

# Non-Gaussian Simultaneous Autoregressive Models with Missing Data

Anjana Wijayawardhana\*, David Gunawan, and Thomas Suesse

School of Mathematics and Applied Statistics, University of Wollongong,  
Wollongong, NSW, Australia

## Abstract

Standard simultaneous autoregressive (SAR) models are usually assumed to have normally distributed errors, an assumption that is often violated in real-world datasets, which are frequently found to exhibit non-normal, skewed, and heavy-tailed characteristics. New SAR models are proposed to capture these non-Gaussian features. In this project, the spatial error model (SEM), a widely used SAR-type model, is considered. Three novel SEMs are introduced that extend the standard Gaussian SEM by incorporating Student's  $t$ -distributed errors after a one-to-one transformation is applied to the response variable. Variational Bayes (VB) estimation methods are developed for these models, and the framework is further extended to handle missing response data. Standard variational Bayes (VB) methods perform well with complete datasets; however, handling missing data requires a Hybrid VB (HVB) approach, which integrates a Markov chain Monte Carlo (MCMC) sampler to generate missing values. The proposed VB methods are evaluated using both simulated and real-world datasets, demonstrating their robustness and effectiveness in dealing with non-normal data and missing data in spatial models. Although the method is demonstrated using SAR models, the proposed model specifications and

---

\*Corresponding author: anjanaw@uow.edu.au

estimation approaches are widely applicable to various types of models for handling non-Gaussian data with missing values.

Keywords: Spatial error models; Student's  $t$  errors; Yeo and Johnson (YJ) transformation; Missing not at random; Variational Bayes approximation

## 1 Introduction

Conventional spatial statistical models, such as simultaneous autoregressive (SAR) models, conditional autoregressive (CAR) models, and kriging models, among others (see Besag (1974); Cressie (1993); Anselin (1988)), typically assume that the data being modeled follow a Gaussian distribution. However, in practice, this assumption is often violated. In this study, we propose novel SAR-type models and their estimation methods, which are particularly useful when the data are non-Gaussian.

SAR models are a broad class of spatial statistical models commonly used for analysing spatially correlated lattice data (Cressie, 1993). Examples of SAR models includes spatial error models (SEMs), spatial autoregressive models (SAMs), and spatial Durbin models (SDMs), and many more; see Anselin (1988), and Cressie (1993). These models account for spatial dependence, making them useful tools for understanding spatial phenomena in fields such as ecology (Ver Hoef et al., 2018), social sciences (Chi and Zhu, 2008, 2019), finance (Calabrese et al., 2017; Agosto et al., 2019).

The estimation of SAR models using methods such as the maximum likelihood estimation (MLE) (Ord, 1975; LeSage, 1997) and the Bayesian methods (De Oliveira and Song, 2008; Wu, 2018), under the assumption of Gaussian errors, has been extensively discussed in the literature. To address the issue of outliers in estimating SEM, Yildirim and Mert Kantar (2020) proposed a robust version of the ML estimator. Estimation methods for SAR models that do not rely on strong distributional assumptions have been developed. For example, Lee (2004) introduced the quasi-maximum likelihood estimator (QMLE) for the SAM. Furthermore, Generalised Method of Moments (GMM) estimators, which require fewer distributional assumptions than traditional ML estimators, are robust to unknown heteroskedasticity and deviations from normality. These estimators

have been proposed by Kelejian and Prucha (1998), Lee and Liu (2010), and Breitung and Wigger (2018). Non-parametric estimation approaches have also been discussed in the literature for modeling SEM with non-Gaussian data (Al-Momani et al., 2017).

Missing values frequently occur in spatial datasets. When estimating SAR models, ignoring missing response values can lead to inconsistency and bias (Wang and Lee, 2013; Benedetti et al., 2020). Various estimation methods for SAR models with randomly missing data have been well developed (see LeSage and Pace (2004); Wang and Lee (2013); Suesse and Zammit-Mangion (2017); Suesse (2018); Wijayawardhana et al. (2024)). However, research on estimating SAR models with non-randomly missing data remains relatively limited. Flores-Lagunes and Schnier (2012) introduced a GMM estimator, while Rabovič and Čížek (2023) proposed a partial ML method for SEM. Furthermore, Doğan and Taşpinar (2018) and Seya et al. (2021) used the Metropolis-Hastings (MH) algorithm, which becomes computationally expensive when dealing with a large number of observations.

Variational Bayes (VB) methods have recently emerged as a faster alternative to Markov chain Monte Carlo (MCMC) for estimating complex statistical models (Chappell et al., 2008; Han et al., 2016; Ong et al., 2018; Gunawan et al., 2021, 2024). Several commonly used VB methods include mean-field variational Bayes (MFVB) (Ormerod and Wand, 2010), integrated non-factorised variational Bayes inference (INFVB) (Han et al., 2013), and Gaussian variational approximation (Ong et al., 2018; Tan and Nott, 2018). Although VB methods offer a more computationally efficient alternative to MCMC, their use in estimating SAR models has been relatively limited. Wu (2018) applied two VB approaches, a hybrid MFVB method and an INFVB method, to estimate spatial autoregressive confused (SAC) and matrix exponential spatial specification (MESS) models. Similarly, Bansal et al. (2021) used MFVB and INFVB to estimate spatial count data models, incorporating a MESS model to capture spatial dependence in error terms. More recently, Wijayawardhana et al. (2025) introduced novel VB methods for estimating SAR models with missing data, demonstrating their effectiveness for moderately large datasets with a high proportion of missing values.

Our article makes several key contributions. First, we introduce novel SAR models designed to capture non-Gaussian characteristics of the response variable, such as skewness and heavy tails. These models extend the standard Gaussian SAR by incorporating Student's t-distributed errors and applying a one-to-one transformation, the Yeo-Johnson (YJ) transformation (Yeo and Johnson, 2000), to the response variable (see Section 2.2 for details). By combining the properties of the Student's  $t$  distribution and the YJ transformation, these models effectively account for heavy-tailedness and skewness, making them well-suited for complex real-world data. Although we illustrate these new model specifications using SEMs, the framework is applicable to any SAR model.

Second, we propose efficient VB methods for estimating these new SEMs, with and without missing values in the response variable. For the missing data case, we specifically consider the missing not at random (MNAR) mechanism, as defined by Rubin (1976), where the probability of a missing value depends on both observed and unobserved responses. In standard VB inference, the joint posterior distribution of missing values and model parameters is approximated using a Gaussian variational approximation (Wijayawardhana et al., 2025). However, it has been shown that the Gaussian variational approximation with a factor covariance structure (Ong et al., 2018), is not sufficiently flexible to jointly approximate the posterior distributions of the SAR model parameters and missing values. Therefore, in this study, we use the standard Gaussian variational approximation of Ong et al. (2018) for SEMs without missing values, while SEMs with missing values are estimated using an extended version of the hybrid VB (HVB) algorithm of Wijayawardhana et al. (2025).

The rest of this paper is organised as follows. Section 2 presents the new SEMs. In Section 3, we present the VB methods to estimate the SEMs with missing data. In Section 4, simulation studies are conducted to evaluate the performance of the new SEMs and VB methods. Section 5 applies the SEMs to a real-world dataset. Section 6 discusses our major results and findings. The paper also has an online supplement with additional technical details and examples.

## 2 Simultaneous Autoregressive Models

This section introduces our proposed SAR models, focusing on the spatial error model (SEM), a widely used SAR-type model. We present three novel SEMs that extend the standard Gaussian SEM.

Let  $\mathbf{y}^* = (y_1^*, y_2^*, \dots, y_n^*)^\top$  be the vector of response variable observed at  $n$  spatial locations  $s_1, \dots, s_n$ ,  $\mathbf{X}$  be the  $n \times (r+1)$  design matrix containing the covariates, and  $\mathbf{W}$  be the  $n \times n$  spatial weight matrix. The SEM is given by

$$\mathbf{y}^* = \mathbf{X}\boldsymbol{\beta} + (\mathbf{I}_n - \rho\mathbf{W})^{-1}\mathbf{e}, \quad (1)$$

where  $\mathbf{e}$  is an  $n \times 1$  vector of error terms,  $\boldsymbol{\beta} = (\beta_0, \beta_1, \dots, \beta_r)^\top$  is an  $(r+1) \times 1$  vector of fixed effects parameters,  $\rho$  is the spatial autocorrelation parameter, which measures the strength and direction of spatial dependence (LeSage and Pace, 2009), and  $\mathbf{I}_n$  is the  $n \times n$  identity matrix.

Section 2.1 discusses SEMs with Gaussian and Student's  $t$  errors. Section 2.2 discusses two SEMs with Yeo-Johnson (Yeo and Johnson, 2000) transformation. Section 2.3 discusses SEMs with missing data.

### 2.1 Spatial error models with Gaussian and Student's $t$ errors

The standard SEM assumes Gaussian errors  $\mathbf{e} \sim N(0, \sigma_e^2 \mathbf{I}_n)$ , where  $\sigma_e^2$  is the variance parameter. This assumption implies that the distribution of  $\mathbf{y}^*$  is also Gaussian, with the mean vector and the covariance matrix given in Table 1. We call this model the SEM-Gau.

Student's  $t$ -distribution has been widely used to model heavy-tailed data in popular statistical models, such as regression (Lange et al., 1989; Fernández and Steel, 1999) and mixed-effects models (Pinheiro et al., 2001; Wang and Lin, 2014). Huang et al. (2021) applied Student's  $t$  errors to spatial autoregressive scalar-on-function regression models. We now discuss SEM-t, which replaces the Gaussian errors in the SEM-Gau model with a Student's  $t$ -distribution. Let  $e_i \sim t_\nu(0, \sigma_e^2)$ , where  $e_i$  is the  $i^{th}$  element of the error vector

$\mathbf{e}$  in Equation (1) and  $t_\nu(0, \sigma_e^2)$  is the Student's t distribution with  $\nu$  degrees of freedom ( $\nu \geq 3$ ), mean zero, and scale parameter  $\sigma_e^2$ . We write Student's t errors,  $e_i$ ,  $i = 1, \dots, n$ , as a scale mixture of normals (Chan et al., 2019),

$$\begin{aligned} e_i \mid \tau_i, \sigma_e^2 &\sim N(0, \sigma_e^2 \tau_i), \\ \tau_i \mid \nu &\sim IG\left(\frac{\nu}{2}, \frac{\nu}{2}\right), \quad i = 1, \dots, n \end{aligned} \tag{2}$$

where  $IG(a, b)$  denotes the inverse gamma distribution with shape parameter  $a$  and scale parameter  $b$ . The conditional distribution of errors presented in Equation (2), can be written in vector notation as

$$\mathbf{e} \mid \boldsymbol{\tau}, \sigma_e^2 \sim N(0, \sigma_e^2 \boldsymbol{\Sigma}_{\boldsymbol{\tau}}), \tag{3}$$

where the matrix  $\boldsymbol{\Sigma}_{\boldsymbol{\tau}} = \text{diag}(\tau_1, \dots, \tau_n)$ . We now incorporate the error structure from Equation (3) into the SEM described in Equation (1). As a result, the distribution of  $\mathbf{y}^*$  given the latent vector  $\boldsymbol{\tau}$  is also Gaussian, with the mean vector and the covariance matrix given in Table 1. We refer to this model as SEM-t. The log-likelihood function of  $\mathbf{y}^*$  for SEM-Gau and SEM-t is expressed as:

$$\log p_{\mathbf{y}^*}(\mathbf{y}^* \mid \boldsymbol{\xi}) = -\frac{n}{2} \log(2\pi) - \frac{n}{2} \log(\sigma_e^2) + \frac{1}{2} \log |\mathbf{M}| - \frac{1}{2\sigma_e^2} \mathbf{r}^\top \mathbf{M} \mathbf{r}, \tag{4}$$

where for the SEM-Gau model,  $\boldsymbol{\xi} = \boldsymbol{\phi}$ , while for the SEM-t model,  $\boldsymbol{\xi} = (\boldsymbol{\phi}^\top, \boldsymbol{\tau}^\top)^\top$ . The definitions for  $\mathbf{r}$ ,  $\mathbf{M}$ , and  $\boldsymbol{\phi}$  are given in Table 1.

## 2.2 Spatial error models with transformations

This section extends the SEM-Gau and SEM-t defined in Section 2.1. We form a novel class of SEMs using an element-wise Yeo and Johnson (YJ) transformation (Yeo and Johnson, 2000) for the response variable,  $\mathbf{y}^*$ , in both the SEM-Gau and SEM-t models.

We assume that the  $i^{th}$  observed response variable ( $y_i$ ) is modeled as,

$$y_i = t_\gamma^{-1}(y_i^*),$$

where  $t_\gamma^{-1}(.)$  is the inverse function of the YJ transformation. For  $0 < \gamma < 2$ , it is defined as:

$$y_i = t_\gamma^{-1}(y_i^*) = \begin{cases} (y_i^* \gamma + 1)^{1/\gamma} - 1 & \text{if } y_i^* \geq 0 \\ 1 - (-(2 - \gamma)y_i^* + 1)^{1/(2-\gamma)} & \text{if } y_i^* < 0. \end{cases} \quad (5)$$

As the YJ transformation makes the data more symmetric and less skewed, applying its inverse transformation moves the data away from symmetry. This implies that  $\mathbf{y} = t_\gamma^{-1}(\mathbf{y}^*) = (t_\gamma^{-1}(y_1^*), t_\gamma^{-1}(y_2^*), \dots, t_\gamma^{-1}(y_n^*))^\top$  becomes an asymmetric, non-Gaussian response variable. The SEM with the YJ transformation (YJ-SEM) is defined as:

$$\mathbf{y} = t_\gamma^{-1}(\mathbf{y}^*) = t_\gamma^{-1}(\mathbf{X}\boldsymbol{\beta} + (\mathbf{I}_n - \rho\mathbf{W})^{-1}\mathbf{e}). \quad (6)$$

The density of  $\mathbf{y}$  for the YJ-SEM is:

$$p_{\mathbf{y}}(\mathbf{y} \mid \boldsymbol{\xi}) = p_{\mathbf{y}^*}(t_\gamma(\mathbf{y})) \prod_{i=1}^n \left( \frac{dt_\gamma(y_i)}{dy_i} \right), \quad i = 1, \dots, n, \quad (7)$$

where  $p_{\mathbf{y}^*}(\cdot)$  is the density of  $\mathbf{y}^*$ ; see Section 2.1, and  $\frac{dt_\gamma(y_i)}{dy_i}$  is the derivative of the YJ transformation with respect to  $y_i$ ; see Section S1 of the online supplement. The YJ-SEM with normally distributed errors (denoted as YJ-SEM-Gau) assumes that the error term in Equation (6) follows a normal distribution:  $\mathbf{e} \sim N(0, \sigma_e^2 \mathbf{I}_n)$ . The YJ-SEM with Student's t-distributed errors (denoted as YJ-SEM-t) assumes that the error term follows the structure specified in Equation (2). The log-likelihood function for  $\mathbf{y}$  in YJ-SEM-Gau and YJ-SEM-t is:

$$\begin{aligned} \log p_{\mathbf{y}}(\mathbf{y} \mid \boldsymbol{\xi}) &= -\frac{n}{2} \log(2\pi) - \frac{n}{2} \log(\sigma_e^2) + \frac{1}{2} \log|\mathbf{M}| - \frac{1}{2\sigma_e^2} \mathbf{r}^\top \mathbf{M} \mathbf{r} \\ &\quad + \sum_{i=1}^n \log \left( \frac{dt_\gamma(y_i)}{dy_i} \right), \end{aligned} \quad (8)$$

where for the YJ-SEM-Gau model,  $\boldsymbol{\xi} = \boldsymbol{\phi}$ , while for the YJ-SEM-t model,  $\boldsymbol{\xi} = (\boldsymbol{\phi}^\top, \boldsymbol{\tau}^\top)^\top$ . The definitions for  $\mathbf{r}$ ,  $\mathbf{M}$ , and  $\boldsymbol{\phi}$  are given in Table 1. Note that  $y_i = y_i^*$  for  $i = 1, \dots, n$ , corresponds to an identity transformation in both SEM-Gau and SEM-t.

The three SEMs, SEM-Gau, SEM-t, and YJ-SEM-Gau, are special cases of the YJ-SEM-t model. The SEM-Gau model is a YJ-SEM-t model with the degrees of freedom parameter ( $\nu$ ) set to  $\infty$  and the YJ parameter ( $\gamma$ ) set to 1, while the YJ-SEM-Gau model is a YJ-SEM-t model with  $\nu = \infty$  and  $\gamma \neq 1$ . Finally, the SEM-t model is also a YJ-SEM-t model with  $\gamma = 1$ .

Table 1: The definitions of  $\mathbf{r}$ ,  $\mathbf{M}$ , and the parameters  $\boldsymbol{\phi}$  for the four spatial error models. Each SEM has a mean vector of  $\mathbf{X}\boldsymbol{\beta}$  and a covariance matrix of the form  $\boldsymbol{\Sigma} = \sigma_e^2 \mathbf{M}^{-1}$ , with  $\mathbf{A} = \mathbf{I}_n - \rho \mathbf{W}$ .

| Model      | $\boldsymbol{\phi}$   | $\mathbf{r}$  | $\mathbf{M}$   |
|------------|---|---|--|
| SEM-Gau    | $(\boldsymbol{\beta}^\top, \sigma_e^2, \rho)^\top$              | $\mathbf{y} - \mathbf{X}\boldsymbol{\beta}$           | $\mathbf{A}^\top \mathbf{A}$                               |
| SEM-t      | $(\boldsymbol{\beta}^\top, \sigma_e^2, \rho, \nu)^\top$         | $\mathbf{y} - \mathbf{X}\boldsymbol{\beta}$           | $\mathbf{A}^\top \boldsymbol{\Sigma}_\tau^{-1} \mathbf{A}$ |
| YJ-SEM-Gau | $(\boldsymbol{\beta}^\top, \sigma_e^2, \rho, \gamma)^\top$      | $t_\gamma(\mathbf{y}) - \mathbf{X}\boldsymbol{\beta}$ | $\mathbf{A}^\top \mathbf{A}$                               |
| YJ-SEM-t   | $(\boldsymbol{\beta}^\top, \sigma_e^2, \rho, \nu, \gamma)^\top$ | $t_\gamma(\mathbf{y}) - \mathbf{X}\boldsymbol{\beta}$ | $\mathbf{A}^\top \boldsymbol{\Sigma}_\tau^{-1} \mathbf{A}$ |

### 2.3 Spatial error models with missing responses

Consider that the response vector  $\mathbf{y}$  of an SEM presented in Sections 2.1 and 2.2 contains missing values. Let  $\mathbf{y}_o$  be the subset of  $\mathbf{y}$  with  $n_o$  observed units, and  $\mathbf{y}_u$  be the subset of  $\mathbf{y}$  with  $n_u$  unobserved units. The complete response vector is  $\mathbf{y} = (\mathbf{y}_o^\top, \mathbf{y}_u^\top)^\top$ . A missing data indicator vector  $\mathbf{m}$  of length  $n$  containing 1's and 0's is defined. If an element in  $\mathbf{y}$  is missing, then the corresponding element in  $\mathbf{m}$  is 1 and 0, otherwise. In the presence of missing values, the vector  $\mathbf{r}$  and the matrices  $\mathbf{X}$  and  $\mathbf{M}$  are decomposed into distinct components as follows:

$$\mathbf{r} = \begin{pmatrix} \mathbf{r}_o \\ \mathbf{r}_u \end{pmatrix}, \quad \mathbf{X} = \begin{pmatrix} \mathbf{X}_o \\ \mathbf{X}_u \end{pmatrix}, \quad \mathbf{M} = \begin{pmatrix} \mathbf{M}_{oo} & \mathbf{M}_{ou} \\ \mathbf{M}_{uo} & \mathbf{M}_{uu} \end{pmatrix}, \quad (9)$$

where  $\mathbf{r}_o$  and  $\mathbf{r}_u$  are subvectors of  $\mathbf{r}$ , corresponding to the observed and unobserved responses, respectively. Similarly,  $\mathbf{X}_o$  and  $\mathbf{X}_u$  represent the design matrices associated

with the observed and unobserved responses. Additionally, the matrices  $\mathbf{M}_{oo}$ ,  $\mathbf{M}_{ou}$ ,  $\mathbf{M}_{uo}$ , and  $\mathbf{M}_{uu}$  are submatrices of  $\mathbf{M}$ .

We assume missing responses follow a missing not at random (MNAR) mechanism (Rubin, 1976). The missing data mechanism is defined by the conditional distribution of  $\mathbf{m}$  given  $\mathbf{y}$ , commonly referred to as the missing data model, denoted by  $p(\mathbf{m}|\mathbf{y}, \boldsymbol{\psi}, \mathbf{X}^*)$ , where  $\mathbf{X}^*$  is an  $n \times (q+1)$  design matrix containing the covariates of the missing data model. These covariates may be a subset of those used in SEMs. Assuming the conditional independence of  $\mathbf{m}$  given  $\mathbf{y}$ ,  $\mathbf{X}^*$ , and  $\boldsymbol{\psi}$ , the density is the product of  $p(m_i | y_i, \mathbf{x}_i^*, \boldsymbol{\psi})$  for  $i = 1, \dots, n$ , where  $m_i$  and  $y_i$  are the  $i^{th}$  elements of  $\mathbf{m}$  and  $\mathbf{y}$ , and  $\mathbf{x}_i^{*\top}$  is the  $i^{th}$  row of  $\mathbf{X}^*$ . The parameter vector  $\boldsymbol{\psi} = (\boldsymbol{\psi}_x^\top, \psi_y)^\top$  consists of the fixed effects vector associated with covariates  $\mathbf{X}^*$ , denoted as  $\boldsymbol{\psi}_x = (\psi_0, \psi_1, \psi_2, \dots, \psi_q)^\top$ , and the fixed effect corresponding to  $\mathbf{y}$ , denoted as  $\psi_y$ . A logistic regression model is used as the missing data model and is given by:

$$p(\mathbf{m} | \mathbf{y}, \mathbf{X}^*, \boldsymbol{\psi}) = \prod_{i=1}^n \frac{e^{(\mathbf{x}_i^{*\top} \boldsymbol{\psi}_x + y_i \psi_y)m_i}}{1 + e^{\mathbf{x}_i^{*\top} \boldsymbol{\psi}_x + y_i \psi_y}}. \quad (10)$$

### 3 Variational Bayes inference for SEMs with missing data

Section 3.1 introduces the variational Bayes (VB) inference method. Section 3.2 discusses the efficient hybrid variational Bayes (HVB) methods for estimating the SEMs with missing data. Section 3.3 discusses the Deviance Information Criterion (DIC) to select the best SEMs. The VB method for the proposed SEMs in Section 2, when there are no missing data, is provided in Section S2 of the online supplement.

#### 3.1 Variational Bayes inference

Variational Bayes (VB) inference approximates a Bayesian posterior distribution by formulating it as an optimisation problem, offering a more computationally efficient alternative to the computationally intensive Markov chain Monte Carlo (MCMC) methods for

complex statistical models. This section presents the VB method for SEMs with missing data.

We assume that some values in the response vector of an SEM are missing under the missing not at random (MNAR) mechanism. Under this assumption, Bayesian estimation of the SEM requires consideration of the joint distribution of the missing data indicator vector  $\mathbf{m}$  and the response vector  $\mathbf{y}$  (Wijayawardhana et al., 2025), which is denoted by  $p(\mathbf{y}, \mathbf{m} | \boldsymbol{\xi}, \boldsymbol{\psi})$ . Using the selection model factorisation (Little and Rubin, 2019),  $p(\mathbf{y}, \mathbf{m} | \boldsymbol{\xi}, \boldsymbol{\psi})$  is expressed as

$$p(\mathbf{y}, \mathbf{m} | \boldsymbol{\xi}, \boldsymbol{\psi}) = p(\mathbf{m} | \mathbf{y}, \boldsymbol{\psi})p(\mathbf{y} | \boldsymbol{\xi}). \quad (11)$$

where  $p(\mathbf{y} | \boldsymbol{\xi})$  is the likelihood of  $\mathbf{y}$ . The log-likelihood for  $\mathbf{y}$  for different SEMs is given in Section 2. Additionally,  $p(\mathbf{m} | \mathbf{y}, \boldsymbol{\psi})$  denotes the density of the missing data model, given in Equation (10).

Consider Bayesian inference to estimate the joint posterior of  $\boldsymbol{\xi}$ ,  $\boldsymbol{\psi}$ , and the missing values  $\mathbf{y}_u$ . For the SEM-Gau and YJ-SEM-Gau models,  $\boldsymbol{\xi} = \boldsymbol{\phi}$ , while for the SEM-t and YJ-SEM-t models,  $\boldsymbol{\xi} = (\boldsymbol{\phi}^\top, \boldsymbol{\tau}^\top)^\top$ ; see Table 1 for the definition of  $\boldsymbol{\phi}$  for each SEM. Let the joint posterior distribution of  $\boldsymbol{\xi}$ ,  $\boldsymbol{\psi}$ , and  $\mathbf{y}_u$  be denoted as  $p(\boldsymbol{\xi}, \boldsymbol{\psi}, \mathbf{y}_u | \mathbf{y}_o, \mathbf{m})$ . We let  $p(\boldsymbol{\xi})$  and  $p(\boldsymbol{\psi})$  as the prior distributions of  $\boldsymbol{\xi}$  and  $\boldsymbol{\psi}$ , respectively. Using the selection model factorisation in Equation (11), the joint posterior distribution  $p(\boldsymbol{\xi}, \boldsymbol{\psi}, \mathbf{y}_u | \mathbf{y}_o, \mathbf{m})$  is given by

$$p(\boldsymbol{\xi}, \boldsymbol{\psi}, \mathbf{y}_u | \mathbf{y}_o, \mathbf{m}) \propto p(\mathbf{m} | \mathbf{y}, \boldsymbol{\psi})p(\mathbf{y} | \boldsymbol{\xi})p(\boldsymbol{\xi})p(\boldsymbol{\psi}). \quad (12)$$

We define  $h(\boldsymbol{\xi}, \boldsymbol{\psi}, \mathbf{y}_u) = p(\mathbf{y} | \boldsymbol{\xi})p(\mathbf{m} | \mathbf{y}, \boldsymbol{\psi})p(\boldsymbol{\xi})p(\boldsymbol{\psi})$ . The term  $h(\boldsymbol{\xi}, \boldsymbol{\psi}, \mathbf{y}_u)$  for each SEM with missing data, along with the total number of parameters to be estimated ( $s_m$ ) for each model are provided in Table 2.

We consider the variational approximation  $q_{\boldsymbol{\lambda}}(\boldsymbol{\xi}, \boldsymbol{\psi}, \mathbf{y}_u)$ , indexed by the variational parameter  $\boldsymbol{\lambda}$  to approximate the joint posterior  $p(\boldsymbol{\xi}, \boldsymbol{\psi}, \mathbf{y}_u | \mathbf{y}_o, \mathbf{m})$ . The VB approach approximates the posterior distribution by minimising the Kullback-Leibler (KL) divergence between  $q_{\boldsymbol{\lambda}}(\boldsymbol{\xi}, \boldsymbol{\psi}, \mathbf{y}_u)$  and  $p(\boldsymbol{\xi}, \boldsymbol{\psi}, \mathbf{y}_u | \mathbf{y}_o, \mathbf{m})$ . Minimising KL divergence between these two distributions is equivalent to maximising the evidence lower bound (ELBO) on

Table 2: The term  $h(\boldsymbol{\xi}, \boldsymbol{\psi}, \mathbf{y}_u) = p(\mathbf{y} \mid \boldsymbol{\xi})p(\mathbf{m} \mid \mathbf{y}, \boldsymbol{\psi})p(\boldsymbol{\xi})p(\boldsymbol{\psi})$ , and the total number of model parameters  $s_m$  (including the length of the latent vector  $\boldsymbol{\tau}$ ) for the SEM-Gau, YJ-SEM-Gau, SEM-t, and YJ-SEM-t models with missing values. The distribution  $p(\boldsymbol{\tau} \mid \boldsymbol{\phi}) = \prod_{i=1}^n p(\tau_i \mid \nu)$  represents the  $n$  independent inverse gamma latent variables used in SEMs with Student- $t$  errors (see Equation (2)).

| Model      | $h(\boldsymbol{\xi}, \boldsymbol{\psi}, \mathbf{y}_u)$   | $s_m$           |
|------------|--|-----------------|
| SEM-Gau    | $p(\mathbf{y} \mid \boldsymbol{\phi})p(\mathbf{m} \mid \mathbf{y}, \boldsymbol{\psi})p(\boldsymbol{\phi})p(\boldsymbol{\psi})$   | $r + q + 5$     |
| SEM-t      | $p(\mathbf{y} \mid \boldsymbol{\tau}, \boldsymbol{\phi})p(\mathbf{m} \mid \mathbf{y}, \boldsymbol{\psi})p(\boldsymbol{\tau} \mid \boldsymbol{\phi})p(\boldsymbol{\phi})p(\boldsymbol{\psi})$ | $r + q + 6 + n$ |
| YJ-SEM-Gau | $p(\mathbf{y} \mid \boldsymbol{\phi})p(\mathbf{m} \mid \mathbf{y}, \boldsymbol{\psi})p(\boldsymbol{\phi})p(\boldsymbol{\psi})$   | $r + q + 6$     |
| YJ-SEM-t   | $p(\mathbf{y} \mid \boldsymbol{\tau}, \boldsymbol{\phi})p(\mathbf{m} \mid \mathbf{y}, \boldsymbol{\psi})p(\boldsymbol{\tau} \mid \boldsymbol{\phi})p(\boldsymbol{\phi})p(\boldsymbol{\psi})$ | $r + q + 7 + n$ |

the marginal likelihood,  $\log p(\mathbf{y}_o, \mathbf{m})$ , denoted by  $\mathcal{L}(\boldsymbol{\lambda})$ , where  $p(\mathbf{y}_o, \mathbf{m}) = \int p(\mathbf{y}_o, \mathbf{m} \mid \boldsymbol{\xi}, \boldsymbol{\psi}, \mathbf{y}_u)p(\mathbf{y}_u \mid \boldsymbol{\xi}, \boldsymbol{\psi})d\boldsymbol{\xi}d\boldsymbol{\psi}d\mathbf{y}_u$  (Blei et al., 2017). Further, the ELBO can be written as an expectation with respect to the variational distribution and is given by

$$\mathcal{L}(\boldsymbol{\lambda}) = E_q [\log h(\boldsymbol{\xi}, \boldsymbol{\psi}, \mathbf{y}_u) - \log q_{\boldsymbol{\lambda}}(\boldsymbol{\xi}, \boldsymbol{\psi}, \mathbf{y}_u)], \quad (13)$$

where  $E_q [\cdot]$  denotes the expectation with respect to  $q_{\boldsymbol{\lambda}}$ . Table 2 provides expressions for  $h(\boldsymbol{\xi}, \boldsymbol{\psi}, \mathbf{y}_u)$  for different SEMs.

To maximise ELBO given in Equation (S6) with respect to variational parameters,  $\boldsymbol{\lambda}$ , stochastic gradient ascent (SGA) methods are used (Nott et al., 2012; Titsias and Lázaro-Gredilla, 2014, 2015). The SGA method updates the initial value for  $\boldsymbol{\lambda}$  (say  $\boldsymbol{\lambda}^{(0)}$ ) according to the iterative scheme,

$$\boldsymbol{\lambda}^{(t+1)} = \boldsymbol{\lambda}^{(t)} + \boldsymbol{a}_t \circ \widehat{\nabla_{\boldsymbol{\lambda}} \mathcal{L}(\boldsymbol{\lambda}^{(t)})}, \quad (14)$$

where  $\widehat{\nabla_{\boldsymbol{\lambda}} \mathcal{L}(\boldsymbol{\lambda})}$  is an unbiased estimate of the gradient  $\nabla_{\boldsymbol{\lambda}} \mathcal{L}(\boldsymbol{\lambda})$ ,  $\boldsymbol{a}_t$  ( $t = 0, 1, \dots$ ), is a vector of adaptive step sizes, obtained using the ADADELTA method (Zeiler, 2012), described in Section S3 of the online supplement to facilitate rapid convergence of the SGA algorithms. The symbol  $\circ$  represents the element-wise product of two vectors. The updating of Equation (14) is done until a stopping criterion is satisfied. In standard VB methods, the missing data vector,  $\mathbf{y}_u$ , is treated as parameters, and the joint posterior distribution of  $\boldsymbol{\xi}$ ,  $\boldsymbol{\psi}$ , and  $\mathbf{y}_u$  is approximated. This is similar to the VB method for the SEMs with full data, outlined in Section S2 of the online supplement.

### 3.2 Hybrid variational Bayes

To efficiently handle missing values  $\mathbf{y}_u$  in SEMs described in Section 2, we extend the hybrid VB method of Wijayawardhana et al. (2025) that uses the Gaussian variational approximation with a factor covariance structure to approximate the posterior distribution of the parameters, while employing an MCMC sampler to generate samples of  $\mathbf{y}_u$  from its conditional distribution, given  $\mathbf{y}_o$ ,  $\mathbf{m}$ ,  $\boldsymbol{\xi}$  and  $\boldsymbol{\psi}$ . We first factorise the variational distribution that approximates  $\boldsymbol{\xi}$ ,  $\boldsymbol{\psi}$ , and  $\mathbf{y}_u$ ,  $q_{\boldsymbol{\lambda}}(\boldsymbol{\xi}, \boldsymbol{\psi}, \mathbf{y}_u)$  as follows:

$$q_{\boldsymbol{\lambda}}(\boldsymbol{\xi}, \boldsymbol{\psi}, \mathbf{y}_u) = p(\mathbf{y}_u \mid \mathbf{y}_o, \mathbf{m}, \boldsymbol{\xi}, \boldsymbol{\psi}) q_{\boldsymbol{\lambda}}^0(\boldsymbol{\xi}, \boldsymbol{\psi}), \quad (15)$$

where  $p(\mathbf{y}_u \mid \mathbf{y}_o, \mathbf{m}, \boldsymbol{\xi}, \boldsymbol{\psi})$  represents the conditional distribution of  $\mathbf{y}_u$ , given the observed data ( $\mathbf{y}_o$ ,  $\mathbf{m}$ ), and the model parameters ( $\boldsymbol{\xi}$  and  $\boldsymbol{\psi}$ ). The term  $q_{\boldsymbol{\lambda}}^0(\boldsymbol{\xi}, \boldsymbol{\psi})$  is the Gaussian variational approximation of Ong et al. (2018), used to approximate the posterior distribution of  $\boldsymbol{\xi}$  and  $\boldsymbol{\psi}$ . We rewrite the ELBO in Equation (S6) by substituting the factorised variational distribution  $q_{\boldsymbol{\lambda}}(\boldsymbol{\xi}, \boldsymbol{\psi}, \mathbf{y}_u)$  from Equation (15). Using Bayes' rule, it is straightforward to show

$$\mathcal{L}(\boldsymbol{\lambda}) = E_q [\log p(\mathbf{y}_o, \mathbf{m} \mid \boldsymbol{\xi}, \boldsymbol{\psi}) + \log p(\boldsymbol{\xi}, \boldsymbol{\psi}) - \log q_{\boldsymbol{\lambda}}^0(\boldsymbol{\xi}, \boldsymbol{\psi})] = \mathcal{L}^0(\boldsymbol{\lambda}), \quad (16)$$

where  $\mathcal{L}^0(\boldsymbol{\lambda})$  is the ELBO resulting from approximating only the posterior distribution of parameters  $\boldsymbol{\xi}$  and  $\boldsymbol{\psi}$ ,  $p(\boldsymbol{\xi}, \boldsymbol{\psi} \mid \mathbf{y}_o, \mathbf{m})$ , directly using the variational distribution  $q_{\boldsymbol{\lambda}}^0(\boldsymbol{\xi}, \boldsymbol{\psi})$ ; see Wijayawardhana et al. (2025) for the complete proof.

We assume that the variational distribution,  $q_{\boldsymbol{\lambda}}^0(\boldsymbol{\xi}, \boldsymbol{\psi})$ , follows a multivariate normal distribution with a factor covariance structure (Ong et al., 2018),  $q_{\boldsymbol{\lambda}}^0(\boldsymbol{\xi}, \boldsymbol{\psi}) \sim N((\boldsymbol{\xi}^\top, \boldsymbol{\psi}^\top)^\top; \boldsymbol{\mu}_{s_m}, \mathbf{B}_{s_m} \mathbf{B}_{s_m}^\top + \mathbf{D}_{s_m}^2)$ , where  $\boldsymbol{\mu}_{s_m}$  is an  $s_m \times 1$  vector of variational means,  $\mathbf{B}_{s_m}$  is an  $s_m \times p$  matrix with the upper triangular elements set to zero, and  $\mathbf{D}_{s_m}$  is an  $s_m \times s_m$  diagonal matrix with positive diagonal elements  $\mathbf{d}_{s_m} = (d_1, \dots, d_{s_m})^\top$ . For all SEMs with missing values, the value of  $s_m$  is provided in Table 2. The vector of variational parameters is given by  $\boldsymbol{\lambda}_{s_m} = (\boldsymbol{\mu}_{s_m}^\top, \text{vech}(\mathbf{B}_{s_m})^\top, \mathbf{d}_{s_m}^\top)^\top$ , where the 'vech' operator vectorises a matrix by stacking its columns from left to right while removing all

the elements above the diagonal (the superdiagonal elements) of the matrix.

In the SGA algorithm (Equation (14)), we compute an unbiased estimate of the ELBO gradient,  $\nabla_{\lambda} \mathcal{L}(\lambda)$ , denoted as  $\widehat{\nabla_{\lambda} \mathcal{L}(\lambda)}$ , at each iteration using the reparameterisation trick (Kingma and Welling, 2013). To do this, we first generate samples from the variational distribution  $q_{\lambda}^0(\xi, \psi)$  by drawing  $\delta^0 = (\eta^0, \epsilon^0) \sim N(\mathbf{0}, \mathbf{I}_{s_m+p})$ , where  $\eta^0$  is a  $p$ -dimensional vector and  $\epsilon^0$  is an  $s_m$ -dimensional vector. Next, we compute  $(\xi^{\top}, \psi^{\top})^{\top} = t^0(\delta^0, \lambda_{s_m}) = \mu_{s_m} + \mathbf{B}_{s_m} \eta^0 + \mathbf{d}_{s_m} \circ \epsilon^0$ . The density of  $\delta^0$  is denoted by  $f_{\delta^0}(\delta^0)$ . Let  $\delta = (\delta^0^{\top}, \mathbf{y}_u^{\top})^{\top}$ , where the product density is expressed as  $f_{\delta}(\delta) = f_{\delta^0}(\delta^0) p(\mathbf{y}_u \mid \mathbf{y}_o, \mathbf{m}, t^0(\delta^0, \lambda_{s_m}))$ . Finally, the transformation from  $\delta$  to the parameter and augmented missing value space is given by  $((\xi^{\top}, \psi^{\top})^{\top}, \mathbf{y}_u^{\top})^{\top} = t(\delta, \lambda_{s_m}) = (t^0(\delta^0, \lambda_{s_m})^{\top}, \mathbf{y}_u^{\top})^{\top} = ((\mu_{s_m} + \mathbf{B}_{s_m} \eta^0 + \mathbf{d}_{s_m} \circ \epsilon^0)^{\top}, \mathbf{y}_u^{\top})^{\top}$ .

The reparameterisation gradient of the ELBO in Equation (16) is derived by differentiating under the integral sign as shown below:

$$\nabla_{\lambda} \mathcal{L}(\lambda) = \mathbb{E}_{f_{\delta}} \left[ \frac{dt^0(\delta^0, \lambda_{s_m})^{\top}}{d\lambda_{s_m}} (\nabla_{(\xi^{\top}, \psi^{\top})^{\top}} \log h(\xi, \psi, \mathbf{y}_u) - \nabla_{(\xi^{\top}, \psi^{\top})^{\top}} \log q_{\lambda}^0(\xi, \psi)) \right], \quad (17)$$

where  $\frac{dt^0(\delta^0, \lambda_{s_m})}{d\lambda_{s_m}}$  is the derivative of the transformation  $t^0(\delta^0, \lambda_{s_m}) = \mu_{s_m} + \mathbf{B}_{s_m} \eta^0 + \mathbf{d}_{s_m} \circ \epsilon^0$  with respect to the variational parameters  $\lambda_{s_m} = (\mu_{s_m}^{\top}, \text{vech}(\mathbf{B}_{s_m})^{\top}, \mathbf{d}_{s_m}^{\top})^{\top}$ ; see Section S4.1 of the online supplement for the proof. The expressions for  $\frac{dt^0(\delta^0, \lambda_{s_m})^{\top}}{d\lambda_{s_m}}$  and  $\nabla_{(\xi^{\top}, \psi^{\top})^{\top}} \log q_{\lambda}^0(\xi, \psi)$  can be found in Section S4.1 of the online supplement. In addition, the expressions for  $\nabla_{(\xi^{\top}, \psi^{\top})^{\top}} \log h(\xi, \psi, \mathbf{y}_u)$  are provided in Section S4.3 for different SEMs.

Algorithm 1 outlines the HVB algorithm. For all four SEMs with missing data, the conditional distribution of missing data;  $p(\mathbf{y}_u \mid \mathbf{y}_o, \mathbf{m}, \xi, \psi)$  is not available in closed form. To sample from  $p(\mathbf{y}_u \mid \mathbf{y}_o, \mathbf{m}, \xi, \psi)$  in step 5 of Algorithm 1, we use the Markov chain Monte Carlo (MCMC) steps outlined in Algorithm 2.

The MCMC steps in Algorithm 2 generate samples from the proposal distribution  $p(\tilde{\mathbf{y}}_u \mid \xi^{(t)}, \mathbf{y}_o)$ , which follows a multivariate Gaussian with the mean vector given by  $\mathbf{X}_u \beta - \mathbf{M}_{uu}^{-1} \mathbf{M}_{uor} \mathbf{r}_o$  and the covariance matrix given by  $\sigma_e^2 \mathbf{M}_{uu}^{-1}$ , for both SEM-Gau and

---

**Algorithm 1** Hybrid variational Bayes (HVB) algorithm.

---

- 1: Initialise  $\boldsymbol{\lambda}_{sm}^{(0)} = (\boldsymbol{\mu}_{sm}^{\top(0)}, \text{vech}(\mathbf{B}_{sm})^{\top(0)}, \mathbf{d}_{sm}^{\top(0)})^\top$  and set  $t = 0$
- 2: **repeat**
- 3:   Generate  $(\boldsymbol{\eta}^{0(t)}, \boldsymbol{\epsilon}^{0(t)}) \sim N(\mathbf{0}, \mathbf{I}_{sm+p})$
- 4:   Generate  $(\boldsymbol{\xi}^{(t)\top}, \boldsymbol{\psi}^{(t)\top})^\top \sim q_{\boldsymbol{\lambda}_{sm}^{(t)}}^0(\boldsymbol{\xi}, \boldsymbol{\psi})$  using its reparameterised representation.
- 5:   Generate  $\mathbf{y}_u^{(t)} \sim p(\mathbf{y}_u \mid \mathbf{y}_o, \mathbf{m}, \boldsymbol{\xi}^{(t)}, \boldsymbol{\psi}^{(t)})$
- 6:   Construct unbiased estimates  $\widehat{\nabla_{\boldsymbol{\mu}_{sm}} \mathcal{L}(\boldsymbol{\lambda})}$ ,  $\widehat{\nabla_{\text{vech}(\mathbf{B}_{sm})} \mathcal{L}(\boldsymbol{\lambda})}$ , and  $\widehat{\nabla_{\mathbf{d}_{sm}} \mathcal{L}(\boldsymbol{\lambda})}$  using Equations (S44), (S45) and (S46) in Section S4.1 of the online supplement.
- 7:   Set adaptive learning rates  $\boldsymbol{\alpha}_{\boldsymbol{\mu}_{sm}}^{(t)}$ ,  $\boldsymbol{\alpha}_{\text{vech}(\mathbf{B}_{sm})}^{(t)}$  and  $\boldsymbol{\alpha}_{\mathbf{d}_{sm}}^{(t)}$ , using ADADELTA described in Section S3 of the online supplement.
- 8:   Set  $\boldsymbol{\mu}_{sm}^{(t+1)} = \boldsymbol{\mu}_{sm}^{(t)} + \boldsymbol{\alpha}_{\boldsymbol{\mu}_{sm}}^{(t)} \circ \widehat{\nabla_{\boldsymbol{\mu}_{sm}} \mathcal{L}(\boldsymbol{\lambda}^{(t)})}$ .
- 9:   Set  $\text{vech}(\mathbf{B}_{sm})^{(t+1)} = \text{vech}(\mathbf{B}_{sm})^{(t)} + \boldsymbol{\alpha}_{\text{vech}(\mathbf{B}_{sm})}^{(t)} \circ \widehat{\nabla_{\text{vech}(\mathbf{B}_{sm})} \mathcal{L}(\boldsymbol{\lambda}^{(t)})}$ .
- 10:   Set  $\mathbf{d}_{sm}^{(t+1)} = \mathbf{d}_{sm}^{(t)} + \boldsymbol{\alpha}_{\mathbf{d}_{sm}}^{(t)} \circ \widehat{\nabla_{\mathbf{d}_{sm}} \mathcal{L}(\boldsymbol{\lambda}^{(t)})}$ .
- 11:   Set  $\boldsymbol{\lambda}_{sm}^{(t+1)} = (\boldsymbol{\mu}_{sm}^{\top(t+1)}, \text{vech}(\mathbf{B}_{sm})^{\top(t+1)}, \mathbf{d}_{sm}^{\top(t+1)})^\top$ , and  $t = t + 1$
- 12: **until** some stopping rule is satisfied

---

SEM-t; see Table 1 and Equation (9) for details on the partitioning of  $\mathbf{r}$ ,  $\mathbf{X}$  and  $\mathbf{M}$  across different SEMs.

For YJ-SEM-Gau and YJ-SEM-t, the proposals are generated in two steps. First, we sample  $\tilde{\mathbf{y}}_u^*$  from the conditional distribution  $p(\tilde{\mathbf{y}}_u^* \mid \boldsymbol{\xi}^{(t)}, \mathbf{y}_o^*)$ , which follows a multivariate Gaussian with the mean vector given by  $\mathbf{X}_u \boldsymbol{\beta} - \mathbf{M}_{uu}^{-1} \mathbf{M}_{uo} (\mathbf{y}_o^* - \mathbf{X}_o \boldsymbol{\beta})$  and the covariance matrix given by  $\sigma_e^2 \mathbf{M}_{uu}^{-1}$ , where  $\mathbf{y}_o^* = t_\gamma(\mathbf{y}_o)$ . Then, we apply the inverse Yeo-Johnson (YJ) transformation to obtain the final proposal:  $\tilde{\mathbf{y}}_u = t_\gamma^{-1}(\tilde{\mathbf{y}}_u^*)$ .

As  $n$  and  $n_u$  increase, the HVB algorithm implemented using the MCMC scheme

---

**Algorithm 2** MCMC steps within the  $t^{th}$  iteration of the HVB algorithm.

---

- 1: Initialise missing values  $\mathbf{y}_{u,0} \sim p(\mathbf{y}_u \mid \boldsymbol{\xi}^{(t)}, \mathbf{y}_o)$
- 2: **for**  $i=1, \dots, N_1$  **do**
- 3:   Sample  $\tilde{\mathbf{y}}_u$  from the proposal distribution  $p(\tilde{\mathbf{y}}_u \mid \boldsymbol{\xi}^{(t)}, \mathbf{y}_o)$ .
- 4:   Sample  $u$  from uniform distribution,  $u \sim \mathcal{U}(0, 1)$
- 5:   Calculate  $a = \min\left(1, \frac{p(\mathbf{m} \mid \tilde{\mathbf{y}}, \boldsymbol{\psi}^{(t)})}{p(\mathbf{m} \mid \mathbf{y}_{i-1}, \boldsymbol{\psi}^{(t)})}\right)$ , where  $\tilde{\mathbf{y}} = (\mathbf{y}_o^\top, \tilde{\mathbf{y}}_u^\top)^\top$  and  $\mathbf{y}_{i-1} = (\mathbf{y}_o^\top, \mathbf{y}_{u,i-1}^\top)^\top$
- 6:   **if**  $a > u$  **then**
- 7:      $\mathbf{y}_{u,i} = \tilde{\mathbf{y}}_u$
- 8:   **else**
- 9:      $\mathbf{y}_{u,i} = \mathbf{y}_{u,i-1}$
- 10:   **end if**
- 11: **end for**
- 12: Output  $\mathbf{y}_u^{(t)} = \mathbf{y}_{u,N_1}$

---

outlined in Algorithm 2 fails to estimate the parameters accurately due to a low acceptance rate. To address this, we partition  $\mathbf{y}_u$  into  $k$  blocks and update one block at a time. The MCMC steps for sampling the missing values one block at a time are detailed in Algorithm S2 in Section S4.2 of the online supplement. We refer to the modified HVB algorithm with block-wise updates as HVB-AllB (which uses MCMC steps in Algorithm S2), and the original version without block-wise updates as HVB-NoB (which uses MCMC steps in Algorithm 2) in the following sections.

### 3.3 Bayesian model comparison

To assess model fit in both the simulation study (Section 4) and the real-world analysis (Section 5), we employ extended versions of the standard Deviance Information Criterion (DIC, Spiegelhalter et al. (2002)) proposed by Celeux et al. (2006). This section first outlines DIC methods for models without missing data, then for those with missing data.

For full data SEMs, both  $\text{DIC}_1$  and  $\text{DIC}_2$  are computed to evaluate model fit, with lower values indicating better fit.  $\text{DIC}_1$  is defined as:

$$\text{DIC}_1 = -4E_{\phi}[\log p(\mathbf{y} \mid \boldsymbol{\phi})] + 2 \log p(\mathbf{y} \mid \bar{\boldsymbol{\phi}}), \quad (18)$$

where  $\bar{\boldsymbol{\phi}}$  is the posterior mean of  $\boldsymbol{\phi}$ , and  $p(\mathbf{y} \mid \boldsymbol{\phi})$  denotes the density of  $\mathbf{y}$  given the model parameters  $\boldsymbol{\phi}$ . Both the expectation and the posterior mean  $\bar{\boldsymbol{\phi}}$  are computed using samples drawn from the approximate posterior distribution estimated by the proposed VB method. For all SEMs, the logarithm of the density  $p(\mathbf{y} \mid \boldsymbol{\phi})$  is provided in Section S5 of the online supplement.

$\text{DIC}_2$  is defined as:

$$\text{DIC}_2 = -4E_{\phi}[\log p(\mathbf{y} \mid \boldsymbol{\phi})] + 2 \log p(\mathbf{y} \mid \hat{\boldsymbol{\phi}}), \quad (19)$$

where  $\hat{\boldsymbol{\phi}}$  is the value of  $\boldsymbol{\phi}$  that maximises the function  $p(\mathbf{y} \mid \boldsymbol{\phi})p(\boldsymbol{\phi})$ , estimated using samples drawn from the approximate posterior obtained by the proposed VB method. The expectation is also computed using these variational posterior samples.

$\text{DIC}_5$  is used to assess model fit for SEMs with missing data and is defined as:

$$\text{DIC}_5 = -4E_{\phi, \psi, \mathbf{y}_u} [\log p(\mathbf{y}, \mathbf{m} \mid \phi, \psi)] + 2 \log p(\mathbf{y}_o, \hat{\mathbf{y}}_u, \mathbf{m} \mid \hat{\phi}, \hat{\psi}), \quad (20)$$

where  $p(\mathbf{y}, \mathbf{m} \mid \phi, \psi)$  is the joint density of  $\mathbf{y}$  and  $\mathbf{m}$ , conditional on model parameters  $\phi$  and  $\psi$ . The values  $\hat{\phi}$ ,  $\hat{\psi}$ , and  $\hat{\mathbf{y}}_u$  are the posterior sample values of  $\phi$ ,  $\psi$  and  $\mathbf{y}_u$  that maximise the density  $p(\mathbf{y}, \mathbf{m} \mid \phi, \psi)p(\phi, \psi)$ , where the samples are drawn from the approximate posterior estimated by the proposed HVB method. The expectation is also computed using these variational posterior samples. Note that  $p(\mathbf{y}, \mathbf{m} \mid \phi, \psi) = p(\mathbf{y} \mid \phi)p(\mathbf{m} \mid \mathbf{y}, \psi)$ ; see the selection model factorisation in Equation (11).

## 4 Simulation study

The simulation study is divided into two subsections. Section 4.1 compares the posterior distributions obtained using variational Bayes (VB) methods with those of Hamiltonian Monte Carlo (HMC, Neal (1996)). The posterior densities estimated using the HMC method are considered as ground truth to assess the accuracy of the VB methods. In Section 4.1, we utilise a small simulated dataset ( $n = 625$ ), as implementing HMC is computationally intensive for SEMs, particularly when handling large datasets with missing data (Wijayawardhana et al., 2025). Section 4.2 uses two moderately large simulated datasets, each considered with and without missing values, and each exhibiting distinct characteristics, to evaluate the robustness of the proposed models and VB methods.

We now describe the prior distributions used in this study for both the VB and HMC methods, applied in the simulation and real-world examples presented in Sections 4.1, 4.2, and 5. To map the parameters  $\sigma_{\mathbf{e}}^2$ ,  $\rho$ ,  $\nu$ , and  $\gamma$  onto the real line, we apply the following transformations:  $\omega' = \log(\sigma_{\mathbf{e}}^2)$ ,  $\rho' = \log(1 + \rho) - \log(1 - \rho)$ ,  $\nu' = \log(\nu - 3)$ , and  $\gamma' = \log(\gamma) - \log(2 - \gamma)$ . Table S3 gives the prior distributions for the transformed parameters.

| Parameter          | $\beta$                                    | $\omega'$                   | $\rho'$                   | $\nu'$                   | $\gamma'$                   | $\psi$                                    |
|--------------------|--|-----------------------------|---------------------------|--------------------------|-----------------------------|---|
| Prior distribution | $N(\mathbf{0}, \sigma_\beta^2 \mathbf{I})$ | $N(0, \sigma_{\omega'}^2)$  | $N(0, \sigma_{\rho'}^2)$  | $N(0, \sigma_{\nu'}^2)$  | $N(0, \sigma_{\gamma'}^2)$  | $N(\mathbf{0}, \sigma_\psi^2 \mathbf{I})$ |
| Hyperparameters    | $\sigma_\beta^2 = 10^2$                    | $\sigma_{\omega'}^2 = 10^2$ | $\sigma_{\rho'}^2 = 10^2$ | $\sigma_{\nu'}^2 = 10^2$ | $\sigma_{\gamma'}^2 = 10^2$ | $\sigma_\psi^2 = 10^2$                    |

Table 3: Prior distributions of model parameters

## 4.1 Assessing the accuracy of variational Bayes approximations

This section compares the accuracy of the proposed VB approximation methods with the computationally intensive, exact HMC methods. The comparison focuses solely on the YJ-SEM-Gau model, both with and without missing data. To facilitate this comparison, a dataset with 625 observations is simulated from the YJ-SEM-Gau model with five covariates generated from standard normal distributions. The weight matrix,  $\mathbf{W}$  is constructed based on a  $25 \times 25$  regular grid, where neighbouring units are defined using the rook neighbourhood criteria, as described in Lloyd (2010).

The model parameters are specified as follows: the fixed effects ( $\beta$ ) are randomly drawn from discrete uniform values between  $-3$  and  $3$  (excluding 0). The error variance parameter is set to  $\sigma_e^2 = 1$  and the spatial autocorrelation parameter is set to  $\rho = 0.8$ . The Yeo Johnson (YJ) parameter is specified as  $\gamma = 1.25$ , inducing moderate left skewness into the simulated response variable. See Figure S1 in Section S7.1 of the online supplement for the kernel density plot of the response variables.

The VB algorithm, outlined in Algorithm S1 in Section S2 of the online supplement, and the HMC algorithm are used to fit the YJ-SEM-Gau model to the simulated dataset. The initial values for the VB algorithm are set as follows: The variational mean vector ( $\mu$ ) is initialised using the estimates of  $\beta$ ,  $\sigma_e^2$ , and  $\rho$  obtained from fitting the SEM-Gau model via maximum likelihood estimation (MLE) method. The initial value for  $\gamma$  is set to 1. For the variational covariance matrix parameters, the elements of  $\mathbf{B}$  and the diagonal elements of  $\mathbf{D}$  are all initialised to 0.01. We use  $p = 4$  factors. The results do not improve when we increase the number of factors. We used similar starting values for the HMC algorithms as well.

Both the VB and HMC algorithms are run for 10,000 iterations, at which point convergence is achieved. For the HMC algorithm, the first 5,000 iterations are treated as burn-in and discarded. Convergence for the VB algorithm is assessed visually by inspecting the plots of variational means over iterations. For the HMC algorithms, convergence is assessed by inspecting trace plots of the model parameters (see Section S9.1 of the online supplement).

The HMC algorithm directly generates posterior samples of the model parameters. In contrast, the VB algorithm first estimates the variational parameters,  $\lambda$ , by running the variational optimisation. Then, 10,000 posterior draws of the model parameters are generated from the variational distribution  $q_\lambda(\xi)$ .

Figure 1 compares the posterior densities of selected model parameters estimated using the VB method and the HMC algorithm implemented via RSTAN (Stan Development Team, 2023) to fit the simulated dataset. For the fixed effect parameter ( $\beta_1$ ), the spatial autocorrelation parameter ( $\rho$ ), the variance parameter ( $\sigma_e^2$ ), and the YJ parameter  $\gamma$ , the posterior densities estimated by both methods are nearly identical and include the true values.

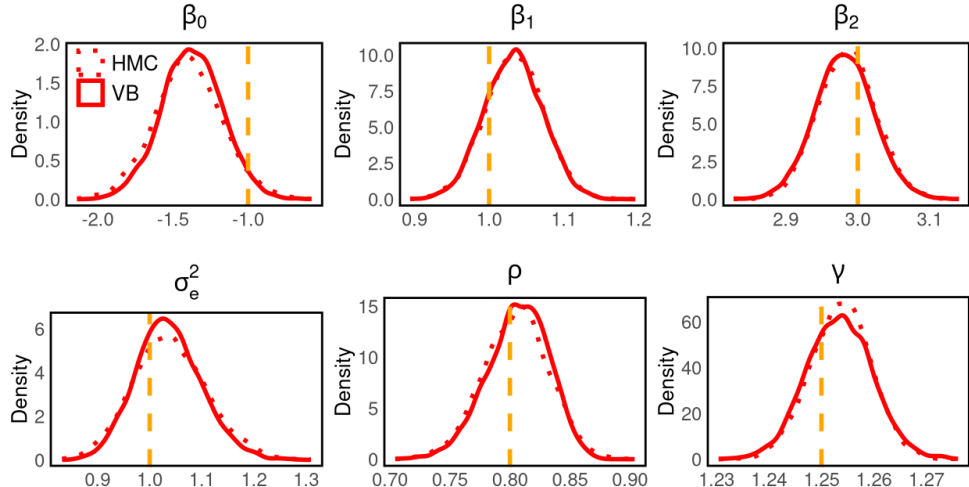


Figure 1: Comparison of posterior densities of selected parameters in the YJ-SEM-Gau model, obtained using the HMC and VB methods on the simulated dataset without missing values. The vertical line represents the true parameter value.

Next, we introduce missing values into the response variable  $\mathbf{y}$  under the MNAR mechanism, using the logistic regression model described in Section 2.3. To do this, we

generate an additional covariate  $\mathbf{x}^*$  from a log-normal distribution with a log-scale mean of 0 and a log-scale standard deviation of 1. This covariate is included in the missing data model, which is specified as a logistic regression model with  $\mathbf{x}^*$  and the response variable  $\mathbf{y}$  as covariates (see Equation (10)). The regression coefficients are set as follows:  $\psi_0 = -1.0$  (intercept),  $\psi_{\mathbf{x}^*} = 0.5$  (the coefficient of  $\mathbf{x}^*$ ), and  $\psi_{\mathbf{y}} = -0.1$  (the coefficient of  $\mathbf{y}$ ). This configuration yields approximately 50% missing values in  $\mathbf{y}$ , corresponding to  $n_u = 320$ .

The HVB-NoB algorithm (without block-wise update) described in Algorithm 1 and the HMC algorithm (implemented via RSTAN) are used to estimate the YJ-SEM-Gau model. The tuning parameter,  $N_1$  of the HVB-NoB algorithm, is set to 10. The initial values for the algorithm are set as follows: the variational mean vector ( $\boldsymbol{\mu}$ ) is initialised using the estimates of  $\boldsymbol{\beta}$ ,  $\sigma_e^2$ , and  $\rho$  obtained by fitting the SEM-Gau model via MLE method. The initial value of the transformation parameter  $\gamma$  is set to 1. All fixed-effect parameters of the missing value model ( $\boldsymbol{\psi}$ ) are initialised to 0.1. For the variational covariance matrix, all elements of  $\mathbf{B}$  and the diagonal elements of  $\mathbf{D}$  are initialised to 0.01. We use  $p = 4$  factors, as increasing the number of factors did not lead to improved results. Similar initial values are used for the HMC algorithm. Both the HVB-NoB and HMC algorithms are run for 10,000 iterations. Convergence diagnostics plots are provided in Section S9.1 of the online supplement.

Now, we briefly explain how the posterior sample of model parameters,  $\boldsymbol{\xi}$ ,  $\boldsymbol{\psi}$ , and missing values  $\mathbf{y}_u$  are generated in the HVB-NoB method. Once the algorithm converges, the set of variational parameters,  $\boldsymbol{\lambda}_{s_m} = (\boldsymbol{\mu}_{s_m}^\top, \text{vech}(\mathbf{B}_{s_m})^\top, \mathbf{d}_{s_m}^\top)^\top$ , is obtained. Given these variational parameters, 10,000 draws from the variational distribution,  $q_\lambda^0(\boldsymbol{\xi}, \boldsymbol{\psi}) \sim N((\boldsymbol{\xi}^\top, \boldsymbol{\psi}^\top)^\top; \boldsymbol{\mu}_{s_m}, \mathbf{B}_{s_m} \mathbf{B}_{s_m}^\top + \mathbf{D}_{s_m}^2)$ , are generated, which form the posterior sample of  $\boldsymbol{\xi}$  and  $\boldsymbol{\psi}$ . Based on this posterior sample of model parameters, the posterior sample of  $\mathbf{y}_u^{(i)}$  is generated from the conditional distribution  $p(\mathbf{y}_u \mid \mathbf{y}_o, \mathbf{m}, \boldsymbol{\xi}^{(i)}, \boldsymbol{\psi}^{(i)})$ , where  $\boldsymbol{\xi}^{(i)}$  and  $\boldsymbol{\psi}^{(i)}$  are the  $i^{th}$  posterior sample for  $i = 1, \dots, 10,000$ .

Figure 2 compares the posterior densities of selected model parameters estimated using HVB-NoB and HMC for fitting the YJ-SEM-Gau model on the simulated dataset

with missing data. For most model parameters, the posterior densities obtained from both methods are nearly identical. However, the posterior density of  $\gamma$  estimated using the HVB-NoB method is slightly overestimated compared to that of the HMC method.

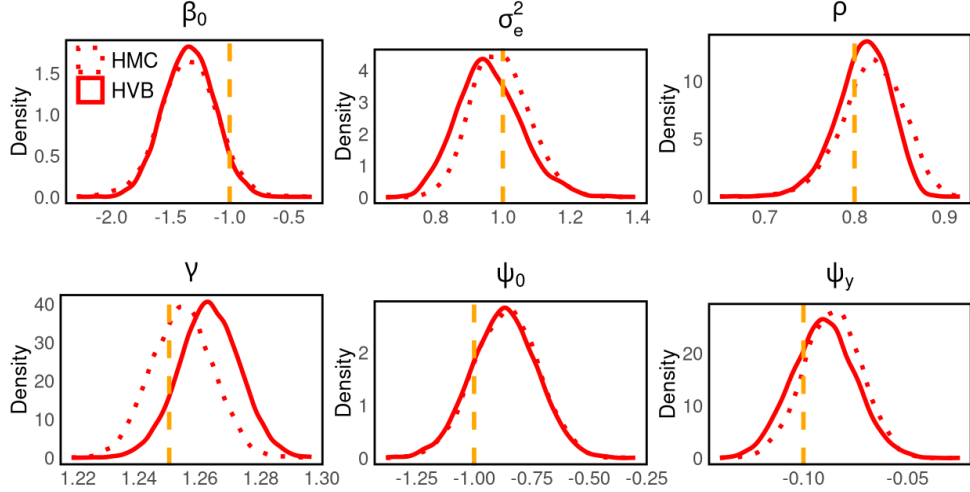


Figure 2: Comparison of posterior densities of selected parameters in the YJ-SEM-Gau model, obtained using the HMC and HVB-NoB methods on the simulated dataset with missing values. The vertical line represents the true parameter value.

Notably, the computation time per iteration of the VB and HVB-NoB algorithms is significantly lower than that of the HMC algorithm. The computation time per iteration for the VB algorithm is approximately 0.0361, while for the HMC algorithm, it is 0.4680 when estimating the YJ-SEM-Gau model without missing data. Similarly, the computation time per iteration for the HVB-NoB algorithm is approximately 0.0542 seconds, while for the HMC algorithm, it is 41.1658 seconds for estimating the YJ-SEM-Gau model with missing data. The high computational cost of the HMC algorithm in estimating SEMs (such as SEM-Gau) with missing data is also highlighted in the findings of Wijayawardhana et al. (2025).

## 4.2 Evaluating the performance of proposed SEMs

This section focuses on evaluating the robustness of the proposed SEMs and the VB methods using moderately large simulated datasets. We use a spatial weight matrix from the *spData* R package (Bivand et al., 2023), based on 25,357 houses sold between 1993 and 1998 in Lucas County, Ohio, USA. Further details on this dataset are provided in

Section 5.

We simulate two datasets from the YJ-SEM-t model using the spatial weight matrix  $\mathbf{W}_{1998}$ , which corresponds to 4,378 houses sold in 1998 in Lucas County, Ohio, USA. In the first dataset, we set the parameters  $\gamma = 0.5$  (right skew) and  $\nu = 4$  (heavy tails). In the second dataset, we set the parameters  $\gamma = 1$  (no skew) and  $\nu = 30$  (light tails). The other parameters are set as follows: 6 fixed effects ( $\beta$ ) are randomly drawn from the discrete uniform values between -3 and 3 (excluding 0),  $\sigma_e^2 = 0.5$ ,  $\rho = 0.8$ , and all covariates are generated from a standard normal distribution,  $N(0, 1)$ . Figure 3 shows kernel density plots of the response variables for both datasets.

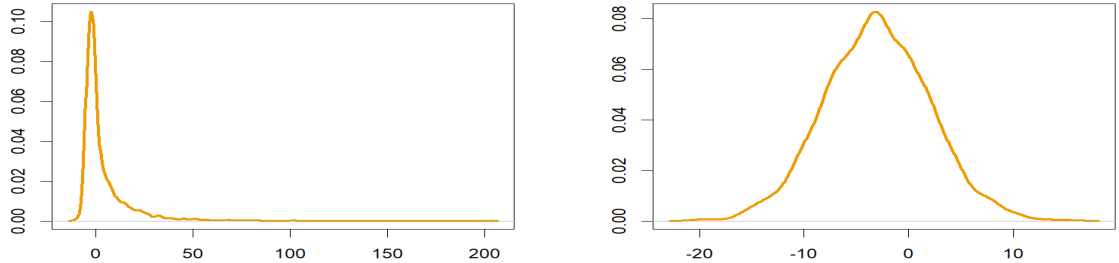


Figure 3: Kernel density plots of the simulated data: The left panel shows the kernel density of the response variable from YJ-SEM-t with  $\nu = 4$  and  $\gamma = 0.5$ , displaying right skewness and heavy tails (referred to as dataset 1). The right panel shows the kernel density of the response variable from YJ-SEM-t with  $\nu = 30$  and  $\gamma = 1$ , which appears nearly symmetric with light tails (referred to as dataset 2).

Section S6 of the online supplement fits the SEM-Gau, SEM-t, YJ-SEM-Gau, and YJ-SEM-t models to simulated datasets 1 and 2 without missing data, and evaluates how effectively these models, along with their VB estimation methods, capture the characteristics of these datasets. Section 4.2.1 introduces missing values into both datasets and evaluates the performance of the models and estimation method (the HVB method) in the presence of missing values.

#### 4.2.1 SEMs with missing data

This section evaluates the accuracy of the HVB method for estimating the SEMs with missing values in the response variable using simulated data. For each simulated dataset,

missing values in the response variable  $\mathbf{y}$  are introduced according to the MNAR mechanism using a logistic regression model defined in Section 2.3. To construct this model, an additional covariate  $\mathbf{x}^*$  is generated from a log-normal distribution with a log-scale mean of 0 and a log-scale standard deviation of 1, and the model is regressed on  $\mathbf{x}^*$  and the response variable  $\mathbf{y}$ . We set  $\psi_0 = 1$  (intercept),  $\psi_{\mathbf{x}^*} = -1$  (the coefficient for  $\mathbf{x}^*$ ), and  $\psi_{\mathbf{y}} = -0.1$  (the coefficient for  $\mathbf{y}$ ). This configuration results in approximately 40% missing values, leading to  $n_u = 1,752$ .

We fit SEM-Gau, SEM-t, YJ-SEM-Gau, and YJ-SEM-t models for the simulated datasets with missing values. As  $n$  and  $n_u$  are large, the HVB-AllB algorithm (Algorithm S2) described in Section S4.2 of the online supplement is used. The tuning parameters for the HVB-AllB algorithm is set as follows: the number of MCMC iterations ( $N_1$ ) is set to 10, and the block size ( $k^*$ ) is defined as 10% of  $n_u$ , resulting in 10 or 11 blocks.

The initial values for the variational parameters corresponding to  $\boldsymbol{\beta}$ ,  $\sigma_e^2$ ,  $\rho$ , and  $\gamma$  are set as described in Section 4.1, while  $\nu$  is initialised with a value of 4. The initial values for the missing data ( $\mathbf{y}_u$ ) are simulated from the conditional distribution  $p(\mathbf{y}_u \mid \boldsymbol{\xi}^{(0)}, \mathbf{y}_o)$ , where  $\boldsymbol{\xi}^{(0)}$  represents the vector of initial parameter values  $\boldsymbol{\xi}$ .

We ran the HVB-AllB algorithm for 10,000 iterations for the SEM-Gau and YJ-SEM-Gau models across both simulated datasets. For the SEM-t and YJ-SEM-t models, more iterations were required to achieve convergence due to the additional complexity introduced by estimating the latent variables  $\boldsymbol{\tau}$  and the degrees of freedom parameter  $\nu$ . Specifically, for simulated dataset 1, SEM-t was run for 20,000 iterations and YJ-SEM-t for 10,000 iterations. For simulated dataset 2, SEM-t required 30,000 iterations, while YJ-SEM-t was run for 20,000 iterations.

Table 4 presents the posterior means and 95% credible intervals for some of the model parameters of the SEM-Gau, YJ-SEM-Gau, SEM-t, and YJ-SEM-t models obtained using the HVB-AllB method applied to the simulated dataset 1 with missing values, along with the computational cost for one VB iteration. The table also includes the  $DIC_5$  values for each model, calculated using the formula in Equation (20). Corresponding posterior density plots of the parameters are given in Section S7.2.2 of the online supplement.

We start by comparing the estimated values of the fixed effects (specifically  $\beta_0$  and  $\beta_1$  for the SEM and  $\psi_0$  and  $\psi_1$  for the missing data model), the variance parameter  $\sigma_e^2$ , and the spatial autocorrelation parameter  $\rho$ , as these parameters are common to all four models. The posterior means for  $\beta_0$ ,  $\beta_1$ ,  $\psi_0$ ,  $\psi_1$ , and  $\rho$  are nearly identical for both YJ-SEM-Gau and YJ-SEM-t, closely matching the true values. In contrast, the estimates from SEM-Gau and SEM-t show significant deviations from the true values. The estimated posterior means of  $\sigma_e^2$  from SEM-Gau, SEM-t, and YJ-SEM-Gau differ considerably from the true value, while the posterior mean from YJ-SEM-t is much closer to the true value. The models incorporating the YJ transformation (YJ-SEM-Gau and YJ-SEM-t) successfully recover the parameter  $\gamma$ . The estimates of  $\nu$  obtained from the SEM-t and YJ-SEM-t models are slightly inaccurate. Furthermore, the posterior means of the estimated missing values from YJ-SEM-t and YJ-SEM-Gau align more closely with the true missing values compared to those from SEM-Gau and SEM-t; see Figure S7 in Section S7.2.2 of the online supplement.

For the simulated dataset 1 with missing values in the response variable, the YJ-SEM-t model provides the best fit, as indicated by the lowest  $DIC_5$  value, among all four models. This result is expected, as the dataset was generated from the YJ-SEM-t model, which incorporates both heavy tails and skewness. The second-best performer is YJ-SEM-Gau, which has the next lowest DIC value. Furthermore, similar to the case without missing values discussed in Section S6 of the online supplement, the relatively small difference in the  $DIC_5$  values between YJ-SEM-t and YJ-SEM-Gau suggests that YJ-SEM-Gau achieves a model fit nearly comparable to that of YJ-SEM-t for this dataset.

The left panel of Figure 4 shows the kernel densities of the true missing values ( $\mathbf{y}_u$ ) and the kernel density of posterior means of the missing values at locations  $s_1, s_2, \dots, s_n$ , estimated from different SEMs for the simulated dataset 1. The densities from both YJ-SEM-Gau and YJ-SEM-t are nearly identical and closely align with the density of the true missing values.

The right panel of Figure 4 presents the posterior density of the maximum missing value ( $\mathbf{y}_{u_{\max}}$ ) predicted by each SEM. The true value of the maximum missing value lies

closer to the posterior densities produced by YJ-SEM-Gau and YJ-SEM-t than to those from SEM-Gau and SEM-t. These outcomes are as expected, since YJ-SEM-Gau and YJ-SEM-t yield similar parameter estimates and DIC values (see Table 4). Figure S8 in Section S7.2.2 of the online supplement provides similar density plots for the simulated dataset 2.

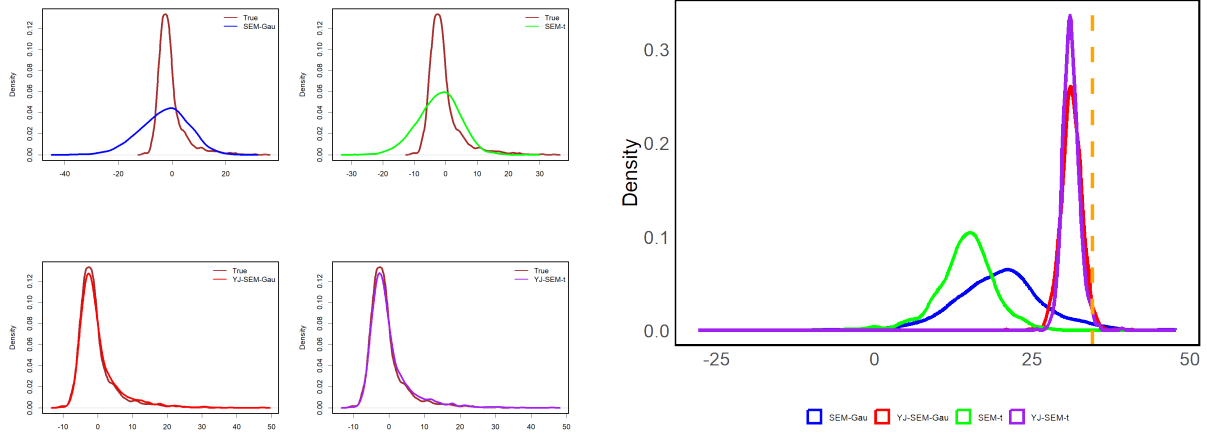


Figure 4: Left panel: The kernel density of the true missing values ( $y_u$ ) and the kernel density of posterior means of the missing values ( $y_u$ ) obtained using the HVB-AllB method for different SEMs for the simulated dataset 1 with missing values. Right panel: The posterior density of the maximum missing value ( $y_{u_{\max}}$ ) obtained by different SEMs for the simulated dataset 1 with missing values. The true value of the maximum missing value is indicated by the vertical line.

Table 5 reports the posterior means and 95% credible intervals for key parameters of the SEM-Gau, SEM-t, YJ-SEM-Gau, and YJ-SEM-t models, obtained using the HVB-AllB method on the simulated dataset 2 with missing values, along with the computational cost for one VB iteration. The table also presents the corresponding  $DIC_5$  values for each model. Posterior density plots for these parameters are provided in Section S7.2.2 of the online supplement. The estimated posterior means for  $\beta_0$ ,  $\beta_1$ ,  $\psi_0$ , and  $\sigma_e^2$  across all four models closely match their true values. Similarly, the estimated posterior mean of  $\gamma$  for the YJ-SEM-Gau and YJ-SEM-t models is also close to the true value. The parameter  $\nu$  is accurately estimated in both the SEM-t and YJ-SEM-t models. In addition, all four models produce posterior means for the estimated missing values that closely match the true values; see Figure S8 in Section S7.2.2 of the online supplement.

Based on the  $DIC_5$  values, the YJ-SEM-t model offers the best fit for the simulated

|                    | SEM-Gau                       | SEM-t                         | YJ-SEM-Gau                    | YJ-SEM-t                      |
|--------------------|-------------------------------|-------------------------------|-------------------------------|-------------------------------|
| $\beta_0 = -1$     | 1.9268<br>(1.6342, 2.2270)    | 1.2929<br>(1.1456, 1.4382)    | -0.9862<br>(-1.0256, -0.9462) | -0.9680<br>(-1.0238, -0.9123) |
| $\beta_1 = 1$      | 1.8848<br>(1.6344, 2.1381)    | 1.3230<br>(1.1675, 1.4797)    | 0.9938<br>(0.9554, 1.0332)    | 0.9835<br>(0.9338, 1.0324)    |
| $\sigma_e^2 = 0.5$ | 77.4912<br>(74.2316, 80.7856) | 24.4549<br>(23.2015, 25.7503) | 0.9994<br>(0.9331, 1.0701)    | 0.7028<br>(0.6615, 0.7451)    |
| $\rho = 0.8$       | 0.2839<br>(0.2527, 0.3144)    | 0.1948<br>(0.1722, 0.2177)    | 0.8007<br>(0.7858, 0.8149)    | 0.8044<br>(0.7922, 0.8159)    |
| $\nu = 4$          | NA                            | 3.3400<br>(3.2319, 3.4772)    | NA                            | 9.5082<br>(9.0327, 10.0109)   |
| $\gamma = 0.5$     | NA                            | NA                            | 0.4965<br>(0.4822, 0.5113)    | 0.4990<br>(0.4882, 0.5099)    |
| $\psi_0 = 1$       | 0.8251<br>(0.7048, 0.9441)    | 0.9171<br>(0.8126, 1.0203)    | 0.9337<br>(0.8193, 1.0442)    | 0.9515<br>(0.8525, 1.0522)    |
| $\psi_y = -0.1$    | -0.0793<br>(-0.0907, -0.0679) | -0.0997<br>(-0.1178, -0.0812) | -0.0794<br>(-0.0924, -0.0663) | -0.0790<br>(-0.0891, -0.0686) |
| DIC <sub>5</sub>   | 36009.5                       | 36302.7                       | 18278.55                      | 17855.59                      |
| CT                 | 0.5894                        | 1.2250                        | 0.6000                        | 1.339                         |

Table 4: Posterior means and 95% credible intervals for selected parameters of different SEMs based on the simulated dataset 1 with missing data, along with the computation time (CT) in seconds for one HVB iteration. The table also presents the DIC<sub>5</sub> values for each model. Parameters labeled as 'NA' indicate that they are not applicable to the corresponding model.

dataset 2 with missing values. In contrast, for the simulated dataset 2 without missing values, the SEM-Gau model provides the best fit; see Section S6 of the online supplement. For the simulated dataset 2 with missing data, the SEM-t model has the second-lowest DIC<sub>5</sub>, indicating it is the second-best performing model.

As shown in Tables 4 and 5, the HVB-AllB algorithms for SEM-t and YJ-SEM-t, which incorporate Student's *t* errors, require significantly more computation time than those for SEM-Gau and YJ-SEM-Gau. This increased computational cost arises from the greater complexity of VB (HVB-AllB) optimisation in models with *t* errors. Specifically, these models introduce an additional length *n* latent variable vector and include the degrees of freedom parameter  $\nu$ , both of which increase the dimensionality and complexity of the VB optimisation.

Our simulations demonstrate that the standard Gaussian VB method for full data and the hybrid VB (HVB-NoB and HVB-AllB) methods for missing data offer accurate yet

|                    | SEM-Gau                       | SEM-t                         | YJ-SEM-Gau                    | YJ-SEM-t                      |
|--------------------|-------------------------------|-------------------------------|-------------------------------|-------------------------------|
| $\beta_0 = -3$     | -3.0131<br>(-3.0495, -2.9764) | -3.0150<br>(-3.0497, -2.9792) | -2.9511<br>(-2.9820, -2.9199) | -2.9467<br>(-2.9767, -2.9161) |
| $\beta_1 = 2$      | 1.9942<br>(1.9582, 2.0309)    | 1.9884<br>(1.9605, 2.0165)    | 1.9803<br>(1.9621, 1.9979)    | 1.9834<br>(1.9568, 2.0096)    |
| $\sigma_e^2 = 0.5$ | 0.5528<br>(0.5222, 0.5849)    | 0.5143<br>(0.4892, 0.5406)    | 0.5450<br>(0.5155, 0.5759)    | 0.5096<br>(0.4826, 0.5377 )   |
| $\rho = 0.8$       | 0.8002<br>(0.7857, 0.8141)    | 0.7990<br>(0.7874, 0.8101)    | 0.8003<br>(0.7892, 0.8113)    | 0.7971<br>(0.7841, 0.8095)    |
| $\nu = 30$         | NA                            | 30.2880<br>(29.1096, 31.4718) | NA                            | 29.7195<br>(27.9820, 31.6032) |
| $\gamma = 1$       | NA                            | NA                            | 1.0032<br>(0.9933, 1.0129)    | 1.0017<br>(0.9961, 1.0074)    |
| $\psi_0 = 0.5$     | 0.4949<br>(0.3847, 0.6044)    | 0.5036<br>(0.4219, 0.5841)    | 0.5477<br>(0.4319, 0.6619)    | 0.5467<br>(0.4742, 0.6204)    |
| $\psi_y = -0.1$    | -0.0956<br>(-0.1210, -0.0706) | -0.1090<br>(-0.1320, -0.0864) | -0.0965<br>(-0.1106, -0.0827) | -0.0972<br>(-0.1137, -0.0809) |
| DIC <sub>5</sub>   | 14713.89                      | 14221.78                      | 14695.32                      | 14164.86                      |
| CT                 | 0.5755                        | 1.2166                        | 0.6048                        | 1.3486                        |

Table 5: Posterior means and 95% credible intervals for selected parameters of different SEMs based on the simulated dataset 2 with missing data, along with the computation time (CT) in seconds for one HVB iteration. The table also presents the DIC<sub>5</sub> values for each model. Parameters labeled as 'NA' indicate that they are not applicable to the corresponding model.

computationally efficient approximations for estimating both Gaussian and non-Gaussian SEMs, outperforming HMC in terms of computational cost. The YJ-SEM-Gau and YJ-SEM-t models are particularly effective for modeling data with pronounced skewness and heavy tails. In most scenarios, the DIC values show that YJ-SEM-Gau performs nearly as well as YJ-SEM-t. Although estimating YJ-SEM-t incurs significantly higher computational cost compared to SEM-Gau (the standard SEM with Gaussian errors), YJ-SEM-Gau has a similar computational cost to SEM-Gau while offering substantial improvements in modeling non-Gaussian data.

## 5 Real data application

We apply the proposed SEMs and VB methods to analyse a dataset of 25,357 single-family homes sold between 1993 and 1998, along with a spatial weight matrix of size 25,357  $\times$  25,357 from Lucas County, Ohio, USA. This dataset is available in the R package

spData (Bivand et al., 2023). The data set includes various house characteristics: house age, the lot size in square feet, the number of rooms, the total living area in square feet, the number of bedrooms, and binary indicators for each year from 1993 to 1998 to represent the year of house sale. For our analysis, we focus on the house price data from 1998, which contains 4,378 observations. We call this dataset Lucas-1998-HP. House prices are typically positive and often exhibit skewness. To transform house prices into the entire real line and reduce skewness, researchers commonly apply logarithmic transformations before modeling (LeSage and Pace, 2004; Wijayawardhana et al., 2024). Accordingly, we apply the natural logarithmic transformation to the house prices in the Lucas-1998-HP dataset. Despite this transformation, the resulting variable still exhibits left skewness (see Figure S9 in Section S8 of the online supplement).

To evaluate the impact of missing data on Gaussian and non-Gaussian SEMs, we use the Lucas-1998-HP dataset, a complete real-world dataset. We first fit the SEMs to the full dataset using the VB algorithm. Then, we intentionally introduce missing values into the response variable and refit the SEMs using the proposed HVB-AllB method. This setup allows for a direct comparison of parameter estimates obtained with and without missing data.

For the Lucas-1998-HP dataset, we fit all four models described in Section 2. The set of independent variables includes various powers of house age (age,  $age^2$ , and  $age^3$ ), the natural logarithm of the lot size in square feet ( $\ln(lotsize)$ ), the number of rooms (rooms), the natural logarithm of the total living area in square feet ( $\ln(LTA)$ ), and the number of bedrooms. The natural logarithm of house price in hundreds of thousands is selected as the dependent variable. Results for the complete dataset (without missing values) are presented in Section 5.1, while Section 5.2 summarises the findings with missing data.

## 5.1 Full Data SEMs

This section presents the results of analysing the Lucas-1998-HP dataset by fitting all four SEMs introduced in Section 2, using the VB algorithms outlined in Section S2 of the online supplement. The starting values for the VB algorithms are obtained as follows:

The variational mean vector ( $\boldsymbol{\mu}$ ) is set to the estimates for  $\boldsymbol{\beta}$ ,  $\sigma_e^2$ , and  $\rho$  obtained from fitting the SEM-Gau model via maximum likelihood estimation (MLE). The initial value for  $\nu$  is set to 4, and the initial value for  $\gamma$  is set to 1. For the variational covariance matrix parameters, the elements of  $\mathbf{B}$  and the diagonal elements of  $\mathbf{D}$  are all initialised to 0.01. We use  $p = 4$  factors.

As in the simulation study with full data described in Section S6 of the online supplement, models with Student- $t$  errors required more iterations to achieve convergence. The VB algorithms were run for 20,000 iterations for the SEM-Gau and YJ-SEM-Gau models and 75,000 iterations for the SEM-t and YJ-SEM-t models, at which point convergence was attained. Convergence was assessed visually by examining the plots of variational means over iterations, which are provided in Section S9.2 of the online supplement.

The estimated posterior means and 95% credible intervals for selected model parameters across different models are summarised in Table 6, along with the corresponding DIC values. According to the  $DIC_1$  and  $DIC_2$  values, the YJ-SEM-t model is the most appropriate SEM for the Lucas-1998-HP dataset, followed by the YJ-SEM-Gau model as the second most suitable.

We now compare estimates of key parameters across different SEMs. A crucial aspect of SEM estimation is identifying the underlying spatial correlation, represented by the parameter  $\rho$ . For the SEM-Gau, YJ-SEM-Gau, and YJ-SEM-t models, the estimated values of  $\rho$  are relatively close, with posterior mean values of 0.6291, 0.6019, and 0.5990, respectively. This suggests a moderate spatial correlation in the Lucas-1998-HP dataset. However, for the SEM-t model, the estimated  $\rho$  is noticeably lower, with a posterior mean value of 0.5475, compared to the other three models.

Similar to linear regression models, the fixed effects  $\boldsymbol{\beta}$  in SEMs represent the influence of covariates on the response variable, which in this case is the logarithm of the house price. An interesting disparity arises in the estimated posterior mean of the fixed effect corresponding to the covariate 'age' ( $\beta_{age}$ ). For the SEM-Gau model,  $\beta_{age}$  is positive, while for the other three models,  $\beta_{age}$  is negative. This suggests that for the SEM-Gau model, the age of the house is associated with an increase in house prices, while for the other

|                        | SEM-Gau                       | SEM-t                         | YJ-SEM-Gau                    | YJ-SEM-t                      |
|------------------------|-------------------------------|-------------------------------|-------------------------------|-------------------------------|
| $intercept$            | -0.4336<br>(-0.4469, -0.4207) | -0.3865<br>(-0.3979, -0.3752) | -0.3020<br>(-0.3278, -0.2765) | -0.2849<br>(-0.3087, -0.2612) |
| $\beta_{age}$          | 0.1650<br>(0.0557, 0.2742)    | -0.4197<br>(-0.5236, -0.3162) | -0.1643<br>(-0.2926, -0.0321) | -0.3201<br>(-0.3984, -0.2405) |
| $\beta_{rooms}$        | 0.0068<br>(-0.0176, 0.0313)   | 0.0188<br>(-0.0018, 0.0395)   | 0.0311<br>(-0.0281, 0.0893)   | 0.0238<br>(-0.0056, 0.0524)   |
| $\beta_{log(lotsize)}$ | 0.1614<br>(0.1480, 0.1752)    | 0.1193<br>(0.1033, 0.1350)    | 0.1441<br>(0.1068, 0.1815)    | 0.1306<br>(0.1192, 0.1420)    |
| $\sigma_e^2$           | 0.1577<br>(0.1516, 0.1641)    | 0.0670<br>(0.0633, 0.0708)    | 0.1031<br>(0.0967, 0.1099)    | 0.0695<br>(0.0647, 0.0744)    |
| $\rho$                 | 0.6291<br>(0.5605, 0.6902)    | 0.5475<br>(0.4900, 0.6015)    | 0.6019<br>(0.5236, 0.6712)    | 0.5990<br>(0.5261, 0.6651)    |
| $\nu$                  | NA                            | 3.0249<br>(3.0000, 3.1324)    | NA                            | 7.9482<br>(7.5327, 8.3940)    |
| $\gamma$               | NA                            | NA                            | 1.5264<br>(1.4783, 1.5728)    | 1.5529<br>(1.5145, 1.5904)    |
| DIC <sub>1</sub>       | 4470.316                      | 4878.664                      | 4329.431                      | 3720.687                      |
| DIC <sub>2</sub>       | 4469.655                      | 5031.204                      | 4332.07                       | 3766.714                      |

Table 6: Posterior means and 95% credible intervals for selected parameters of different SEMs for the Lucas-1998-HP dataset (no missing values). The table also includes DIC values for each model. Parameters labeled as 'NA' indicate that they are not applicable to the corresponding model.

models, the age of the house is linked to a decrease in house prices. The estimated posterior means of the fixed effect for the number of rooms ( $\beta_{rooms}$ ) are 0.0068, 0.0188, 0.0311, and 0.0238 for the SEM-Gau, SEM-t, YJ-SEM-Gau, and YJ-SEM-t models, respectively. These estimates suggest that the effect of the number of rooms on house prices varies across models. Notably, the YJ-SEM-Gau model shows the strongest positive influence, while the SEM-Gau model exhibits the weakest.

Additionally, the SEM-t, YJ-SEM-Gau, and YJ-SEM-t models provide further insights into the characteristics of the dataset. The posterior mean of  $\nu = 3.0249$  for SEM-t and  $\nu = 7.9482$  for YJ-SEM-t suggest that the log-transformed house price distribution exhibits heavy tails. Furthermore, the posterior means of  $\gamma$ , 1.5264 for YJ-SEM-Gau and 1.5529 for YJ-SEM-t, suggest left skewness in the response variable, effectively capturing the asymmetry in the distribution of log-transformed house prices. These distributional features are visually evident in the kernel density plot of the response variable (see Figure S9 in Section S8 of the online supplement).

## 5.2 SEMs with missing data

This section discusses the analysis of the Lucas-1998-HP dataset with missing data in the response variable. We use the age of the house and the response variable of SEMs (logarithm of the house price) as the covariates in the missing data model. The missing data model has three parameters,  $\psi = (\psi_0, \psi_{\mathbf{x}^*}, \psi_{\mathbf{y}})$ . We set the values  $\psi_0 = 0.1$ ,  $\psi_{\mathbf{x}^*} = 0.1$ , and  $\psi_{\mathbf{y}} = -0.1$ . With these settings, approximately 50% of the responses are missing, resulting in  $n_u = 2,348$ .

Since both  $n$  and  $n_u$  are large, we utilise the HVB-AllB algorithm. We set the number of MCMC iterations  $N_1$  to 10 and the block size to 10% of  $n_u$ , resulting in 11 blocks. The starting values for the HVB-AllB algorithms are obtained as follows: the variational mean vector ( $\boldsymbol{\mu}$ ) is set to the estimates of  $\boldsymbol{\beta}$ ,  $\sigma_e^2$ , and  $\rho$  obtained from fitting the SEM-Gau model with only the observed data,  $\mathbf{y}_o$ , using MLE. The initial value for  $\nu$  is set to 4, and the initial value for  $\gamma$  is set to 1. For the parameters of the missing data generating model ( $\psi_0$ ,  $\psi_{\mathbf{x}^*}$ , and  $\psi_{\mathbf{y}}$ ), all coefficients are set to an initial value of 0.01. For the variational covariance matrix parameters, the elements of  $\mathbf{B}$  and the diagonal elements of  $\mathbf{D}$  are all initialised to 0.01. The initial values for the missing data ( $\mathbf{y}_u$ ) are simulated from the conditional distribution  $p(\mathbf{y}_u \mid \boldsymbol{\xi}^{(0)}, \mathbf{y}_o)$ , where  $\boldsymbol{\xi}^{(0)}$  represents the vector of initial parameter values for  $\boldsymbol{\xi}$ . We use  $p = 4$  factors.

Similar to the simulation study with missing data, models with Student's  $t$  errors required a relatively large number of iterations to converge. Therefore, we ran the HVB-AllB algorithm for 10,000 iterations for the SEM-Gau and YJ-SEM-Gau models, 40,000 iterations for the SEM-t model, and 20,000 iterations for the YJ-SEM-t model. Convergence plots can be found in Section S9.2 of the online supplement.

The estimated posterior means and 95% credible intervals for selected model parameters across different models are summarised in Table 7, along with the corresponding  $DIC_5$  values. According to the  $DIC_5$  values, the YJ-SEM-t model is the most appropriate SEM for the Lucas-1998-HP dataset with missing data, followed by the YJ-SEM-Gau model as the second best model.

The estimated parameters from different SEMs are now briefly discussed. For the

|                        | SEM-Gau                       | SEM-t                         | YJ-SEM-Gau                    | YJ-SEM-t                      |
|------------------------|-------------------------------|-------------------------------|-------------------------------|-------------------------------|
| $intercept$            | -0.4189<br>(-0.4413, -0.3960) | -0.3721<br>(-0.3886, -0.3562) | -0.2856<br>(-0.3008, -0.2703) | -0.2752<br>(-0.2956, -0.2544) |
| $\beta_{age}$          | 0.1935<br>(0.0335, 0.3510)    | -0.4640<br>(-0.5990, -0.3324) | -0.1473<br>(-0.2598, -0.0345) | -0.3768<br>(-0.4870, -0.2687) |
| $\beta_{rooms}$        | 0.0010<br>(-0.0409, 0.0432)   | 0.0179<br>(-0.0132, 0.0491)   | 0.0341<br>(0.0021, 0.0655)    | 0.0438<br>(0.0053, 0.0816)    |
| $\beta_{log(lotsize)}$ | 0.1360<br>(0.1097, 0.1620)    | 0.1124<br>(0.0952, 0.1293)    | 0.1173<br>(0.1020, 0.1323)    | 0.1219<br>(0.0786, 0.1651)    |
| $\sigma_e^2$           | 0.1463<br>(0.1378, 0.1553)    | 0.0696<br>(0.0649, 0.0746)    | 0.0894<br>(0.0847, 0.0943)    | 0.0657<br>(0.0617, 0.0699)    |
| $\rho$                 | 0.5872<br>(0.4810, 0.6818)    | 0.5686<br>(0.4553, 0.6695)    | 0.5494<br>(0.4337, 0.6502)    | 0.5377<br>(0.4325, 0.6322)    |
| $\nu$                  | NA                            | 4.1165<br>(3.9476, 4.3046)    | NA                            | 10.6394<br>(10.2060, 11.1003) |
| $\gamma$               | NA                            | NA                            | 1.5814<br>(1.5297, 1.6299)    | 1.5998<br>(1.5552, 1.6415)    |
| $\psi_0 = 0.1$         | 0.1128<br>(0.0193, 0.2064)    | 0.2075<br>(0.1361, 0.2806)    | 0.1110<br>(0.0349, 0.1865)    | 0.1317<br>(0.0595, 0.2033)    |
| DIC <sub>5</sub>       | 8074.382                      | 7734.356                      | 7309.394                      | 6657.172                      |

Table 7: Posterior means and 95% credible intervals for selected parameters of different SEMs for the Lucas-1998-HP dataset with missing data. The table also includes DIC<sub>5</sub> values for each model. Parameters labeled as 'NA' indicate that they are not applicable to the corresponding model.

spatial autocorrelation parameter,  $\rho$ , the posterior mean estimates across all SEMs are slightly lower than those obtained without missing values, shown in Table 6. However, these estimates still indicate a moderate spatial correlation in the Lucas-1998-HP dataset, consistent with the conclusions drawn from SEMs fitted without missing values in Section 5.1.

The posterior mean estimates for the fixed effects ( $\beta$ ) in the SEMs lead to the same conclusions as those drawn from the Lucas-1998-HP dataset without missing values. For example, the posterior mean estimate of  $\beta_{age}$  in the SEM-Gau model suggests a positive effect of age on house prices, whereas the estimates from the other three models indicate a negative effect. Moreover, the estimated intercepts in the missing data model,  $\psi_0$ , are close to the true value of 0.1 for all models except SEM-t.

The posterior mean estimates of  $\nu$  for the SEM-t and YJ-SEM-t models indicate moderate to strong heavy-tailed behavior. Meanwhile, the estimated  $\gamma$  values for the YJ-

SEM-Gau and YJ-SEM-t models suggest left skewness in the data. These conclusions are consistent with the findings from the analysis without missing data discussed in Section 5.1.

## 6 Conclusion

Our article introduces three novel simultaneous autoregressive (SAR) models for non-Gaussian spatial data. Specifically, we extend the conventional spatial error model (SEM-Gau), a widely used SAR model, to accommodate skewed and heavy tailed features of real datasets. The novel SEMs are SEM-t, YJ-SEM-Gau, and YJ-SEM-t. The SEM-t assumes that the error terms follow a Student's t distribution, allowing heavier tails than a Gaussian distribution. The YJ-SEM-Gau retains Gaussian errors but applies the Yeo-Johnson (YJ) transformation to handle asymmetric response variables. The YJ-SEM-t combines these approaches by assuming Student's t errors while incorporating the YJ transformation to account for skewness in the response variable. These extensions improve the robustness of SAR models in analysing complex spatial datasets. Additionally, we develop efficient variational Bayes (VB) methods to estimate these models with and without missing data. For cases with missing data, our approach assumes a missing not at random (MNAR) mechanism. Standard VB methods are inadequate for accurately estimating these SEMs in the presence of missing data; therefore, we employ hybrid VB (HVB) algorithms to address this challenge. The posterior distributions obtained from the proposed VB and HVB approximation methods are compared with those of the exact Hamiltonian Monte Carlo (HMC) method.

The empirical results show that: (1) The VB and HVB methods yield posterior density estimates for most model parameters that are similar to those obtained using the HMC method when estimating SEMs with and without missing values; (2) For models with Student's  $t$  errors (SEM-t and YJ-SEM-t), the posterior approximation of the degrees of freedom parameter ( $\nu$ ) from the VB and HVB methods exhibits slight deviations compared to the true value; (3) For both VB and HVB algorithms, models with Stu-

dent's t errors require more computation time per iteration than models with Gaussian errors (SEM-Gau and YJ-SEM-Gau); (4) In general, models with Gaussian errors tend to converge in fewer iterations compared to those with Student's t errors; (5) YJ-SEM-t is able to model complex response variable with skewness and heavy tails and is the best model for the Lucas-1998-HP dataset, both with and without missing data.

## References

Agosto, A., Giudici, P., and Leach, T. (2019). Spatial regression models to improve P2P credit risk management. *Frontiers in Artificial Intelligence*, 2:6.

Al-Momani, M., Hussein, A. A., and Ahmed, S. E. (2017). Penalty and related estimation strategies in the spatial error model. *Statistica Neerlandica*, 71(1):4–30.

Anselin, L. (1988). *Spatial Econometrics: Methods and Models*, volume 4. Springer Science & Business Media.

Bansal, P., Krueger, R., and Graham, D. J. (2021). Fast Bayesian estimation of spatial count data models. *Computational Statistics & Data Analysis*, 157:107152.

Benedetti, R., Suesse, T., and Piersimoni, F. (2020). Spatial auto-correlation and auto-regressive models estimation from sample survey data. *Biometrical Journal*, 62(6):1494–1507.

Besag, J. (1974). Spatial interaction and the statistical analysis of lattice systems. *Journal of the Royal Statistical Society. Series B (Methodological)*, 36(2):192–236.

Bivand, R., Nowosad, J., and Lovelace, R. (2023). *spData: Datasets for spatial analysis*. R package version 2.2.2.

Blei, D. M., Kucukelbir, A., and McAuliffe, J. D. (2017). Variational inference: A review for statisticians. *Journal of the American Statistical Association*, 112(518):859–877.

Breitung, J. and Wigger, C. (2018). Alternative GMM estimators for spatial regression models. *Spatial Economic Analysis*, 13(2):148–170.

Calabrese, R., Elkink, J. A., and Giudici, P. S. (2017). Measuring bank contagion in Europe using binary spatial regression models. *Journal of the Operational Research Society*, 68(12):1503–1511.

Celeux, G., Forbes, F., Robert, C. P., and Titterington, D. M. (2006). Deviance information criteria for missing data models. *Bayesian Analysis*, 1(4):651 – 673.

Chan, J., Koop, G., Poirier, D. J., and Tobias, J. L. (2019). *Bayesian Econometric Methods*. Econometric Exercises. Cambridge University Press, 2<sup>nd</sup> edition.

Chappell, M. A., Groves, A. R., Whitcher, B., and Woolrich, M. W. (2008). Variational Bayesian inference for a nonlinear forward model. *IEEE Transactions on Signal Processing*, 57(1):223–236.

Chi, G. and Zhu, J. (2008). Spatial regression models for demographic analysis. *Population Research and Policy Review*, 27:17–42.

Chi, G. and Zhu, J. (2019). *Spatial Regression Models for the Social Sciences*. SAGE publications.

Cressie, N. (1993). *Statistics for Spatial Data*. Wiley Series in Probability and Statistics. Wiley.

De Oliveira, V. and Song, J. J. (2008). Bayesian analysis of simultaneous autoregressive models. *Sankhyā: The Indian Journal of Statistics, Series B*, 70:323–350.

Doğan, O. and Taşpinar, S. (2018). Bayesian inference in spatial sample selection models. *Oxford Bulletin of Economics and Statistics*, 80(1):90–121.

Fernández, C. and Steel, M. F. (1999). Multivariate Student-t regression models: Pitfalls and inference. *Biometrika*, 86(1):153–167.

Flores-Lagunes, A. and Schnier, K. E. (2012). Estimation of sample selection models with spatial dependence. *Journal of Applied Econometrics*, 27(2):173–204.

Gunawan, D., Kohn, R., and Nott, D. (2021). Variational Bayes approximation of factor stochastic volatility models. *International Journal of Forecasting*, 37(4):1355–1375.

Gunawan, D., Kohn, R., and Nott, D. (2024). Flexible variational Bayes based on a copula of a mixture. *Journal of Computational and Graphical Statistics*, 33(2):665–680.

Han, S., Liao, X., and Carin, L. (2013). Integrated non-factorized variational inference. In *Advances in Neural Information Processing Systems*, volume 26. Curran Associates, Inc.

Han, S., Liao, X., Dunson, D., and Carin, L. (2016). Variational Gaussian copula inference. In Gretton, A. and Robert, C. C., editors, *Proceedings of the 19th International Conference on Artificial Intelligence and Statistics*, volume 51 of *Proceedings of Machine Learning Research*, pages 829–838, Cadiz, Spain. PMLR.

Huang, T., Saporta, G., Wang, H., and Wang, S. (2021). A robust spatial autoregressive scalar-on-function regression with t-distribution. *Advances in Data Analysis and Classification*, 15:57–81.

Kelejian, H. H. and Prucha, I. R. (1998). A generalized spatial two-stage least squares procedure for estimating a spatial autoregressive model with autoregressive disturbances. *The Journal of Real Estate Finance and Economics*, 17(1):99–121.

Kingma, D. P. and Welling, M. (2013). Auto-encoding variational Bayes. *arXiv preprint arXiv:1312.6114*.

Lange, K. L., Little, R. J. A., and Taylor, J. M. G. (1989). Robust statistical modeling using the t distribution. *Journal of the American Statistical Association*, 84(408):881–896.

Lee, L.-F. (2004). Asymptotic distributions of quasi-maximum likelihood estimators for spatial autoregressive models. *Econometrica*, 72(6):1899–1925.

Lee, L.-f. and Liu, X. (2010). Efficient GMM estimation of high order spatial autoregressive models with autoregressive disturbances. *Econometric Theory*, 26(1):187–230.

LeSage, J. and Pace, R. K. (2009). *Introduction to Spatial Econometrics*. Chapman and Hall/CRC.

LeSage, J. P. (1997). Bayesian estimation of spatial autoregressive models. *International Regional Science Review*, 20(1-2):113–129.

LeSage, J. P. and Pace, R. K. (2004). Models for spatially dependent missing data. *The Journal of Real Estate Finance and Economics*, 29(2):233–254.

Little, R. J. and Rubin, D. B. (2019). *Statistical Analysis with Missing Data*, volume 793. John Wiley & Sons.

Lloyd, C. (2010). *Spatial Data Analysis: An Introduction for GIS Users*. Knovel Library. OUP Oxford.

Neal, R. M. (1996). *Bayesian Learning for Neural Networks*, volume 118 of *Lecture Notes in Statistics*. Springer, New York, NY.

Neal, R. M. et al. (2011). MCMC using Hamiltonian dynamics. *Handbook of Markov chain Monte Carlo*, 2(11):2.

Nott, D. J., Tan, S. L., Villani, M., and Kohn, R. (2012). Regression density estimation with variational methods and stochastic approximation. *Journal of Computational and Graphical Statistics*, 21(3):797–820.

Ong, V. M.-H., Nott, D. J., and Smith, M. S. (2018). Gaussian variational approximation with a factor covariance structure. *Journal of Computational and Graphical Statistics*, 27(3):465–478.

Ord, K. (1975). Estimation methods for models of spatial interaction. *Journal of the American Statistical Association*, 70(349):120–126.

Ormerod, J. T. and Wand, M. P. (2010). Explaining variational approximations. *The American Statistician*, 64(2):140–153.

Pinheiro, J. C., Liu, C., and Wu, Y. N. (2001). Efficient algorithms for robust estimation in linear mixed-effects models using the multivariate t distribution. *Journal of Computational and Graphical Statistics*, 10(2):249–276.

Poyiadjis, G., Doucet, A., and Singh, S. S. (2011). Particle approximations of the score and observed information matrix in state space models with application to parameter estimation. *Biometrika*, 98(1):65–80.

Rabovič, R. and Čížek, P. (2023). Estimation of spatial sample selection models: A partial maximum likelihood approach. *Journal of Econometrics*, 232(1):214–243.

Rezende, D. J., Mohamed, S., and Wierstra, D. (2014). Stochastic backpropagation and approximate inference in deep generative models. In Xing, E. P. and Jebara, T., editors, *Proceedings of the 31st International Conference on Machine Learning*, volume 32 of *Proceedings of Machine Learning Research*, pages 1278–1286, Beijing, China. PMLR.

Robbins, H. and Monro, S. (1951). A stochastic approximation method. *The Annals of Mathematical Statistics*, 22(3):400 – 407.

Rubin, D. B. (1976). Inference and missing data. *Biometrika*, 63(3):581–592.

Seya, H., Tomari, M., and Uno, S. (2021). Parameter estimation in spatial econometric models with non-random missing data. *Applied Economics Letters*, 28(6):440–446.

Spiegelhalter, D. J., Best, N. G., Carlin, B. P., and Van Der Linde, A. (2002). Bayesian measures of model complexity and fit. *Journal of the Royal Statistical Society: Series B (statistical methodology)*, 64(4):583–639.

Stan Development Team (2023). RStan: The R interface to Stan. R package version 2.21.8.

Suesse, T. (2018). Marginal maximum likelihood estimation of SAR models with missing data. *Computational Statistics & Data Analysis*, 120:98–110.

Suesse, T. and Zammit-Mangion, A. (2017). Computational aspects of the EM algorithm for spatial econometric models with missing data. *Journal of Statistical Computation and Simulation*, 87(9):1767–1786.

Tan, L. S. and Nott, D. J. (2018). Gaussian variational approximation with sparse precision matrices. *Statistics and Computing*, 28:259–275.

Titsias, M. and Lázaro-Gredilla, M. (2015). Local expectation gradients for black box variational inference. In Cortes, C., Lawrence, N., Lee, D., Sugiyama, M., and Garnett, R., editors, *Advances in Neural Information Processing Systems*, volume 28. Curran Associates, Inc.

Titsias, M. and Lázaro-Gredilla, M. (2014). Doubly stochastic variational Bayes for non-conjugate inference. In Xing, E. P. and Jebara, T., editors, *Proceedings of the 31st International Conference on Machine Learning*, volume 32 of *Proceedings of Machine Learning Research*, pages 1971–1979, Beijing, China. PMLR.

Ver Hoef, J. M., Peterson, E. E., Hooten, M. B., Hanks, E. M., and Fortin, M.-J. (2018). Spatial autoregressive models for statistical inference from ecological data. *Ecological Monographs*, 88(1):36–59.

Wang, W. and Lee, L.-F. (2013). Estimation of spatial autoregressive models with randomly missing data in the dependent variable. *The Econometrics Journal*, 16(1):73–102.

Wang, W.-L. and Lin, T.-I. (2014). Multivariate t nonlinear mixed-effects models for multi-outcome longitudinal data with missing values. *Statistics in Medicine*, 33(17):3029–3046.

Wijayawardhana, A., Gunawan, D., and Suesse, T. (2024). A marginal maximum likelihood approach for hierarchical simultaneous autoregressive models with missing data. *Mathematics*, 12(23).

Wijayawardhana, A., Gunawan, D., and Suesse, T. (2025). Variational Bayes inference for simultaneous autoregressive models with missing data. *Statistics and Computing*, 35(3):68.

Wu, G. (2018). Fast and scalable variational Bayes estimation of spatial econometric models for Gaussian data. *Spatial Statistics*, 24:32–53.

Yeo, I.-K. and Johnson, R. A. (2000). A new family of power transformations to improve normality or symmetry. *Biometrika*, 87(4):954–959.

Yildirim, V. and Mert Kantar, Y. (2020). Robust estimation approach for spatial error model. *Journal of Statistical Computation and Simulation*, 90(9):1618–1638.

Zeiler, M. D. (2012). ADADELTA: An adaptive learning rate method. *ArXiv*, abs/1212.5701.

# Online Supplement for Non-Gaussian Simultaneous Autoregressive Models with Missing Data

We use the following notation in the online supplement. Equation (1), Table 1, Figure 1, and Algorithm 1, etc, refer to the main paper, while Equation (S1), Table S1, Figure S1, and Algorithm S1, etc, refer to the supplement.

## S1 Yeo and Johnson transformation and its derivatives

This section provides the Yeo and Johnson (YJ) transformation (Yeo and Johnson, 2000) and its derivatives, which are used to construct the YJ-SEM-Gau and YJ-SEM-t models discussed in Section 2.2 of the main paper.

Let the random variable  $y_i$  be asymmetric. The Yeo–Johnson (YJ) transformation, denoted  $t_\gamma(y_i)$ , is used to make  $y_i$  more symmetric, and is defined by:

$$y_i^* = t_\gamma(y_i) = \begin{cases} \frac{(y_i+1)^\gamma - 1}{\gamma} & \text{if } y_i \geq 0, \\ -\frac{(-y_i+1)^{2-\gamma} - 1}{2-\gamma} & \text{if } y_i < 0, \end{cases} \quad (\text{S1})$$

where  $0 < \gamma < 2$ .

The density function of SEMs with YJ transformations includes the derivative of the YJ transformation with respect to  $y_i$ , as shown in Equation (7) of the main paper. This derivative is equal to

$$\frac{dt_\gamma(y_i)}{dy_i} = \begin{cases} (y_i + 1)^{\gamma-1} & \text{if } y_i \geq 0, \\ (-y_i + 1)^{1-\gamma} & \text{if } y_i < 0. \end{cases} \quad (\text{S2})$$

Table S1: The definitions of  $\mathbf{r}$ ,  $\mathbf{M}$ , and the parameters  $\phi$  for the four spatial error models. Each SEM has a mean vector of  $\mathbf{X}\beta$  and a covariance matrix of the form  $\Sigma = \sigma_e^2 \mathbf{M}^{-1}$ , with  $\mathbf{A} = \mathbf{I}_n - \rho \mathbf{W}$ .

| Model      | $\phi$   | $\mathbf{r}$                             | $\mathbf{M}$                                  |
|------------|--|--|---|
| SEM-Gau    | $(\beta^\top, \sigma_e^2, \rho)^\top$              | $\mathbf{y} - \mathbf{X}\beta$           | $\mathbf{A}^\top \mathbf{A}$                  |
| SEM-t      | $(\beta^\top, \sigma_e^2, \rho, \nu)^\top$         | $\mathbf{y} - \mathbf{X}\beta$           | $\mathbf{A}^\top \Sigma_\tau^{-1} \mathbf{A}$ |
| YJ-SEM-Gau | $(\beta^\top, \sigma_e^2, \rho, \gamma)^\top$      | $t_\gamma(\mathbf{y}) - \mathbf{X}\beta$ | $\mathbf{A}^\top \mathbf{A}$                  |
| YJ-SEM-t   | $(\beta^\top, \sigma_e^2, \rho, \nu, \gamma)^\top$ | $t_\gamma(\mathbf{y}) - \mathbf{X}\beta$ | $\mathbf{A}^\top \Sigma_\tau^{-1} \mathbf{A}$ |

## S2 Variational Bayes approximation for SEMs with full data

Consider Bayesian inference for the parameter vector of SEMs,  $\xi$ . For SEM-Gau and YJ-SEM-Gau, we have  $\xi = \phi$ , while for SEM-t and YJ-SEM-t,  $\xi = (\phi^\top, \tau^\top)^\top$ . See Table S1 for the definition of  $\phi$  for each SEM. Let the prior distribution of  $\xi$  be denoted by  $p(\xi)$ . Then, the posterior distribution of  $\xi$  given the data  $\mathbf{y}$  is denoted by  $p(\xi | \mathbf{y})$  and is given by:

$$p(\xi | \mathbf{y}) \propto p(\mathbf{y} | \xi) p(\xi), \quad (\text{S3})$$

where the term  $p(\mathbf{y} | \xi)$  represents the likelihood of  $\mathbf{y}$ , and the log-likelihood of  $\mathbf{y}$  for different SEMs are given in Section 2 of the main paper. We define  $p(\mathbf{y} | \xi)p(\xi) = h(\xi)$ . The terms  $h(\xi)$  for each SEM, along with the total length of the parameter vector to be estimated in each model (i.e., the length of the vector  $\xi$ ), are provided in Table S2.

Table S2: The term  $h(\xi) = p(\mathbf{y} | \xi)p(\xi)$ , and the total number of model parameters  $s$  (including the length of the latent vector  $\tau$  if exists) for the SEM-Gau, YJ-SEM-Gau, SEM-t, and YJ-SEM-t models. The distribution  $p(\tau | \phi) = \prod_{i=1}^n p(\tau_i | \nu)$  represents the  $n$  independent inverse gamma latent variables used in SEMs with Student- $t$  errors (see Equation (2) on the main paper).

| Model      | $h(\xi) = p(\mathbf{y}   \xi)p(\xi)$              | $s$         |
|------------|---|-------------|
| SEM-Gau    | $p(\mathbf{y}   \phi)p(\phi)$                     | $r + 3$     |
| SEM-t      | $p(\mathbf{y}   \tau, \phi)p(\tau   \phi)p(\phi)$ | $r + 4 + n$ |
| YJ-SEM-Gau | $p(\mathbf{y}   \phi)p(\phi)$                     | $r + 4$     |
| YJ-SEM-t   | $p(\mathbf{y}   \tau, \phi)p(\tau   \phi)p(\phi)$ | $r + 5 + n$ |

Now we explain how variational Bayes (VB) inference is used to approximate the posterior distribution in Equation (S3). We use the variational distribution  $q_\lambda(\xi)$ , indexed

by the variational parameter  $\boldsymbol{\lambda}$  to approximate the posterior  $p(\boldsymbol{\xi} \mid \mathbf{y})$ . The VB approach approximates this posterior distribution by minimising the Kullback-Leibler (KL) divergence between  $q_{\boldsymbol{\lambda}}(\boldsymbol{\xi})$  and  $p(\boldsymbol{\xi} \mid \mathbf{y})$ . The KL divergence between these two distributions is

$$\begin{aligned} \text{KL}(\boldsymbol{\lambda}) &= \text{KL}(q_{\boldsymbol{\lambda}}(\boldsymbol{\xi}) \mid\mid p(\boldsymbol{\xi} \mid \mathbf{y})) \\ &= \int \log \left( \frac{q_{\boldsymbol{\lambda}}(\boldsymbol{\xi})}{p(\boldsymbol{\xi} \mid \mathbf{y})} \right) q_{\boldsymbol{\lambda}}(\boldsymbol{\xi}) d\boldsymbol{\xi}. \end{aligned} \quad (\text{S4})$$

Minimising KL divergence between  $q_{\boldsymbol{\lambda}}(\boldsymbol{\xi})$  and  $p(\boldsymbol{\xi} \mid \mathbf{y})$  is equivalent to maximising evidence lower bound (ELBO) on the marginal log-likelihood,  $\log p(\mathbf{y})$ , denoted by  $\mathcal{L}(\boldsymbol{\lambda})$ , with  $p(\mathbf{y}) = \int p(\mathbf{y} \mid \boldsymbol{\xi}) p(\boldsymbol{\xi}) d\boldsymbol{\xi}$  (Blei et al., 2017). The ELBO is

$$\mathcal{L}(\boldsymbol{\lambda}) = \int \log \left( \frac{h(\boldsymbol{\xi})}{q_{\boldsymbol{\lambda}}(\boldsymbol{\xi})} \right) q_{\boldsymbol{\lambda}}(\boldsymbol{\xi}) d\boldsymbol{\xi}, \quad (\text{S5})$$

where  $h(\boldsymbol{\xi}) = p(\mathbf{y} \mid \boldsymbol{\xi}) p(\boldsymbol{\xi})$ . Table S2 presents the expressions for  $h(\boldsymbol{\xi})$  for each of the SEMs. The ELBO in Equation (S5) can be written as an expectation with respect to  $q_{\boldsymbol{\lambda}}$ ,

$$\mathcal{L}(\boldsymbol{\lambda}) = E_q [\log h(\boldsymbol{\xi}) - \log q_{\boldsymbol{\lambda}}(\boldsymbol{\xi})], \quad (\text{S6})$$

where  $E_q [\cdot]$  denotes the expectation with respect to  $q_{\boldsymbol{\lambda}}$ .

We employ the Gaussian variational approximation, where we select  $q_{\boldsymbol{\lambda}}$  to be a multivariate normal distribution. As a result, the variational parameters  $\boldsymbol{\lambda}$  consist of both the mean vector and the distinct elements of the covariance matrix. We impose a factorised covariance structure (Ong et al., 2018) on the covariance matrix of  $q_{\boldsymbol{\lambda}}$ , which reduces the number of distinct elements in the covariance matrix. Under a factor covariance structure for the covariance matrix, the variational distribution is parameterised as  $q_{\boldsymbol{\lambda}}(\boldsymbol{\xi}) \sim N(\boldsymbol{\xi}; \boldsymbol{\mu}, \mathbf{B}\mathbf{B}^T + \mathbf{D}^2)$ , where  $\boldsymbol{\mu}$  is the  $s \times 1$  mean vector,  $\mathbf{B}$  is an  $s \times p$  full rank matrix with  $p \ll s$ , and  $\mathbf{D}$  is an  $s \times s$  diagonal matrix having diagonal elements  $\mathbf{d} = (d_1, \dots, d_s)$ . For all SEMs, the total number of parameters,  $s$  is provided in Table S2. We further impose the restriction that the upper triangular elements of  $\mathbf{B}$  are all zero.

Since the ELBO in Equation (S6) does not have a closed-form solution for all four models, we use stochastic gradient ascent (SGA) methods (Nott et al., 2012; Titsias and Lázaro-Gredilla, 2014, 2015) to maximise the ELBO with respect to the variational parameters,  $\boldsymbol{\lambda}$ . Let  $\nabla_{\boldsymbol{\lambda}} \mathcal{L}(\boldsymbol{\lambda})$  be the gradient of the objective function to be optimised,  $\mathcal{L}(\boldsymbol{\lambda})$ , and  $\widehat{\nabla_{\boldsymbol{\lambda}} \mathcal{L}(\boldsymbol{\lambda})}$  an unbiased estimate of  $\nabla_{\boldsymbol{\lambda}} \mathcal{L}(\boldsymbol{\lambda})$ . The SGA method updates  $\boldsymbol{\lambda}$  iteratively, starting from an initial value  $\boldsymbol{\lambda}^{(0)}$ , according to the following scheme:

$$\boldsymbol{\lambda}^{(t+1)} = \boldsymbol{\lambda}^{(t)} + \boldsymbol{a}_t \circ \widehat{\nabla_{\boldsymbol{\lambda}} \mathcal{L}(\boldsymbol{\lambda}^{(t)})}, \quad (\text{S7})$$

and continues until a stopping criterion is satisfied, where  $\boldsymbol{a}_t$  ( $t = 0, 1, \dots$ ) represents the vector-valued learning rates that satisfy the Robbins-Monro conditions ( $\sum_t \boldsymbol{a}_t = \infty$  and  $\sum_t (\boldsymbol{a}_t)^2 \leq \infty$ ) to ensure convergence of the sequence  $\boldsymbol{\lambda}^{(t)}$  to a local optimum as  $t \rightarrow \infty$  (Robbins and Monro, 1951). The symbol  $\circ$  denotes the element-wise product. To speed up convergence, we use the ADADELTA algorithm for adaptive learning rates (Zeiler, 2012), detailed in Section S3.

Minimising the variance of the gradient estimator,  $\widehat{\nabla_{\boldsymbol{\lambda}} \mathcal{L}(\boldsymbol{\lambda})}$ , is crucial for both stability and fast convergence of the SGA algorithm, which we address using the reparameterisation trick (Kingma and Welling, 2013; Rezende et al., 2014).

We now briefly explain how the reparameterisation trick, combined with a factor covariance structure for the Gaussian variational distribution, is used to obtain efficient gradient estimates in this article. More detailed information can be found in Ong et al. (2018).

To apply the reparameterisation trick, we begin by sampling from  $q_{\boldsymbol{\lambda}}(\boldsymbol{\xi})$ . This involves first drawing  $\boldsymbol{\zeta} = (\boldsymbol{\eta}^{\top}, \boldsymbol{\epsilon}^{\top})^{\top}$ , where  $\boldsymbol{\eta}$  is a  $p$ -dimensional vector and  $\boldsymbol{\epsilon}$  is an  $s$ -dimensional vector, from a fixed distribution  $f_{\boldsymbol{\zeta}}(\boldsymbol{\zeta})$  that is independent of the variational parameters. Next, we compute  $\boldsymbol{\xi} = u(\boldsymbol{\zeta}, \boldsymbol{\lambda}) = \boldsymbol{\mu} + \mathbf{B}\boldsymbol{\eta} + \mathbf{d} \circ \boldsymbol{\epsilon}$ . We let,  $f_{\boldsymbol{\zeta}}(\boldsymbol{\zeta})$  to follow a standard normal distribution. i.e.  $\boldsymbol{\zeta} = (\boldsymbol{\eta}^{\top}, \boldsymbol{\epsilon}^{\top})^{\top} \sim N(\mathbf{0}, \mathbf{I}_{s+p})$ , where  $\mathbf{0}$  is the zero mean vector of size  $s + p$  and  $\mathbf{I}_{s+p}$  is the identity matrix of the same size. Then, the expectation in

Equation (S6) is expressed with respect to the distribution  $f_\zeta$  as

$$\begin{aligned}\mathcal{L}(\boldsymbol{\lambda}) &= E_q [\log h(\boldsymbol{\xi}) - \log q_{\boldsymbol{\lambda}}(\boldsymbol{\xi})] \\ &= E_{f_\zeta} [\log h(u(\boldsymbol{\zeta}, \boldsymbol{\lambda})) - \log q_{\boldsymbol{\lambda}}(u(\boldsymbol{\zeta}, \boldsymbol{\lambda}))],\end{aligned}\tag{S8}$$

and differentiating  $\mathcal{L}(\boldsymbol{\lambda})$  under the integral sign, we obtain

$$\begin{aligned}\nabla_{\boldsymbol{\lambda}} \mathcal{L}(\boldsymbol{\lambda}) &= E_{f_\zeta} [\nabla_{\boldsymbol{\lambda}} \log h(u(\boldsymbol{\zeta}, \boldsymbol{\lambda})) - \nabla_{\boldsymbol{\lambda}} \log q_{\boldsymbol{\lambda}}(u(\boldsymbol{\zeta}, \boldsymbol{\lambda}))], \\ &= E_{f_\zeta} \left[ \frac{du(\boldsymbol{\zeta}, \boldsymbol{\lambda})^\top}{d\boldsymbol{\lambda}} \{ \nabla_{\boldsymbol{\xi}} \log h(\boldsymbol{\xi}) - \nabla_{\boldsymbol{\xi}} \log q_{\boldsymbol{\lambda}}(\boldsymbol{\xi}) \} \right],\end{aligned}\tag{S9}$$

where  $\frac{du(\boldsymbol{\zeta}, \boldsymbol{\lambda})}{d\boldsymbol{\lambda}}$  is the derivative of the transformation  $u(\boldsymbol{\zeta}, \boldsymbol{\lambda}) = \boldsymbol{\mu} + \mathbf{B}\boldsymbol{\eta} + \mathbf{d} \circ \boldsymbol{\epsilon}$  with respect to the variational parameters  $\boldsymbol{\lambda} = (\boldsymbol{\mu}^\top, \text{vech}(\mathbf{B})^\top, \mathbf{d}^\top)^\top$ , where the "vech" operator vectorises a matrix by stacking its columns from left to right while removing all the elements above the diagonal (the superdiagonal elements) of the matrix. The gradients  $\frac{du(\boldsymbol{\zeta}, \boldsymbol{\lambda})}{d\boldsymbol{\lambda}}$  and  $\nabla_{\boldsymbol{\xi}} \log q_{\boldsymbol{\lambda}}(\boldsymbol{\xi})$  are provided in Section S2.1. The expressions for  $\nabla_{\boldsymbol{\xi}} \log h(\boldsymbol{\xi})$  differ for each SEM and can be found in Section S2.2.

Algorithm S1 outlines the VB algorithm for estimating SEMs with full data. The unbiased estimate of the gradient,  $\widehat{\nabla_{\boldsymbol{\lambda}} \mathcal{L}(\boldsymbol{\lambda})}$ , presented in step 4 of Algorithm S1 can be constructed using the reparameterisation trick described earlier, with a single sample drawn from  $f_\zeta(\boldsymbol{\zeta})$ .

## S2.1 Expressions for $\frac{du(\boldsymbol{\zeta}, \boldsymbol{\lambda})}{d\boldsymbol{\lambda}}$

In the reparameterisation gradient given in Equation (S9),  $\frac{du(\boldsymbol{\zeta}, \boldsymbol{\lambda})}{d\boldsymbol{\lambda}}$  is the derivative of the transformation  $u(\boldsymbol{\zeta}, \boldsymbol{\lambda}) = \boldsymbol{\mu} + \mathbf{B}\boldsymbol{\eta} + \mathbf{d} \circ \boldsymbol{\epsilon}$  with respect to the variational parameters  $\boldsymbol{\lambda} = (\boldsymbol{\mu}^\top, \text{vech}(\mathbf{B})^\top, \mathbf{d}^\top)^\top$ . We write that  $u(\boldsymbol{\zeta}, \boldsymbol{\lambda}) = \boldsymbol{\mu} + (\boldsymbol{\eta}^\top \otimes \mathbf{I}_s) \text{vech}(\mathbf{B}) + \mathbf{d} \circ \boldsymbol{\epsilon}$ , where  $\otimes$  represents the Kronecker product, and  $\mathbf{I}_s$  is the identity matrix of size  $s$ . It can be shown that  $\nabla_{\boldsymbol{\xi}} \log q_{\boldsymbol{\lambda}}(\boldsymbol{\xi}) = -(\mathbf{B}\mathbf{B}^\top + \mathbf{D}^2)^{-1}(\boldsymbol{\xi} - \boldsymbol{\mu})$ ,

$$\frac{du(\boldsymbol{\zeta}, \boldsymbol{\lambda})}{d\boldsymbol{\mu}} = \mathbf{I}_s \quad \text{and} \quad \frac{du(\boldsymbol{\zeta}, \boldsymbol{\lambda})}{d\text{vech}(\mathbf{B})} = \boldsymbol{\eta}^\top \otimes \mathbf{I}_s.\tag{S10}$$

---

**Algorithm S1** Variational Bayes algorithm

---

- 1: Initialise  $\boldsymbol{\lambda}^{(0)} = (\boldsymbol{\mu}^{\top(0)}, \text{vech}(\mathbf{B})^{\top(0)}, \mathbf{d}^{\top(0)})^\top$  and set  $t = 0$
- 2: **repeat**
- 3:   Generate  $(\boldsymbol{\eta}^{(t)}, \boldsymbol{\epsilon}^{(t)}) \sim N(\mathbf{0}, \mathbf{I}_{s+p})$
- 4:   Construct unbiased estimates  $\widehat{\nabla_{\boldsymbol{\mu}} \mathcal{L}(\boldsymbol{\lambda})}$ ,  $\widehat{\nabla_{\text{vech}(\mathbf{B})} \mathcal{L}(\boldsymbol{\lambda})}$ , and  $\widehat{\nabla_{\mathbf{d}} \mathcal{L}(\boldsymbol{\lambda})}$  using Equations (S11), (S12) and (S13) in Section S2.1 at  $\boldsymbol{\lambda}^{(t)}$ .
- 5:   Set adaptive learning rates for the variational means,  $\boldsymbol{a}_{\boldsymbol{\mu}}^{(t)}$  and the variational parameters  $\text{vech}(\mathbf{B})$  and  $\mathbf{d}$ ,  $\boldsymbol{a}_{\text{vech}(\mathbf{B})}^{(t)}$  and  $\boldsymbol{a}_{\mathbf{d}}^{(t)}$ , respectively, using ADADELTA described in Section S3 of the online supplement.
- 6:   Set  $\boldsymbol{\mu}^{(t+1)} = \boldsymbol{\mu}^{(t)} + \boldsymbol{a}_{\boldsymbol{\mu}}^{(t)} \circ \widehat{\nabla_{\boldsymbol{\mu}} \mathcal{L}(\boldsymbol{\lambda}^{(t)})}$ .
- 7:   Set  $\text{vech}(\mathbf{B})^{(t+1)} = \text{vech}(\mathbf{B})^{(t)} + \boldsymbol{a}_{\text{vech}(\mathbf{B})}^{(t)} \circ \widehat{\nabla_{\text{vech}(\mathbf{B})} \mathcal{L}(\boldsymbol{\lambda}^{(t)})}$ .
- 8:   Set  $\mathbf{d}^{(t+1)} = \mathbf{d}^{(t)} + \boldsymbol{a}_{\mathbf{d}}^{(t)} \circ \widehat{\nabla_{\mathbf{d}} \mathcal{L}(\boldsymbol{\lambda}^{(t)})}$ .
- 9:   Set  $\boldsymbol{\lambda}^{(t+1)} = (\boldsymbol{\mu}^{\top(t+1)}, \text{vech}(\mathbf{B})^{\top(t+1)}, \mathbf{d}^{\top(t+1)})$ , and  $t = t + 1$
- 10: **until** some stopping rule is satisfied

---

The derivatives of the lower bound with respect to variational parameters are:

$$\begin{aligned} \nabla_{\boldsymbol{\mu}} \mathcal{L}(\boldsymbol{\lambda}) &= E_{f_{\boldsymbol{\zeta}}} [\nabla_{\boldsymbol{\xi}} \log h(\boldsymbol{\mu} + \mathbf{B}\boldsymbol{\eta} + \mathbf{d} \circ \boldsymbol{\epsilon}) \\ &\quad + (\mathbf{B}\mathbf{B}^\top + \mathbf{D}^2)^{-1}(\mathbf{B}\boldsymbol{\eta} + \mathbf{d} \circ \boldsymbol{\epsilon})], \end{aligned} \quad (\text{S11})$$

$$\begin{aligned} \nabla_{\text{vech}(\mathbf{B})} \mathcal{L}(\boldsymbol{\lambda}) &= E_{f_{\boldsymbol{\zeta}}} [\nabla_{\boldsymbol{\xi}} \log h(\boldsymbol{\mu} + \mathbf{B}\boldsymbol{\eta} + \mathbf{d} \circ \boldsymbol{\epsilon}) \boldsymbol{\eta}^\top \\ &\quad + (\mathbf{B}\mathbf{B}^\top + \mathbf{D}^2)^{-1}(\mathbf{B}\boldsymbol{\eta} + \mathbf{d} \circ \boldsymbol{\epsilon}) \boldsymbol{\eta}^\top], \end{aligned} \quad (\text{S12})$$

and

$$\begin{aligned} \nabla_{\mathbf{d}} \mathcal{L}(\boldsymbol{\lambda}) &= E_{f_{\boldsymbol{\zeta}}} [\text{diag}(\nabla_{\boldsymbol{\xi}} \log h(\boldsymbol{\mu} + \mathbf{B}\boldsymbol{\eta} + \mathbf{d} \circ \boldsymbol{\epsilon})) \boldsymbol{\epsilon}^\top \\ &\quad + (\mathbf{B}\mathbf{B}^\top + \mathbf{D}^2)^{-1}(\mathbf{B}\boldsymbol{\eta} + \mathbf{d} \circ \boldsymbol{\epsilon}) \boldsymbol{\epsilon}^\top], \end{aligned} \quad (\text{S13})$$

where  $\text{diag}(\cdot)$  is the vector of diagonal elements extracted from a square matrix. The analytical expressions for  $\nabla_{\boldsymbol{\xi}} \log h(\boldsymbol{\mu} + \mathbf{B}\boldsymbol{\eta} + \mathbf{d} \circ \boldsymbol{\epsilon}) = \nabla_{\boldsymbol{\xi}} \log h(\boldsymbol{\xi})$  in Equations (S11)-(S13) for different SEMs are provided in Section S2.2.

## S2.2 Expressions for $\nabla_{\boldsymbol{\xi}} \log h(\boldsymbol{\mu} + \mathbf{B}\boldsymbol{\eta} + \mathbf{d} \circ \boldsymbol{\epsilon}) = \nabla_{\boldsymbol{\xi}} \log h(\boldsymbol{\xi})$

The term  $h(\boldsymbol{\xi})$  represents the likelihood multiplied by the prior distribution (see Section S2). For different SEMs, the expressions for  $h(\boldsymbol{\xi})$  are given in Table S2. Table S3

shows the prior distributions used for the model parameters in this study. In this section, we compute the derivatives of  $\log h(\boldsymbol{\xi})$  with respect to the model parameter vector  $\boldsymbol{\xi}$ , denoted as  $\nabla_{\boldsymbol{\xi}} \log h(\boldsymbol{\xi})$ . These derivatives are necessary for computing the reparameterisation gradient, as outlined in Equation (S9), for each SEM.

| Parameter          | $\boldsymbol{\beta}$                                      | $\omega'$                   | $\rho'$                   | $\nu'$                   | $\gamma'$                   | $\boldsymbol{\psi}$                                      |
|--------------------|---|-----------------------------|---------------------------|--------------------------|-----------------------------|--|
| Prior distribution | $N(\mathbf{0}, \sigma_{\boldsymbol{\beta}}^2 \mathbf{I})$ | $N(0, \sigma_{\omega'}^2)$  | $N(0, \sigma_{\rho'}^2)$  | $N(0, \sigma_{\nu'}^2)$  | $N(0, \sigma_{\gamma'}^2)$  | $N(\mathbf{0}, \sigma_{\boldsymbol{\psi}}^2 \mathbf{I})$ |
| Hyperparameters    | $\sigma_{\boldsymbol{\beta}}^2 = 10^2$                    | $\sigma_{\omega'}^2 = 10^2$ | $\sigma_{\rho'}^2 = 10^2$ | $\sigma_{\nu'}^2 = 10^2$ | $\sigma_{\gamma'}^2 = 10^2$ | $\sigma_{\boldsymbol{\psi}}^2 = 10^2$                    |

Table S3: Prior distributions of model parameters

### S2.2.1 Derivatives for SEM-Gau

For SEM-Gau,  $h(\boldsymbol{\xi}) = p(\mathbf{y} \mid \boldsymbol{\phi})p(\boldsymbol{\phi})$ , where  $\boldsymbol{\phi} = (\boldsymbol{\beta}^\top, \sigma_{\mathbf{e}}^2, \rho)^\top$ . The logarithm of  $h(\boldsymbol{\xi})$  is  $\log p(\mathbf{y} \mid \boldsymbol{\phi}) + \log p(\boldsymbol{\phi})$ . Note that, for  $\sigma_{\mathbf{e}}^2$ , and  $\rho$ , we utilise the transformations described in Section 4 of the main paper, and put prior on the transformed parameters as in Table S3. This leads to

$$\log h(\boldsymbol{\xi}) \propto -\frac{n}{2}\omega' + \frac{1}{2}\log|\mathbf{M}| - \frac{e^{-\omega'}}{2}\mathbf{r}^\top \mathbf{M}\mathbf{r} - \frac{\boldsymbol{\beta}^\top \boldsymbol{\beta}}{2\sigma_{\boldsymbol{\beta}}^2} - \frac{\omega'^2}{2\sigma_{\omega'}^2} - \frac{\rho'^2}{2\sigma_{\rho'}^2}, \quad (\text{S14})$$

where the values of  $\sigma_{\boldsymbol{\beta}}^2$ ,  $\sigma_{\omega'}^2$ , and  $\sigma_{\rho'}^2$  are each set to 100, as detailed in Table S3, while  $\mathbf{r}$  and  $\mathbf{M}$  are provided in Table S1.

The derivative of  $\log h(\boldsymbol{\xi})$  in Equation (S14) with respect to  $\boldsymbol{\beta}$  is

$$\frac{\partial \log h(\boldsymbol{\xi})}{\partial \boldsymbol{\beta}} = e^{-\omega'} \mathbf{r}^\top \mathbf{M} \mathbf{X} - \frac{\boldsymbol{\beta}^\top}{\sigma_{\boldsymbol{\beta}}^2}, \quad (\text{S15})$$

the derivative of  $\log h(\boldsymbol{\xi})$  with respect to  $\omega'$  is

$$\frac{\partial \log h(\boldsymbol{\xi})}{\partial \omega'} = -\frac{n}{2} + \frac{e^{-\omega'}}{2}\mathbf{r}^\top \mathbf{M}\mathbf{r} - \frac{\omega'}{\sigma_{\omega'}^2}, \quad (\text{S16})$$

and the derivative of  $\log h(\boldsymbol{\xi})$  with respect to  $\rho'$  is

$$\frac{\partial \log h(\boldsymbol{\xi})}{\partial \rho'} = \left( \frac{1}{2} \text{tr} \left\{ (\mathbf{A}^\top \mathbf{A})^{-1} \left( \frac{\partial \mathbf{A}^\top \mathbf{A}}{\partial \rho} \right) \right\} - \frac{e^{-\omega'}}{2} \mathbf{r}^\top \left( \frac{\partial \mathbf{A}^\top \mathbf{A}}{\partial \rho} \right) \mathbf{r} \right) \left( \frac{\partial \rho}{\partial \rho'} \right) - \frac{\rho'}{\sigma_{\rho'}^2}, \quad (\text{S17})$$

where  $\text{tr}\{\cdot\}$  denotes the trace operator, which computes the sum of the diagonal elements of a matrix,

$$\begin{aligned} \left( \frac{\partial \mathbf{A}^\top \mathbf{A}}{\partial \rho} \right) &= -(\mathbf{W}^\top + \mathbf{W}) + 2\rho \mathbf{W}^\top \mathbf{W}, \\ \left( \frac{\partial \rho}{\partial \rho'} \right) &= \frac{2e^{\rho'}}{(1 + e^{\rho'})^2}. \end{aligned}$$

### S2.2.2 Gradients for SEM-t

For SEM-t,  $h(\boldsymbol{\xi}) = p(\mathbf{y} \mid \boldsymbol{\tau}, \boldsymbol{\phi})p(\boldsymbol{\tau} \mid \boldsymbol{\phi})p(\boldsymbol{\phi})$ , where  $\boldsymbol{\phi} = (\boldsymbol{\beta}^\top, \sigma_{\mathbf{e}}^2, \rho, \nu)^\top$ . The logarithm of  $h(\boldsymbol{\xi})$  is  $p(\mathbf{y} \mid \boldsymbol{\tau}, \boldsymbol{\phi}) + \log p(\boldsymbol{\tau} \mid \boldsymbol{\phi}) + \log p(\boldsymbol{\phi})$ . Note that, for  $\sigma_{\mathbf{e}}^2$ ,  $\rho$  and  $\nu$ , we utilise the transformations described in Section 4 of the main paper, and put prior on the transformed parameters as in Table S3. This leads to

$$\begin{aligned} \log h(\boldsymbol{\xi}) &\propto -\frac{n}{2}\omega' + \frac{1}{2}\log|\mathbf{M}| - \frac{e^{-\omega'}}{2}\mathbf{r}^\top \mathbf{M}\mathbf{r} \\ &\quad + \sum_{i=1}^n \log p(\tau_i \mid \nu) + \log \left| \frac{\partial \tau_i}{\partial \tau'_i} \right| - \frac{\boldsymbol{\beta}^\top \boldsymbol{\beta}}{2\sigma_{\boldsymbol{\beta}}^2} - \frac{\omega'^2}{2\sigma_{\omega'}^2} - \frac{\rho'^2}{2\sigma_{\rho'}^2} - \frac{\nu'^2}{2\sigma_{\nu'}^2}, \end{aligned} \quad (\text{S18})$$

where the values of  $\sigma_{\boldsymbol{\beta}}^2$ ,  $\sigma_{\omega'}^2$ ,  $\sigma_{\rho'}^2$ , and  $\sigma_{\nu'}^2$  are each set to 100, as detailed in Table S3, while  $\mathbf{r}$  and  $\mathbf{M}$  are provided in Table S1. The term  $\left| \frac{\partial \tau_i}{\partial \tau'_i} \right|$  represents the derivative of the inverse transformation  $\tau_i = e^{\tau'_i}$ , which maps the latent variable  $\tau_i$ , for  $i = 1, \dots, n$ , onto the real line using the transformation  $\tau'_i = \log(\tau_i)$ .

The derivative of  $\log h(\boldsymbol{\xi})$  in Equation (S18) with respect to  $\boldsymbol{\beta}$  is

$$\frac{\partial \log h(\boldsymbol{\xi})}{\partial \boldsymbol{\beta}} = e^{-\omega'} \mathbf{r}^\top \mathbf{M} \mathbf{X} - \frac{\boldsymbol{\beta}^\top}{\sigma_{\boldsymbol{\beta}}^2}, \quad (\text{S19})$$

the derivative of  $\log h(\boldsymbol{\xi})$  with respect to  $\omega'$  is

$$\frac{\partial \log h(\boldsymbol{\xi})}{\partial \omega'} = -\frac{n}{2} + \frac{e^{-\omega'}}{2} \mathbf{r}^\top \mathbf{M} \mathbf{r} - \frac{\omega'}{\sigma_{\omega'}^2}, \quad (\text{S20})$$

the derivative of  $\log h(\boldsymbol{\xi})$  with respect to  $\rho'$  is

$$\frac{\partial \log h(\boldsymbol{\xi})}{\partial \rho'} = \left( \frac{1}{2} \text{tr} \left\{ (\mathbf{A}^\top \mathbf{A})^{-1} \left( \frac{\partial \mathbf{A}^\top \mathbf{A}}{\partial \rho} \right) \right\} + e^{-\omega'} (\mathbf{A}\mathbf{r})^\top \boldsymbol{\Sigma}_\tau^{-1} \mathbf{W}\mathbf{r} \right) \left( \frac{\partial \rho}{\partial \rho'} \right) - \frac{\rho'}{\sigma_{\rho'}^2}, \quad (\text{S21})$$

and the derivative of  $\log h(\boldsymbol{\xi})$  with respect to  $\nu'$  is

$$\begin{aligned} \frac{\partial \log h(\boldsymbol{\xi})}{\partial \nu'} = & n \left( \frac{\partial \log \Gamma \left( \frac{e^{\nu'}+3}{2} \right)}{\partial \nu'} \right) - \frac{e^{\nu'}}{2} \sum_{i=1}^n \left( \tau'_i + e^{-\tau'_i} \right) - \frac{ne^{\nu'}}{2} \log \left( \frac{2}{e^{\nu'}+3} \right) + \frac{ne^{\nu'}}{2} \\ & - \frac{\nu'}{\sigma_{\nu'}^2}, \end{aligned} \quad (\text{S22})$$

where  $\frac{\partial \log \Gamma \left( \frac{e^{\nu'}+3}{2} \right)}{\partial \nu'}$  is the derivative of the log-gamma function, which is computed numerically using R.

The derivative of  $\log h(\boldsymbol{\xi})$  with respect to  $i^{th}$  element of the vector  $\boldsymbol{\tau}'$ ,  $\tau'_i$  is

$$\frac{\partial \log h(\boldsymbol{\xi})}{\partial \tau'_i} = -\frac{1}{2} + \frac{1}{2} e^{-\omega'} (\mathbf{r}_{\mathbf{A}i})^2 e^{\tau'_i} + \left( \frac{e^{\nu'+3}}{2} \right) \left( -1 + e^{-\tau'_i} \right), \quad (\text{S23})$$

where  $\mathbf{r}_{\mathbf{A}i}$  is the  $i^{th}$  element of the vector  $\mathbf{A}\mathbf{r}$ .

### S2.2.3 Gradients for YJ-SEM-Gau

For YJ-SEM-Gau,  $h(\boldsymbol{\xi}) = p(\mathbf{y} \mid \boldsymbol{\phi})p(\boldsymbol{\phi})$ , where  $\boldsymbol{\phi} = (\boldsymbol{\beta}^\top, \sigma_{\mathbf{e}}^2, \rho, \gamma)^\top$ . The logarithm of  $h(\boldsymbol{\xi})$  is  $\log p(\mathbf{y} \mid \boldsymbol{\phi}) + \log p(\boldsymbol{\phi})$ . Note that, for  $\sigma_{\mathbf{e}}^2$ ,  $\rho$  and  $\gamma$ , we utilise the transformations described in Section 4 of the main paper, and put prior on the transformed parameters as in Table S3. This leads to

$$\begin{aligned} \log h(\boldsymbol{\xi}) \propto & -\frac{n}{2} \omega' + \frac{1}{2} \log |\mathbf{M}| - \frac{e^{-\omega'}}{2} \mathbf{r}^\top \mathbf{M} \mathbf{r} + \sum_{i=1}^n \log \left( \frac{dt_\gamma(y_i)}{dy_i} \right) \\ & - \frac{\boldsymbol{\beta}^\top \boldsymbol{\beta}}{2\sigma_{\boldsymbol{\beta}}^2} - \frac{\omega'^2}{2\sigma_{\omega'}^2} - \frac{\rho'^2}{2\sigma_{\rho'}^2} - \frac{\gamma'^2}{2\sigma_{\gamma'}^2}, \end{aligned} \quad (\text{S24})$$

where the values of  $\sigma_{\boldsymbol{\beta}}^2$ ,  $\sigma_{\omega'}^2$ ,  $\sigma_{\rho'}^2$ , and  $\sigma_{\gamma'}^2$  are each set to 100, as detailed in Table S3, while  $\mathbf{r}$  and  $\mathbf{M}$  are provided in Table S1.

The derivative of  $\log h(\boldsymbol{\xi})$  in Equation (S24) with respect to  $\boldsymbol{\beta}$  is

$$\frac{\partial \log h(\boldsymbol{\xi})}{\partial \boldsymbol{\beta}} = e^{-\omega'} \mathbf{r}^\top \mathbf{M} \mathbf{X} - \frac{\boldsymbol{\beta}^\top}{\sigma_{\boldsymbol{\beta}}^2}, \quad (\text{S25})$$

the derivative of  $\log h(\boldsymbol{\xi})$  with respect to  $\omega'$  is

$$\frac{\partial \log h(\boldsymbol{\xi})}{\partial \omega'} = -\frac{n}{2} + \frac{e^{-\omega'}}{2} \mathbf{r}^\top \mathbf{M} \mathbf{r} - \frac{\omega'}{\sigma_{\omega'}^2}, \quad (\text{S26})$$

the derivative of  $\log h(\boldsymbol{\xi})$  with respect to  $\rho'$  is

$$\frac{\partial \log h(\boldsymbol{\xi})}{\partial \rho'} = \left( \frac{1}{2} \text{tr} \left\{ (\mathbf{A}^\top \mathbf{A})^{-1} \left( \frac{\partial \mathbf{A}^\top \mathbf{A}}{\partial \rho} \right) \right\} - \frac{e^{-\omega'}}{2} \mathbf{r}^\top \left( \frac{\partial \mathbf{A}^\top \mathbf{A}}{\partial \rho} \right) \mathbf{r} \right) \left( \frac{\partial \rho}{\partial \rho'} \right) - \frac{\rho'}{\sigma_{\rho'}^2}, \quad (\text{S27})$$

and the derivative of  $\log h(\boldsymbol{\xi})$  with respect to  $\gamma'$  is

$$\frac{\partial \log h(\boldsymbol{\xi})}{\partial \gamma'} = \left( -e^{-\omega'} \mathbf{r}^\top \mathbf{M} \left( \frac{\partial t_\gamma(\mathbf{y})}{\partial \gamma} \right) + \sum_{i=0}^n \frac{\partial \log \left( \frac{dt_\gamma(y_i)}{dy_i} \right)}{\partial \gamma} \right) \left( \frac{\partial \gamma}{\partial \gamma'} \right) - \frac{\gamma'}{\sigma_{\gamma'}^2}, \quad (\text{S28})$$

where  $\frac{\partial t_\gamma(\mathbf{y})}{\partial \gamma} = \left( \frac{\partial t_\gamma(y_1)}{\partial \gamma}, \frac{\partial t_\gamma(y_2)}{\partial \gamma}, \dots, \frac{\partial t_\gamma(y_n)}{\partial \gamma} \right)^\top$ , with the  $i^{th}$  elements of the vector is equal to

$$\frac{\partial t_\gamma(y_i)}{\partial \gamma} = \begin{cases} \frac{(y_i+1)^\gamma (\gamma \log(y_i+1)-1)+1}{\gamma^2} & \text{if } y_i \geq 0, \\ \frac{(2-\gamma)(-y_i+1)^{(2-\gamma)} \log(-y_i+1)-(-y_i+1)^{2-\gamma}+1}{(2-\gamma)^2} & \text{if } y_i < 0, \end{cases}$$

$$\frac{\partial \log \left( \frac{dt_\gamma(y_i)}{dy_i} \right)}{\partial \gamma} = \begin{cases} \log(y_i+1) & \text{if } y_i \geq 0, \\ -\log(y_i+1) & \text{if } y_i < 0, \end{cases}$$

and

$$\frac{\partial \gamma}{\partial \gamma'} = \frac{2e^{\gamma'}}{(1+e^{\gamma'})^2}.$$

#### S2.2.4 Gradients for YJ-SEM-t

For YJ-SEM-t,  $h(\boldsymbol{\xi}) = p(\mathbf{y} \mid \boldsymbol{\tau}, \boldsymbol{\phi})p(\boldsymbol{\tau} \mid \boldsymbol{\phi})p(\boldsymbol{\phi})$ , where  $\boldsymbol{\phi} = (\boldsymbol{\beta}^\top, \sigma_{\mathbf{e}}^2, \rho, \nu, \gamma)^\top$ . The logarithm of  $h(\boldsymbol{\xi})$  is  $\log p(\mathbf{y} \mid \boldsymbol{\tau}, \boldsymbol{\phi}) + \log p(\boldsymbol{\tau} \mid \boldsymbol{\phi}) + \log p(\boldsymbol{\phi})$ . Note that, for  $\sigma_{\mathbf{e}}^2$ ,  $\rho$ ,  $\nu$ , and  $\gamma$ , we utilise the transformations described in Section 4 of the main paper, and put prior

on the transformed parameters as in Table S3. This leads to

$$\begin{aligned} \log h(\boldsymbol{\xi}) \propto & -\frac{n}{2}\omega' + \frac{1}{2}\log|\mathbf{M}| - \frac{e^{-\omega'}}{2}\mathbf{r}^\top \mathbf{M}\mathbf{r} + \sum_{i=1}^n \log\left(\frac{dt_\gamma(y_i)}{dy_i}\right) \\ & + \sum_{i=1}^n \log p(\tau_i \mid \nu) + \log\left|\frac{\partial\tau_i}{\partial\tau'_i}\right| - \frac{\boldsymbol{\beta}^\top \boldsymbol{\beta}}{2\sigma_{\boldsymbol{\beta}}^2} - \frac{\omega'^2}{2\sigma_{\omega'}^2} - \frac{\rho'^2}{2\sigma_{\rho'}^2} - \frac{\nu'^2}{2\sigma_{\nu'}^2}, \end{aligned} \quad (\text{S29})$$

where the values of  $\sigma_{\boldsymbol{\beta}}^2$ ,  $\sigma_{\omega'}^2$ ,  $\sigma_{\rho'}^2$ ,  $\sigma_{\nu'}^2$ , and  $\sigma_\gamma^2$  are each set to 100, as detailed in Table S3, while  $\mathbf{r}$  and  $\mathbf{M}$  are provided in Table S1.

The derivative of  $\log h(\boldsymbol{\xi})$  in Equation (S29) with respect to  $\boldsymbol{\beta}$  is

$$\frac{\partial \log h(\boldsymbol{\xi})}{\partial \boldsymbol{\beta}} = e^{-\omega'} \mathbf{r}^\top \mathbf{M} \mathbf{X} - \frac{\boldsymbol{\beta}^\top}{\sigma_{\boldsymbol{\beta}}^2}, \quad (\text{S30})$$

the derivative of  $\log h(\boldsymbol{\xi})$  with respect to  $\omega'$  is

$$\frac{\partial \log h(\boldsymbol{\xi})}{\partial \omega'} = -\frac{n}{2} + \frac{e^{-\omega'}}{2}\mathbf{r}^\top \mathbf{M}\mathbf{r} - \frac{\omega'}{\sigma_{\omega'}^2}, \quad (\text{S31})$$

the derivative of  $\log h(\boldsymbol{\xi})$  with respect to  $\rho'$  is

$$\frac{\partial \log h(\boldsymbol{\xi})}{\partial \rho'} = \left( \frac{1}{2} \text{tr} \left\{ (\mathbf{A}^\top \mathbf{A})^{-1} \left( \frac{\partial \mathbf{A}^\top \mathbf{A}}{\partial \rho} \right) \right\} + e^{-\omega'} (\mathbf{A}\mathbf{r})^\top \boldsymbol{\Sigma}_\tau^{-1} \mathbf{W} \mathbf{r} \right) \left( \frac{\partial \rho}{\partial \rho'} \right) - \frac{\rho'}{\sigma_{\rho'}^2}, \quad (\text{S32})$$

the derivative of  $\log h(\boldsymbol{\xi})$  with respect to  $\nu'$  is

$$\begin{aligned} \frac{\partial \log h(\boldsymbol{\xi})}{\partial \nu'} = & n \left( \frac{\partial \log \Gamma\left(\frac{e^{\nu'}+3}{2}\right)}{\partial \nu'} \right) - \frac{e^{\nu'}}{2} \sum_{i=1}^n \left( \tau'_i + e^{-\tau'_i} \right) - \frac{ne^{\nu'}}{2} \log\left(\frac{2}{e^{\nu'}+3}\right) + \frac{ne^{\nu'}}{2} \\ & - \frac{\nu'}{\sigma_{\nu'}^2}, \end{aligned} \quad (\text{S33})$$

and the derivative of  $\log h(\boldsymbol{\xi})$  with respect to  $\gamma'$  is

$$\frac{\partial \log h(\boldsymbol{\xi})}{\partial \gamma'} = \left( -e^{-\omega'} \mathbf{r}^\top \mathbf{M} \left( \frac{\partial t_\gamma(\mathbf{y})}{\partial \gamma} \right) + \sum_{i=0}^n \frac{\partial \log\left(\frac{dt_\gamma(y_i)}{dy_i}\right)}{\partial \gamma} \right) \left( \frac{\partial \gamma}{\partial \gamma'} \right) - \frac{\gamma'}{\sigma_{\gamma'}^2}. \quad (\text{S34})$$

The derivative of  $\log h(\boldsymbol{\xi})$  with respect to  $i^{th}$  element of the vector  $\boldsymbol{\tau}'$ ,  $\tau'_i$  is

$$\frac{\partial \log h(\boldsymbol{\xi})}{\partial \tau'_i} = -\frac{1}{2} + \frac{1}{2}e^{-\omega'}(\mathbf{r}_{\mathbf{A}i})^2 e^{\tau'_i} + \left(\frac{e^{\nu'+3}}{2}\right) \left(-1 + e^{-\tau'_i}\right), \quad (\text{S35})$$

where  $\mathbf{r}_{\mathbf{A}i}$  is the  $i^{th}$  element of the vector  $\mathbf{A}\mathbf{r}$ .

### S3 Calculate adaptive learning rates using ADADELTA

The adaptive learning rates (step sizes) for the VB algorithms are calculated using the ADADELTA algorithm (Zeiler, 2012). The ADADELTA algorithm is now briefly described. Different step sizes are used for each element in variational parameters  $\boldsymbol{\lambda}$ .

The update for the  $i^{th}$  element of  $\boldsymbol{\lambda}$  is

$$\boldsymbol{\lambda}_i^{(t+1)} = \boldsymbol{\lambda}_i^{(t)} + \Delta \boldsymbol{\lambda}_i^{(t)}, \quad (\text{S36})$$

where, the step size  $\Delta \boldsymbol{\lambda}_i^{(t)}$  is  $a_i^{(t)} g_{\boldsymbol{\lambda}_i}^{(t)}$ . The term  $g_{\boldsymbol{\lambda}_i}^{(t)}$  denotes the  $i^{th}$  component of  $\widehat{\nabla_{\boldsymbol{\lambda}} \mathcal{L}(\boldsymbol{\lambda}^{(t)})}$  and  $a_i^{(t)}$  is defined as:

$$a_i^{(t)} = \sqrt{\frac{E(\Delta_{\boldsymbol{\lambda}_i}^2)^{(t-1)} + \alpha}{E(g_{\boldsymbol{\lambda}_i}^2)^{(t)} + \alpha}}, \quad (\text{S37})$$

where  $\alpha$  is a small positive constant,  $E(\Delta_{\boldsymbol{\lambda}_i}^2)^{(t)}$  and  $E(g_{\boldsymbol{\lambda}_i}^2)^{(t)}$  are decayed moving average estimates of  $\Delta \boldsymbol{\lambda}_i^{(t)2}$  and  $g_{\boldsymbol{\lambda}_i}^{(t)2}$ , defined by

$$E(\Delta_{\boldsymbol{\lambda}_i}^2)^{(t)} = v E(\Delta_{\boldsymbol{\lambda}_i}^2)^{(t-1)} + (1-v) \Delta \boldsymbol{\lambda}_i^{(t)2}, \quad (\text{S38})$$

and

$$E(g_{\boldsymbol{\lambda}_i}^2)^{(t)} = v E(g_{\boldsymbol{\lambda}_i}^2)^{(t-1)} + (1-v) g_{\boldsymbol{\lambda}_i}^{(t)2}, \quad (\text{S39})$$

where the variable  $v$  is a decay constant. We use the default tuning parameter choices  $\alpha = 10^{-6}$  and  $v = 0.95$ , and initialize  $E(\Delta_{\boldsymbol{\lambda}_i}^2)^{(0)} = E(g_{\boldsymbol{\lambda}_i}^2)^{(0)} = 0$ .

## S4 Additional Derivation of HVB algorithms for estimating SEMs with missing data

### S4.1 Derivation of the reparameterisation gradient for HVB algorithm

Since  $\mathcal{L}(\boldsymbol{\lambda}) = E_q [\log p(\mathbf{y}_o, \mathbf{m} \mid \boldsymbol{\xi}, \boldsymbol{\psi}) + \log p(\boldsymbol{\xi}, \boldsymbol{\psi}) - \log q_{\boldsymbol{\lambda}}^0(\boldsymbol{\xi}, \boldsymbol{\psi})] = \mathcal{L}^0(\boldsymbol{\lambda})$  as shown in Equation (16) of the main paper. Then, the reparameterisation gradient of  $\mathcal{L}$  is the same as that of  $\mathcal{L}^0$ , given by

$$\nabla_{\boldsymbol{\lambda}} \mathcal{L}(\boldsymbol{\lambda}) = E_{f_{\boldsymbol{\delta}^0}} \left[ \frac{dt^0(\boldsymbol{\delta}^0, \boldsymbol{\lambda}_{s_m})^\top}{d\boldsymbol{\lambda}_{s_m}} \left( \nabla_{(\boldsymbol{\xi}^\top, \boldsymbol{\psi}^\top)^\top} \log p(\boldsymbol{\xi}, \boldsymbol{\psi}) \right. \right. \\ \left. \left. + \nabla_{(\boldsymbol{\xi}^\top, \boldsymbol{\psi}^\top)^\top} \log p(\mathbf{y}_o, \mathbf{m} \mid \boldsymbol{\xi}, \boldsymbol{\psi}) - \nabla_{(\boldsymbol{\xi}^\top, \boldsymbol{\psi}^\top)^\top} \log q_{\boldsymbol{\lambda}}^0(\boldsymbol{\theta}) \right) \right], \quad (\text{S40})$$

where, the random vector  $\boldsymbol{\delta}^0$  has density  $f_{\boldsymbol{\delta}^0}$ , which follows a standard normal, and does not depend on  $\boldsymbol{\lambda}_{s_m}$ , and  $t^0$  is the one-to-one vector-valued transformation from  $\boldsymbol{\delta}^0 = (\boldsymbol{\eta}^{0\top}, \boldsymbol{\epsilon}^{0\top})^\top$  to the parameter vector, such that  $(\boldsymbol{\xi}^\top, \boldsymbol{\psi}^\top)^\top = t^0(\boldsymbol{\delta}^0, \boldsymbol{\lambda}_{s_m}) = \boldsymbol{\mu}_{s_m} + \mathbf{B}_{s_m} \boldsymbol{\eta}^0 + \mathbf{d}_{s_m} \circ \boldsymbol{\epsilon}^0$ .

Then, the Fisher's identity is given by

$$\nabla_{(\boldsymbol{\xi}^\top, \boldsymbol{\psi}^\top)^\top} \log p(\mathbf{y}_o, \mathbf{m} \mid \boldsymbol{\xi}, \boldsymbol{\psi}) = \int \nabla_{(\boldsymbol{\xi}^\top, \boldsymbol{\psi}^\top)^\top} [\log (p(\mathbf{y}_o, \mathbf{m} \mid \mathbf{y}_u, \boldsymbol{\xi}, \boldsymbol{\psi}) p(\mathbf{y}_u \mid \boldsymbol{\xi}))] \\ p(\mathbf{y}_u \mid \mathbf{y}_o, \mathbf{m}, \boldsymbol{\xi}, \boldsymbol{\psi}) d\mathbf{y}_u, \quad (\text{S41})$$

see Poyiadjis et al. (2011). Substituting this expression into Equation (S40), and writing  $E_{f_{\boldsymbol{\delta}}}(\cdot)$  for expectation with respect to  $f_{\boldsymbol{\delta}}(\boldsymbol{\delta}) = f_{\boldsymbol{\delta}^0}(\boldsymbol{\delta}^0) p(\mathbf{y}_u \mid \mathbf{y}_o, \mathbf{m}, \boldsymbol{\xi}, \boldsymbol{\psi})$  and because

$h(\boldsymbol{\xi}, \boldsymbol{\psi}, \mathbf{y}_u) = p(\mathbf{y}_o, \mathbf{m} \mid \mathbf{y}_u, \boldsymbol{\xi}, \boldsymbol{\psi})p(\mathbf{y}_u \mid \boldsymbol{\xi})p(\boldsymbol{\xi}, \boldsymbol{\psi})$ , we get

$$\begin{aligned}
\nabla_{\boldsymbol{\lambda}} \mathcal{L}(\boldsymbol{\lambda}) &= E_{f_{\boldsymbol{\delta}}} \left[ \frac{dt^0(\boldsymbol{\delta}^0, \boldsymbol{\lambda}_{s_m})^\top}{d\boldsymbol{\lambda}_{s_m}} \left( \nabla_{(\boldsymbol{\xi}^\top, \boldsymbol{\psi}^\top)^\top} \log p(\boldsymbol{\xi}, \boldsymbol{\psi}) \right. \right. \\
&\quad + \nabla_{(\boldsymbol{\xi}^\top, \boldsymbol{\psi}^\top)^\top} \log p(\mathbf{y}_u \mid \boldsymbol{\xi}) + \nabla_{(\boldsymbol{\xi}^\top, \boldsymbol{\psi}^\top)^\top} \log p(\mathbf{y}_o, \mathbf{m} \mid \mathbf{y}_u, \boldsymbol{\xi}, \boldsymbol{\psi}) \\
&\quad \left. \left. - \nabla_{(\boldsymbol{\xi}^\top, \boldsymbol{\psi}^\top)^\top} \log q_{\boldsymbol{\lambda}}^0(\boldsymbol{\xi}, \boldsymbol{\psi}) \right) \right] \\
&= E_{f_{\boldsymbol{\delta}}} \left[ \frac{dt^0(\boldsymbol{\delta}^0, \boldsymbol{\lambda}_{s_m})^\top}{d\boldsymbol{\lambda}_{s_m}} \left( \nabla_{(\boldsymbol{\xi}^\top, \boldsymbol{\psi}^\top)^\top} \log h(\boldsymbol{\xi}, \boldsymbol{\psi}, \mathbf{y}_u) - \nabla_{(\boldsymbol{\xi}^\top, \boldsymbol{\psi}^\top)^\top} \log q_{\boldsymbol{\lambda}}^0(\boldsymbol{\xi}, \boldsymbol{\psi}) \right) \right]. \tag{S42}
\end{aligned}$$

The term  $\frac{dt^0(\boldsymbol{\delta}^0, \boldsymbol{\lambda}_{s_m})}{d\boldsymbol{\lambda}_{s_m}}$  in Equation (S42) is the derivative of the transformation  $t^0(\boldsymbol{\delta}^0, \boldsymbol{\lambda}_{s_m}) = \boldsymbol{\mu}_{s_m} + \mathbf{B}_{s_m} \boldsymbol{\eta}^0 + \mathbf{d}_{s_m} \circ \boldsymbol{\epsilon}^0$  with respect to the variational parameters  $\boldsymbol{\lambda}_{s_m} = (\boldsymbol{\mu}_{s_m}^\top, \text{vech}(\mathbf{B}_{s_m})^\top, \mathbf{d}_{s_m}^\top)^\top$ . We can express that  $t^0(\boldsymbol{\delta}^0, \boldsymbol{\lambda}_{s_m}) = \boldsymbol{\mu}_{s_m} + (\boldsymbol{\eta}^0 \otimes \mathbf{I}_{s_m}) \text{vech}(\mathbf{B}_{s_m}) + \mathbf{d}_{s_m} \circ \boldsymbol{\epsilon}^0$ , where  $\mathbf{I}_{s_m}$  is the identity matrix of size  $s_m$ , and it can be further shown that  $\nabla_{(\boldsymbol{\xi}^\top, \boldsymbol{\psi}^\top)^\top} \log q_{\boldsymbol{\lambda}}^0(\boldsymbol{\xi}, \boldsymbol{\psi}) = -(\mathbf{B}_{s_m} \mathbf{B}_{s_m}^\top + \mathbf{D}_{s_m}^2)^{-1}((\boldsymbol{\xi}^\top, \boldsymbol{\psi}^\top)^\top - \boldsymbol{\mu}_{s_m})$ ,

$$\frac{dt^0(\boldsymbol{\delta}^0, \boldsymbol{\lambda}_{s_m})}{d\boldsymbol{\mu}_{s_m}} = \mathbf{I}_{s_m} \quad \text{and} \quad \frac{dt^0(\boldsymbol{\delta}^0, \boldsymbol{\lambda}_{s_m})}{d\text{vech}(\mathbf{B}_{s_m})} = \boldsymbol{\eta}^{0\top} \otimes \mathbf{I}_{s_m}. \tag{S43}$$

Then the derivatives of  $\mathcal{L}(\boldsymbol{\lambda})$  with respect to  $\boldsymbol{\mu}_{s_m}$ ,  $\text{vech}(\mathbf{B}_{s_m})$ , and  $\mathbf{d}_{s_m}$  are:

$$\begin{aligned}
\nabla_{\boldsymbol{\mu}_{s_m}} \mathcal{L}(\boldsymbol{\lambda}) &= E_{f_{\boldsymbol{\delta}}} [\nabla_{(\boldsymbol{\xi}^\top, \boldsymbol{\psi}^\top)^\top} \log h(\boldsymbol{\mu}_{s_m} + \mathbf{B}_{s_m} \boldsymbol{\eta}^0 + \mathbf{d}_{s_m} \circ \boldsymbol{\epsilon}^0, \mathbf{y}_u) \\
&\quad + (\mathbf{B}_{s_m} \mathbf{B}_{s_m}^\top + \mathbf{D}_{s_m}^2)^{-1}(\mathbf{B}_{s_m} \boldsymbol{\eta}^0 + \mathbf{d}_{s_m} \circ \boldsymbol{\epsilon}^0)], \tag{S44}
\end{aligned}$$

$$\begin{aligned}
\nabla_{\text{vech}(\mathbf{B}_{s_m})} \mathcal{L}(\boldsymbol{\lambda}) &= E_{f_{\boldsymbol{\delta}}} [\nabla_{(\boldsymbol{\xi}^\top, \boldsymbol{\psi}^\top)^\top} \log h(\boldsymbol{\mu}_{s_m} + \mathbf{B}_{s_m} \boldsymbol{\eta}^0 + \mathbf{d}_{s_m} \circ \boldsymbol{\epsilon}^0, \mathbf{y}_u) \boldsymbol{\eta}^{0\top} \\
&\quad + (\mathbf{B}_{s_m} \mathbf{B}_{s_m}^\top + \mathbf{D}_{s_m}^2)^{-1}(\mathbf{B}_{s_m} \boldsymbol{\eta}^0 + \mathbf{d}_{s_m} \circ \boldsymbol{\epsilon}^0) \boldsymbol{\eta}^{0\top}], \tag{S45}
\end{aligned}$$

$$\begin{aligned}
\nabla_{\mathbf{d}_{s_m}} \mathcal{L}(\boldsymbol{\lambda}) &= E_{f_{\boldsymbol{\delta}}} [\text{diag}(\nabla_{(\boldsymbol{\xi}^\top, \boldsymbol{\psi}^\top)^\top} \log h(\boldsymbol{\mu}_{s_m} + \mathbf{B}_{s_m} \boldsymbol{\eta}^0 + \mathbf{d}_{s_m} \circ \boldsymbol{\epsilon}^0, \mathbf{y}_u) \boldsymbol{\epsilon}^{0\top} \\
&\quad + (\mathbf{B}_{s_m} \mathbf{B}_{s_m}^\top + \mathbf{D}_{s_m}^2)^{-1}(\mathbf{B}_{s_m} \boldsymbol{\eta}^0 + \mathbf{d}_{s_m} \circ \boldsymbol{\epsilon}^0) \boldsymbol{\epsilon}^{0\top})]. \tag{S46}
\end{aligned}$$

The expressions for  $\nabla_{(\boldsymbol{\xi}^\top, \boldsymbol{\psi}^\top)^\top} \log h(\boldsymbol{\mu}_{s_m} + \mathbf{B}_{s_m} \boldsymbol{\eta}^0 + \mathbf{d}_{s_m} \circ \boldsymbol{\epsilon}^0, \mathbf{y}_u) = \nabla_{(\boldsymbol{\xi}^\top, \boldsymbol{\psi}^\top)^\top} \log h(\boldsymbol{\xi}, \boldsymbol{\psi}, \mathbf{y}_u)$  in Equations (S44)-(S46) can be found in Section S4.3. The expectations in these gradients are estimated using a single sample of  $\boldsymbol{\delta} = (\boldsymbol{\delta}^{0\top}, \mathbf{y}_u^\top)^\top$ , which is drawn from  $f_{\boldsymbol{\delta}^0}$ , and  $p(\mathbf{y}_u \mid \boldsymbol{\xi}, \boldsymbol{\psi}, \mathbf{y}_o, \mathbf{m}) = p(\mathbf{y}_u \mid t^0(\boldsymbol{\delta}^0, \boldsymbol{\lambda}_{s_m}), \mathbf{y}_o, \mathbf{m})$ ; see

Wijayawardhana et al. (2025) for further details.

## S4.2 HVB-AllB algorithm

This section presents the HVB-AllB algorithm for estimating SEMs with missing values, which is particularly suited for cases where both  $n$  and  $n_u$  are large.

The MCMC steps in Algorithm 2 of the main paper generates samples from the conditional distribution  $p(\mathbf{y}_u \mid \mathbf{y}_o, \mathbf{m}, \boldsymbol{\xi}, \boldsymbol{\psi})$ . However, as  $n$  and  $n_u$  increase, the HVB algorithm implemented using these MCMC steps does not estimate the parameters accurately because of the low acceptance percentage. To improve the acceptance percentage, we partition  $\mathbf{y}_u$  into  $k$  blocks and update one block at a time.

We start with partitioning the unobserved responses vector into  $k$  blocks, such that  $\mathbf{y}_u = (\mathbf{y}_{u_1}^\top, \dots, \mathbf{y}_{u_k}^\top)^\top$ . Using proposals from  $p(\mathbf{y}_{u_j} \mid \boldsymbol{\xi}^{(t)}, \mathbf{y}_o, \mathbf{y}_u^{(-j)})$ , the Algorithm S2 outlines the MCMC steps for sampling the missing values one block at a time, for  $j = 1, \dots, k$ , where  $\mathbf{y}_{u_j}$  is the updated block and  $\mathbf{y}_u^{(-j)} = (\mathbf{y}_{u_1}^\top, \dots, \mathbf{y}_{u_{j-1}}^\top, \mathbf{y}_{u_{j+1}}^\top, \dots, \mathbf{y}_{u_k}^\top)^\top$  is the remaining blocks. The complete response vector  $\mathbf{y}$  can now be written as  $\mathbf{y} = (\mathbf{y}_{s_j}^\top, \mathbf{y}_{u_j}^\top)^\top$ , where  $\mathbf{y}_{s_j} = (\mathbf{y}_o^\top, \mathbf{y}_u^{(-j)^\top})^\top$ . Based on this partitioning of  $\mathbf{y}$ , the following partitioned vector and matrices are defined:

$$\mathbf{r} = \begin{pmatrix} \mathbf{r}_{s_j} \\ \mathbf{r}_{u_j} \end{pmatrix}, \quad \mathbf{X} = \begin{pmatrix} \mathbf{X}_{s_j} \\ \mathbf{X}_{u_j} \end{pmatrix}, \quad \mathbf{M} = \begin{pmatrix} \mathbf{M}_{s_j s_j} & \mathbf{M}_{s_j u_j} \\ \mathbf{M}_{u_j s_j} & \mathbf{M}_{u_j u_j} \end{pmatrix}, \quad (\text{S47})$$

where  $\mathbf{r}_{s_j}$  is the corresponding sub-vector of  $\mathbf{r}$  for the observed responses ( $\mathbf{y}_o$ ), and the unobserved responses that are not in the  $j^{th}$  block ( $\mathbf{y}_u^{(-j)}$ ). i.e.  $\mathbf{r}_{s_j} = (\mathbf{r}_o^\top, \mathbf{r}_{u^{(-j)}}^\top)^\top$  and  $\mathbf{r}_{u_j}$  is the corresponding sub vector of  $\mathbf{r}$  for  $j^{th}$  block of unobserved responses,  $\mathbf{y}_{u_j}$ . Similarly,  $\mathbf{X}_{s_j}$  and  $\mathbf{X}_{u_j}$  are represent the sub-matrices of  $\mathbf{X}$ , and  $\mathbf{M}_{s_j s_j}$ ,  $\mathbf{M}_{s_j u_j}$ ,  $\mathbf{M}_{u_j s_j}$ , and  $\mathbf{M}_{u_j u_j}$  are sub-matrices of  $\mathbf{M}$ .

In step 4 of the Algorithm S2, proposals from the conditional distributions,  $p(\tilde{\mathbf{y}}_{u_j} \mid \boldsymbol{\xi}^{(t)}, \mathbf{y}_{s_j})$  needs to be generated. For the SEM-Gau, and SEM-t, this distribution follows a multivariate Gaussian distribution with the mean  $\mathbf{X}_{u_j} \boldsymbol{\beta} - \mathbf{M}_{u_j u_j}^{-1} \mathbf{M}_{u_j s_j} \mathbf{r}_{s_j}$  and the covariance matrix  $\sigma_e^2 \mathbf{M}_{u_j u_j}^{-1}$ .

---

**Algorithm S2** MCMC steps within the  $t^{th}$  iteration of the HVB algorithm under MNAR. The missing values are updated one block at a time.

---

```

1: Initialise missing values  $\mathbf{y}_{u,0} = (\mathbf{y}_{u_1,0}^\top, \dots, \mathbf{y}_{u_k,0}^\top)^\top \sim p(\mathbf{y}_u \mid \boldsymbol{\xi}^{(t)}, \mathbf{y}_o)$ 
2: for  $i=1, \dots, N_1$  do
3:   for  $j=1, \dots, k$  do
4:     Sample  $\tilde{\mathbf{y}}_{u_j}$  from the proposal distribution  $p(\tilde{\mathbf{y}}_{u_j} \mid \boldsymbol{\xi}^{(t)}, \mathbf{y}_o, \mathbf{y}_{u,i-1}^{(-j)})$ , where  $\mathbf{y}_{u,i-1}^{(-j)} = (\mathbf{y}_{u_1,i}^\top, \mathbf{y}_{u_2,i}^\top, \dots, \mathbf{y}_{u_{j-1},i}^\top, \mathbf{y}_{u_{j+1},i-1}^\top, \dots, \mathbf{y}_{u_k,i-1}^\top)^\top$ .
5:     Sample  $u$  from uniform distribution,  $u \sim \mathcal{U}(0, 1)$ 
6:     Calculate  $a = \min\left(1, \frac{p(\mathbf{m}|\tilde{\mathbf{y}}, \boldsymbol{\psi}^{(t)})}{p(\mathbf{m}|\mathbf{y}_{i-1}, \boldsymbol{\psi}^{(t)})}\right)$ , where  $\tilde{\mathbf{y}} = (\mathbf{y}_o^\top, \mathbf{y}_u^{(-j)\top}, \tilde{\mathbf{y}}_{u_j}^\top)^\top$  and  $\mathbf{y}_{i-1} = (\mathbf{y}_o^\top, \mathbf{y}_u^{(-j)\top}, \mathbf{y}_{u_{j-1}}^\top)^\top$ 
7:     if  $a > u$  then
8:        $\mathbf{y}_{u_j,i} = \mathbf{y}_{u_j}^*$ 
9:     else
10:       $\mathbf{y}_{u_j,i} = \mathbf{y}_{u_j,i-1}$ 
11:    end if
12:  end for
13:   $\mathbf{y}_{u,i} = (\mathbf{y}_{u_1,i}^\top, \dots, \mathbf{y}_{u_k,i}^\top)^\top$ 
14: end for
15: Output  $\mathbf{y}_u^{(t)} = \mathbf{y}_{u,N_1}$ 

```

---

For YJ-SEM-Gau and YJ-SEM-t, the proposals are generated in two steps. First, we sample  $\tilde{\mathbf{y}}_{u_j}^*$  from the full conditional distribution  $p(\tilde{\mathbf{y}}_{u_j}^* \mid \boldsymbol{\xi}^{(t)}, \mathbf{y}_{s_j})$ , which follows a multivariate Gaussian with the mean vector given by  $\mathbf{X}_{u_j}\boldsymbol{\beta} - \mathbf{M}_{u_j u_j}^{-1}\mathbf{M}_{u_j s_j}(\mathbf{y}_{s_j}^* - \mathbf{X}_{s_j}\boldsymbol{\beta})$  and the covariance matrix  $\sigma_e^2 \mathbf{M}_{u_j u_j}^{-1}$ , where  $\mathbf{y}_{s_j}^* = t_\gamma(\mathbf{y}_{s_j})$ . Then, we apply the inverse Yeo-Johnson (YJ) transformation to obtain the final proposal:  $\tilde{\mathbf{y}}_{u_j} = t_\gamma^{-1}(\tilde{\mathbf{y}}_{u_j}^*)$ .

### S4.3 Expressions for $\nabla_{(\boldsymbol{\xi}^\top, \boldsymbol{\psi}^\top)^\top} \log h(\boldsymbol{\xi}, \boldsymbol{\psi}, \mathbf{y}_u)$

This section presents the derivatives  $\nabla_{(\boldsymbol{\xi}^\top, \boldsymbol{\psi}^\top)^\top} \log h(\boldsymbol{\xi}, \boldsymbol{\psi}, \mathbf{y}_u)$ , which are required to compute the gradients of the reparameterised ELBO, defined in Equation (17) of the main paper for different SEMs with missing data.

#### S4.3.1 Derivatives for SEM-Gau

For SEM-Gau with missing data,  $h(\boldsymbol{\xi}, \boldsymbol{\psi}, \mathbf{y}_u) = p(\mathbf{y} \mid \boldsymbol{\phi})p(\mathbf{m} \mid \mathbf{y}, \boldsymbol{\psi})p(\boldsymbol{\phi})p(\boldsymbol{\psi})$ , where  $\boldsymbol{\phi} = (\boldsymbol{\beta}^\top, \sigma_e^2, \rho)^\top$ . The logarithm of  $h(\boldsymbol{\xi}, \boldsymbol{\psi}, \mathbf{y}_u)$  is  $\log p(\mathbf{y} \mid \boldsymbol{\phi}) + \log p(\mathbf{m} \mid \mathbf{y}, \boldsymbol{\psi}) + \log p(\boldsymbol{\phi}) + \log p(\boldsymbol{\psi})$ . Note that, for  $\sigma_e^2$ , and  $\rho$ , we utilise the transformations described in Section 4 of the main paper, and put prior on the transformed parameters as in Table S3.

This leads to

$$\begin{aligned} \log h(\boldsymbol{\xi}, \boldsymbol{\psi}, \mathbf{y}_u) &\propto -\frac{n}{2}\omega' + \frac{1}{2}\log|\mathbf{M}| - \frac{e^{-\omega'}}{2}\mathbf{r}^\top \mathbf{M}\mathbf{r} \\ &+ \sum_{i=1}^n m_i(\mathbf{x}_i^* \boldsymbol{\psi}_x + y_i \boldsymbol{\psi}_y) - \log(1 + e^{(\mathbf{x}_i^* \boldsymbol{\psi}_x + y_i \boldsymbol{\psi}_y)}) \\ &- \frac{\boldsymbol{\beta}^\top \boldsymbol{\beta}}{2\sigma_{\boldsymbol{\beta}}^2} - \frac{\omega'^2}{2\sigma_{\omega'}^2} - \frac{\rho'^2}{2\sigma_{\rho'}^2} - \frac{\boldsymbol{\psi}^\top \boldsymbol{\psi}}{2\sigma_{\boldsymbol{\psi}}^2}, \end{aligned} \quad (\text{S48})$$

where the values of  $\sigma_{\boldsymbol{\beta}}^2$ ,  $\sigma_{\omega'}^2$ ,  $\sigma_{\rho'}^2$ , and  $\sigma_{\boldsymbol{\psi}}^2$  are each set to 100, as detailed in Table S3, while  $\mathbf{r}$  and  $\mathbf{M}$  are provided in Table S1.

The derivatives of  $\log h(\boldsymbol{\xi}, \boldsymbol{\psi}, \mathbf{y}_u)$  in Equation (S48) with respect to  $\boldsymbol{\beta}$ ,  $\omega'$ , and  $\rho'$  are similar to that of without missing data given in Equations (S15), (S16), and (S17), respectively. The derivative of  $\log h(\boldsymbol{\xi}, \boldsymbol{\psi}, \mathbf{y}_u)$  with respect to  $\boldsymbol{\psi}$  is

$$\frac{\partial \log h(\boldsymbol{\xi}, \boldsymbol{\psi}, \mathbf{y}_u)}{\partial \boldsymbol{\psi}} = \sum_{i=1}^n \left( m_i - \frac{e^{\mathbf{x}_i^* \top \boldsymbol{\psi}_x + y_i \boldsymbol{\psi}_y}}{1 + e^{\mathbf{x}_i^* \top \boldsymbol{\psi}_x + y_i \boldsymbol{\psi}_y}} \right) \mathbf{z}_i - \frac{\boldsymbol{\psi}^\top}{\sigma_{\boldsymbol{\psi}}^2}, \quad (\text{S49})$$

where  $\mathbf{z}_i = (\mathbf{x}_i^*, y_i)$  is the vector containing the  $i^{th}$  row vector of matrix  $\mathbf{X}^*$ , and the  $i^{th}$  element of the vector  $\mathbf{y}$ , see Section 2.3 of the main paper.

#### S4.3.2 Derivatives for SEM-t

For SEM-t with missing data,  $h(\boldsymbol{\xi}, \boldsymbol{\psi}, \mathbf{y}_u) = p(\mathbf{y} \mid \boldsymbol{\tau}, \boldsymbol{\phi})p(\mathbf{m} \mid \mathbf{y}, \boldsymbol{\psi})p(\boldsymbol{\tau} \mid \boldsymbol{\phi})p(\boldsymbol{\phi})p(\boldsymbol{\psi})$ , where  $\boldsymbol{\phi} = (\boldsymbol{\beta}^\top, \sigma_{\boldsymbol{\epsilon}}^2, \nu, \rho)^\top$ . The logarithm of  $h(\boldsymbol{\xi}, \boldsymbol{\psi}, \mathbf{y}_u)$  is  $\log p(\mathbf{y} \mid \boldsymbol{\tau}, \boldsymbol{\phi}) + \log p(\mathbf{m} \mid \mathbf{y}, \boldsymbol{\psi}) + \log p(\boldsymbol{\tau} \mid \boldsymbol{\phi}) + \log p(\boldsymbol{\phi}) + \log p(\boldsymbol{\psi})$ . Note that, for  $\sigma_{\boldsymbol{\epsilon}}^2$ ,  $\rho$ , and  $\nu$ , we utilise the transformations described in Section 4 of the main paper, and put prior on the transformed parameters as in Table S3. This leads to

$$\begin{aligned} \log h(\boldsymbol{\xi}, \boldsymbol{\psi}, \mathbf{y}_u) &\propto -\frac{n}{2}\omega' + \frac{1}{2}\log|\mathbf{M}| - \frac{e^{-\omega'}}{2}\mathbf{r}^\top \mathbf{M}\mathbf{r} \\ &+ \sum_{i=1}^n m_i(\mathbf{x}_i^* \boldsymbol{\psi}_x + y_i \boldsymbol{\psi}_y) - \log(1 + e^{(\mathbf{x}_i^* \boldsymbol{\psi}_x + y_i \boldsymbol{\psi}_y)}) \\ &+ \sum_{i=1}^n \log p(\tau_i \mid \nu) + \log \left| \frac{\partial \tau_i}{\partial \tau'_i} \right| - \frac{\boldsymbol{\beta}^\top \boldsymbol{\beta}}{2\sigma_{\boldsymbol{\beta}}^2} - \frac{\omega'^2}{2\sigma_{\omega'}^2} - \frac{\rho'^2}{2\sigma_{\rho'}^2} - \frac{\nu'^2}{2\sigma_{\nu'}^2}, \end{aligned} \quad (\text{S50})$$

where the values of  $\sigma_{\boldsymbol{\beta}}^2$ ,  $\sigma_{\omega'}^2$ ,  $\sigma_{\rho'}^2$ ,  $\sigma_{\nu'}^2$ , and  $\sigma_{\boldsymbol{\psi}}^2$  are each set to 100, as detailed in Table S3,

while  $\mathbf{r}$  and  $\mathbf{M}$  are provided in Table S1.

The derivatives of  $\log h(\boldsymbol{\xi}, \boldsymbol{\psi}, \mathbf{y}_u)$  in Equation (S50) with respect to  $\boldsymbol{\beta}$ ,  $\omega'$ ,  $\rho'$ ,  $\nu'$  and  $\tau'_i$  are similar to that of without missing data given in Equations (S19), (S20), (S21), (S22), and (S23), respectively. The derivative of  $\log h(\boldsymbol{\xi}, \boldsymbol{\psi}, \mathbf{y}_u)$  with respect to  $\boldsymbol{\psi}$  is similar to that of SEM-Gau given in Equation (S49).

#### S4.3.3 Derivatives for YJ-SEM-Gau

For YJ-SEM-Gau with missing data,  $h(\boldsymbol{\xi}, \boldsymbol{\psi}, \mathbf{y}_u) = p(\mathbf{y} \mid \boldsymbol{\phi})p(\mathbf{m} \mid \mathbf{y}, \boldsymbol{\psi})p(\boldsymbol{\phi})p(\boldsymbol{\psi})$ , where  $\boldsymbol{\phi} = (\boldsymbol{\beta}^\top, \sigma_e^2, \rho, \gamma)^\top$ . The logarithm of  $h(\boldsymbol{\xi}, \boldsymbol{\psi}, \mathbf{y}_u)$  is  $\log p(\mathbf{y} \mid \boldsymbol{\phi}) + \log p(\mathbf{m} \mid \mathbf{y}, \boldsymbol{\psi}) + \log p(\boldsymbol{\phi}) + \log p(\boldsymbol{\psi})$ . Note that, for  $\sigma_e^2$ ,  $\rho$ , and  $\gamma$ , we utilise the transformations described in Section 4 of the main paper, and put prior on the transformed parameters as in Table S3. This leads to

$$\begin{aligned} \log h(\boldsymbol{\xi}, \boldsymbol{\psi}, \mathbf{y}_u) \propto & -\frac{n}{2}\omega' + \frac{1}{2}\log|\mathbf{M}| - \frac{e^{-\omega'}}{2}\mathbf{r}^\top \mathbf{M}\mathbf{r} + \sum_{i=1}^n \log\left(\frac{dt_\gamma(y_i)}{dy_i}\right) \\ & + \sum_{i=1}^n m_i(\mathbf{x}_i^* \boldsymbol{\psi}_x + y_i \boldsymbol{\psi}_y) - \log(1 + e^{(\mathbf{x}_i^* \boldsymbol{\psi}_x + y_i \boldsymbol{\psi}_y)}) \\ & - \frac{\boldsymbol{\beta}^\top \boldsymbol{\beta}}{2\sigma_{\beta}^2} - \frac{\omega'^2}{2\sigma_{\omega'}^2} - \frac{\rho'^2}{2\sigma_{\rho'}^2} - \frac{\gamma'^2}{2\sigma_{\gamma'}^2} - \frac{\boldsymbol{\psi}^\top \boldsymbol{\psi}}{2\sigma_{\psi}^2}, \end{aligned} \quad (\text{S51})$$

where the values of  $\sigma_{\beta}^2$ ,  $\sigma_{\omega'}^2$ ,  $\sigma_{\rho'}^2$ ,  $\sigma_{\nu'}^2$ ,  $\sigma_{\gamma'}^2$ , and  $\sigma_{\psi}^2$  are each set to 100, as detailed in Table S3, while  $\mathbf{r}$  and  $\mathbf{M}$  are provided in Table S1.

The derivatives of  $\log h(\boldsymbol{\xi}, \boldsymbol{\psi}, \mathbf{y}_u)$  in Equation (S51) with respect to  $\boldsymbol{\beta}$ ,  $\omega'$ ,  $\rho'$ , and  $\gamma'$  are similar to that of without missing data given in Equations (S25), (S26), (S27), and (S28), respectively. The derivative of  $\log h(\boldsymbol{\xi}, \boldsymbol{\psi}, \mathbf{y}_u)$  with respect to  $\boldsymbol{\psi}$  is similar to that of SEM-Gau given in Equation (S49).

#### S4.3.4 Derivatives for YJ-SEM-t

For YJ-SEM-t with missing data,  $h(\boldsymbol{\xi}, \boldsymbol{\psi}, \mathbf{y}_u) = p(\mathbf{y} \mid \boldsymbol{\tau}, \boldsymbol{\phi})p(\mathbf{m} \mid \mathbf{y}, \boldsymbol{\psi})p(\boldsymbol{\tau} \mid \boldsymbol{\phi})p(\boldsymbol{\phi})p(\boldsymbol{\psi})$ , where  $\boldsymbol{\phi} = (\boldsymbol{\beta}^\top, \sigma_e^2, \rho, \nu, \gamma)^\top$ . The logarithm of  $h(\boldsymbol{\xi}, \boldsymbol{\psi}, \mathbf{y}_u)$  is  $\log p(\mathbf{y} \mid \boldsymbol{\tau}, \boldsymbol{\phi}) + \log p(\mathbf{m} \mid \mathbf{y}, \boldsymbol{\psi}) + \log p(\boldsymbol{\tau} \mid \boldsymbol{\phi}) + \log p(\boldsymbol{\phi}) + \log p(\boldsymbol{\psi})$ . Note that, for  $\sigma_e^2$ ,  $\rho$ ,  $\nu$ , and  $\gamma$ , we utilise the transformations described in Section 4 of the main paper, and put prior on the

transformed parameters as in Table S3. This leads to

$$\begin{aligned}
\log h(\boldsymbol{\xi}, \boldsymbol{\psi}, \mathbf{y}_u) \propto & -\frac{n}{2}\omega' + \frac{1}{2}\log|\mathbf{M}| - \frac{e^{-\omega'}}{2}\mathbf{r}^\top \mathbf{M}\mathbf{r} + \sum_{i=1}^n \log \left( \frac{dt_\gamma(y_i)}{dy_i} \right) \\
& + \sum_{i=1}^n m_i(\mathbf{x}_i^* \boldsymbol{\psi}_x + y_i \boldsymbol{\psi}_y) - \log(1 + e^{(\mathbf{x}_i^* \boldsymbol{\psi}_x + y_i \boldsymbol{\psi}_y)}) \\
& + \sum_{i=1}^n \log p(\tau_i \mid \nu) + \log \left| \frac{\partial \tau_i}{\partial \tau'_i} \right| - \frac{\boldsymbol{\beta}^\top \boldsymbol{\beta}}{2\sigma_{\boldsymbol{\beta}}^2} - \frac{\omega'^2}{2\sigma_{\omega'}^2} - \frac{\rho'^2}{2\sigma_{\rho'}^2} - \frac{\nu'^2}{2\sigma_{\nu'}^2} - \frac{\gamma'^2}{2\sigma_{\gamma'}^2},
\end{aligned} \tag{S52}$$

where the values of  $\sigma_{\boldsymbol{\beta}}^2$ ,  $\sigma_{\omega'}^2$ ,  $\sigma_{\rho'}^2$ ,  $\sigma_{\nu'}^2$ ,  $\sigma_{\gamma'}^2$ , and  $\sigma_{\psi}^2$  are each set to 100, as detailed in Table S3, while  $\mathbf{r}$  and  $\mathbf{M}$  are provided in Table S1.

The derivatives of  $\log h(\boldsymbol{\xi}, \boldsymbol{\psi}, \mathbf{y}_u)$  in Equation S52 with respect to  $\boldsymbol{\beta}$ ,  $\omega'$ ,  $\rho'$ ,  $\nu'$ ,  $\gamma'$  and  $\tau'_i$  are similar to that of without missing data given in Equations (S30), (S31), (S32), (S33), (S34), and (S35), respectively. The derivative of  $\log h(\boldsymbol{\xi}, \boldsymbol{\psi}, \mathbf{y}_u)$  with respect to  $\boldsymbol{\psi}$  is similar to that of SEM-Gau given in Equation (S49).

## S5 Bayesian model comparison of spatial error models

This section presents expressions for the term  $\log p(\mathbf{y} \mid \boldsymbol{\phi})$ , which are used to compute the Deviance Information Criterion (DIC) (Celeux et al., 2006) for the various SEMs discussed in Section 3.3 of the main paper.

Note that for SEM-Gau, and YJ-SEM-Gau,  $\boldsymbol{\xi} = \boldsymbol{\phi}$ , meaning for these two models  $p(\mathbf{y} \mid \boldsymbol{\phi}) = p(\mathbf{y} \mid \boldsymbol{\xi})$ . For the SEM-Gau model,  $p(\mathbf{y} \mid \boldsymbol{\xi})$  is Gaussian; see Section 2.1 of the main paper. The log-likelihood is given by:

$$\log p(\mathbf{y} \mid \boldsymbol{\phi}) = -\frac{n}{2}\log(2\pi) - \frac{n}{2}\log(\sigma_e^2) + \frac{1}{2}\log|\mathbf{M}| - \frac{1}{2\sigma_e^2}\mathbf{r}^\top \mathbf{M}\mathbf{r}, \tag{S53}$$

where  $\mathbf{M}$ , and  $\mathbf{r}$  are given in Table S1.

For the YJ-SEM-Gau,  $p(\mathbf{y} \mid \boldsymbol{\phi}) = p(\mathbf{y} \mid \boldsymbol{\xi})$  is derived in Section 2.2 of the main paper,

and the log-likelihood is given by:

$$\begin{aligned}\log p(\mathbf{y} \mid \boldsymbol{\phi}) &= -\frac{n}{2} \log(2\pi) - \frac{n}{2} \log(\sigma_e^2) + \frac{1}{2} \log|\mathbf{M}| - \frac{1}{2\sigma_e^2} \mathbf{r}^\top \mathbf{M} \mathbf{r} \\ &\quad + \sum_{i=1}^n \log \left( \frac{dt_\gamma(y_i)}{dy_i} \right),\end{aligned}\tag{S54}$$

where  $\mathbf{M}$ , and  $\mathbf{r}$  are given in Table S1, while  $\frac{dt_\gamma(y_i)}{dy_i}$  is given in Equation (S2).

For the SEM-t model,

$$p(\mathbf{y} \mid \boldsymbol{\phi}) = \int_0^\infty \dots \int_0^\infty p(\mathbf{y} \mid \boldsymbol{\tau}, \boldsymbol{\phi}) p(\tau_1 \mid \boldsymbol{\phi}) \dots p(\tau_n \mid \boldsymbol{\phi}) d\tau_1 \dots d\tau_n \tag{S55}$$

where  $p(\mathbf{y} \mid \boldsymbol{\tau}, \boldsymbol{\phi})$  is multivariate Gaussian, with its mean vector and covariance matrix specified in Table S1. Each  $p(\tau_i \mid \boldsymbol{\phi})$  (for  $i = 1, \dots, n$ ) follows an inverse gamma distribution with both shape and scale parameters equal to  $\nu/2$ ; see Section 2.1 of the main paper. This hierarchical representation implies that the marginal distribution  $p(\mathbf{y} \mid \boldsymbol{\phi})$  is a multivariate Student's  $t$ -distribution with mean vector  $\mathbf{X}\boldsymbol{\beta}$ , scale matrix  $\sigma_e^2(\mathbf{A}^\top \mathbf{A})^{-1}$ , and degrees of freedom  $\nu$ . The log-likelihood is given by:

$$\begin{aligned}\log p(\mathbf{y} \mid \boldsymbol{\phi}) &= \log \Gamma \left( \frac{\nu+2}{2} \right) - \log \Gamma \left( \frac{\nu}{2} \right) + \frac{1}{2} \log|\mathbf{A}^\top \mathbf{A}| \\ &\quad - \frac{n}{2} \log(\pi\nu\sigma_e^2) - \frac{(n+\nu)}{2} \log \left( 1 + \frac{1}{\nu\sigma_e^2} \mathbf{r}^\top \mathbf{A}^\top \mathbf{A} \mathbf{r} \right),\end{aligned}\tag{S56}$$

where  $\mathbf{r} = \mathbf{y} - \mathbf{X}\boldsymbol{\beta}$ .

Similarly, logarithm of  $p(\mathbf{y} \mid \boldsymbol{\phi})$  for YJ-SEM-t can be derived as

$$\begin{aligned}\log p(\mathbf{y} \mid \boldsymbol{\phi}) &= \log \Gamma \left( \frac{\nu+2}{2} \right) - \log \Gamma \left( \frac{\nu}{2} \right) + \frac{1}{2} \log|\mathbf{A}^\top \mathbf{A}| \\ &\quad - \frac{n}{2} \log(\pi\nu\sigma_e^2) - \frac{(n+\nu)}{2} \log \left( 1 + \frac{1}{\nu\sigma_e^2} \mathbf{r}^\top \mathbf{A}^\top \mathbf{A} \mathbf{r} \right) \\ &\quad + \sum_{i=1}^n \log \left( \frac{dt_\gamma(y_i)}{dy_i} \right),\end{aligned}\tag{S57}$$

where  $\mathbf{r} = t_\gamma(\mathbf{y}) - \mathbf{X}\boldsymbol{\beta}$ .

## S6 Simulation study with full data SEMs

This section fits the SEM-Gau, SEM-t, YJ-SEM-Gau, and YJ-SEM-t models to simulated datasets 1 and 2 (without missing data) in Section 4.2 of the main paper, and evaluates how effectively these models, along with their VB estimation methods, capture the characteristics of these datasets.

The initial values for the VB algorithms are set as follows: The variational mean vector ( $\boldsymbol{\mu}$ ) is initialised using the estimates of  $\boldsymbol{\beta}$ ,  $\sigma_e^2$ , and  $\rho$  obtained from fitting the SEM-Gau model via maximum likelihood estimation (MLE). The initial values for  $\nu$  and  $\gamma$  are set to 4 and 1, respectively. For the variational covariance matrix parameters, the elements of  $\mathbf{B}$  and the diagonal elements of  $\mathbf{D}$  are all initialised to 0.01. We use  $p = 4$  factors.

After some experimentation, we found that the models with Student's  $t$  errors required a relatively large number of iterations to converge. This increased computational demand is attributed to the added complexity of estimating both the latent variables  $\boldsymbol{\tau}$  and the degrees of freedom parameter  $\nu$ . For simulated dataset 1, the VB algorithms were run for 10,000 iterations for both SEM-Gau and YJ-SEM-Gau, and 20,000 iterations for SEM-t and YJ-SEM-t. For simulated dataset 2, convergence was achieved after 10,000 iterations for SEM-Gau and YJ-SEM-Gau, and 40,000 iterations for SEM-t and YJ-SEM-t. Convergence is assessed visually by inspecting the variational mean plots over iterations, which are presented in Section S9.1. Then, we generate 10,000 draws of model parameters from the variational distribution  $q_{\boldsymbol{\lambda}}(\boldsymbol{\xi})$ .

Table S4 shows the posterior means and the 95% credible intervals for some of the model parameters of the SEM-Gau, SEM-t, YJ-SEM-Gau, and YJ-SEM-t models obtained using the Gaussian variational approximation method described in Section S2 applied to the simulated dataset 1. The table also includes the computation times (in seconds) for one VB iteration, as well as the  $DIC_1$  and  $DIC_2$  values for each model, calculated using Equations (18) and (19) of the main paper, respectively. The plots of posterior densities of the parameters are provided in Section S7.2.1.

We begin by comparing the estimated values of the fixed effects (specifically  $\beta_0$  and

$\beta_1$ ), the variance parameter  $\sigma_e^2$ , and the spatial autocorrelation parameter  $\rho$ , as these parameters are present in all four models. Accurate estimation of these parameters is crucial for interpreting the underlying spatial relationships and the effect of covariates on the response variable in SEMs. The posterior means for  $\beta_0$ ,  $\beta_1$  and  $\rho$  are nearly identical for YJ-SEM-Gau and YJ-SEM-t, closely matching the true values of  $-1$  for  $\beta_0$ ,  $1$  for  $\beta_1$ , and  $0.8$  for  $\rho$ . In contrast, the estimates from SEM-Gau and SEM-t show significant deviations from the true values. The estimated posterior means of  $\sigma_e^2$  from SEM-Gau, SEM-t, and YJ-SEM-Gau deviate considerably from the true value, while the posterior mean obtained from YJ-SEM-t is much closer to the true value, as expected. The models incorporating the YJ transformation, YJ-SEM-Gau and YJ-SEM-t, successfully recover the parameter  $\gamma$ . The degrees of freedom ( $\nu$ ) estimated by the SEM-t and YJ-SEM-t models show slight deviations from the true value.

For the simulated dataset 1, the model fit assessment indicates that YJ-SEM-t is the best-performing model, as it achieves the lowest  $DIC_1$  and  $DIC_2$  values among all four models. This outcome is expected, given that the dataset was simulated from YJ-SEM-t. The second-best model is YJ-SEM-Gau, which has the next lowest DIC values. Notably, the difference in DIC between YJ-SEM-t and YJ-SEM-Gau is minimal, suggesting that YJ-SEM-Gau provides a model fit nearly as good as YJ-SEM-t for this dataset.

Table S5 presents the posterior means and 95% credible intervals for selected model parameters obtained from the SEM-Gau, SEM-t, YJ-SEM-Gau, and YJ-SEM-t models applied to the simulated dataset 2, along with the computational cost for one VB iteration. The table also includes the  $DIC_1$  and  $DIC_2$  values for each model. Corresponding posterior density plots of the parameters are provided in Section S7.2.1. Unlike the simulated dataset 1, which is skewed and heavy tails, the simulated dataset 2 is more symmetrical with lighter tails. The posterior mean estimates for parameters  $\beta_0$ ,  $\beta_1$ ,  $\sigma_e^2$ , and  $\rho$  across all four models closely match their true values. Likewise, the posterior mean estimate of  $\nu$  for SEM-t and YJ-SEM-t is close to the true value of 30, while the posterior mean estimate of  $\gamma$  for YJ-SEM-Gau and YJ-SEM-t is close to the true value of 1. The overall accuracy of parameter estimation across all models is further supported

|                    | SEM-Gau                       | SEM-t                      | YJ-SEM-Gau                    | YJ-SEM-t                      |
|--------------------|-------------------------------|----------------------------|-------------------------------|-------------------------------|
| $\beta_0 = -1$     | 3.1962<br>(2.9423, 3.4453)    | 0.9017<br>(0.8048, 0.9978) | -1.0319<br>(-1.0709, -0.9931) | -1.0065<br>(-1.0391, -0.9742) |
| $\beta_1 = 1$      | 1.5352<br>(1.3089, 1.7603)    | 0.9097<br>(0.8079, 1.0136) | 0.9941<br>(0.9669, 1.0212)    | 0.9880<br>(0.9568, 1.0192)    |
| $\sigma_e^2 = 0.5$ | 58.4686<br>(56.0301, 60.9582) | 8.2516<br>(7.7781, 8.7454) | 1.0362<br>(0.9909, 1.0823)    | 0.6318<br>(0.6090, 0.6554)    |
| $\rho = 0.8$       | 0.2274<br>(0.1969, 0.2577)    | 0.1626<br>(0.1416, 0.1835) | 0.7945<br>(0.7832, 0.8053)    | 0.7925<br>(0.7798, 0.8048)    |
| $\nu = 4$          | NA                            | 3.0049<br>(3.0000, 3.0063) | NA                            | 5.9993<br>(5.7126, 6.3156)    |
| $\gamma = 0.5$     | NA                            | NA                         | 0.4964<br>(0.4918, 0.5010)    | 0.4985<br>(0.4954, 0.5016)    |
| DIC <sub>1</sub>   | 30328.85                      | 31535.42                   | 14734.73                      | 14732.85                      |
| DIC <sub>2</sub>   | 30328.34                      | 31655.98                   | 14737.32                      | 14732.32                      |
| CT                 | 0.1322                        | 0.1206                     | 0.6715                        | 0.7252                        |

Table S4: Posterior means and 95% credible intervals for selected parameters of different SEMs based on the simulated dataset 1 (full data), along with the computation time (CT) in seconds for one VB iteration. The table also presents the DIC values for each model. Parameters labeled as 'NA' indicate that they are not applicable to the corresponding model.

by the nearly identical DIC<sub>1</sub> and DIC<sub>2</sub> values, with SEM-Gau having the lowest values, indicating the best fit for the simulated dataset 2, as expected.

According to the computation times presented in Tables S4 and S5, VB algorithms for both SEM-t and YJ-SEM-t, which incorporate Student's *t* errors, require significantly more computation time compared to SEM-Gau and YJ-SEM-Gau. This is because, in models with *t* errors, the VB optimisation is substantially more complex than in models with Gaussian errors. Specifically, for models with Student's *t* errors, the set of model parameters is  $\xi = (\phi^\top, \tau^\top)^\top$ , whereas for models with Gaussian errors, it simplifies to  $\xi = \phi$ . Here,  $\tau$  is a latent variable vector of length *n*; see Section 2.1 of the main paper.

## S7 Additional figures for simulation study in Section 4

This section provides additional figures related to the simulation study presented in Section 4 of the main paper, and Section S6.

|                    | SEM-Gau                       | SEM-t                         | YJ-SEM-Gau                    | YJ-SEM-t                      |
|--------------------|-------------------------------|-------------------------------|-------------------------------|-------------------------------|
| $\beta_0 = -3$     | -2.9976<br>(-3.0258, -2.9692) | -3.0008<br>(-3.0305, -2.9707) | -2.9781<br>(-3.0108, -2.9449) | -2.9808<br>(-3.0033, -2.9584) |
| $\beta_1 = 2$      | 1.9968<br>(1.9773, 2.0161)    | 1.9947<br>(1.9774, 2.0121)    | 1.9920<br>(1.9739, 2.0104)    | 1.9950<br>(1.9716, 2.0183)    |
| $\sigma_e^2 = 0.5$ | 0.5414<br>(0.5175, 0.5661)    | 0.4921<br>(0.4734, 0.5113)    | 0.5378<br>(0.5167, 0.5598)    | 0.4981<br>(0.4775, 0.5192)    |
| $\rho = 0.8$       | 0.7987<br>(0.7880, 0.8091)    | 0.7970<br>(0.7856, 0.8080)    | 0.7984<br>(0.7873, 0.8091)    | 0.7977<br>(0.7857, 0.8092)    |
| $\nu = 30$         | NA                            | 22.7544<br>(21.8282, 23.7190) | NA                            | 26.1797<br>(24.8903, 27.5045) |
| $\gamma = 1$       | NA                            | NA                            | 1.0028<br>(0.9998, 1.0057)    | 1.0035<br>(0.9987, 1.0083)    |
| DIC <sub>1</sub>   | 11315.17                      | 11320.44                      | 11475.1                       | 11324.83                      |
| DIC <sub>2</sub>   | 11314.81                      | 11321.4                       | 11535.12                      | 11324.85                      |
| CT                 | 0.1280                        | 0.6718                        | 0.1197                        | 0.7241                        |

Table S5: Posterior means and 95% credible intervals for selected parameters of different SEMs based on the simulated dataset 2 (full data), along with the computation time (CT) in seconds for one VB iteration. The table also presents the DIC values for each model. Parameters labeled as 'NA' indicate that they are not applicable to the corresponding model.

## S7.1 Comparison of VB and HVB methods

Section 4.1 of the main paper compares the estimated posterior densities of the model parameters for the YJ-SEM-Gau model using VB (including HVB) and HMC (Neal, 1996) methods, both with and without missing data, based on a simulated dataset. To generate the data, the model parameters are set as follows: the fixed effects ( $\beta$ ) are randomly drawn from discrete uniform values between  $-3$  and  $3$  (excluding 0). The error variance parameter is set to  $\sigma_e^2 = 1$  and the spatial autoregressive parameter is  $\rho = 0.8$ . The Yeo-Johnson transformation parameter is set to  $\gamma = 1.25$ , which introduces moderate left skewness in the simulated response variable. The kernel density plot of the simulated response variable is provided in Figure S1. As expected, the density is moderately skewed to the left.

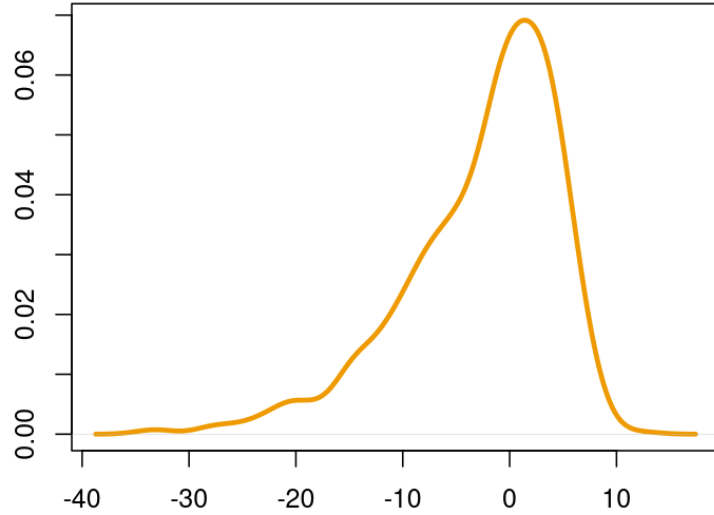


Figure S1: Kernel density plot of the simulated response variable generated using the YJ-SEM-Gau model with  $\gamma = 1.25$  in the simulation study of Section 4.1 of the main paper.

## S7.2 Evaluating the performance of proposed SEMs

### S7.2.1 Simulation study with full data

This section presents further figures from Section S6.

Figures S2 and S3 compare the posterior densities of selected model parameters obtained using the proposed VB method, applied to different SEMs (without missing values) for simulated dataset 1 and simulated dataset 2, respectively.

As shown in Figure S2, the YJ-SEM-t model is able to recover the true parameter values more accurately than the other three models, as expected, since the simulated dataset 1 was simulated using the YJ-SEM-t model. In contrast, as shown in Figure S3, all four models successfully recover the true values of the parameters.

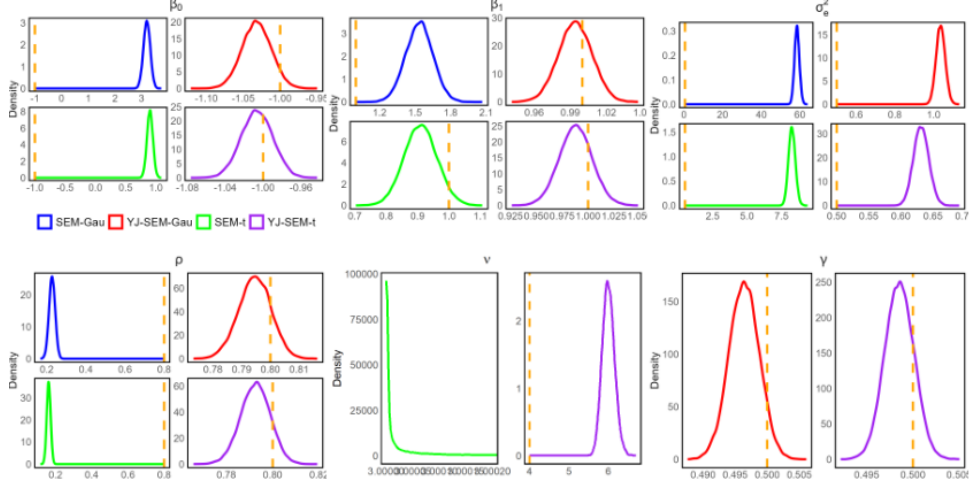


Figure S2: Posterior densities of some of the parameters for the SEM-Gau, YJ-SEM-Gau, SEM-t, and YJ-SEM-t models, fitted to the simulated dataset 1, using the VB method. The vertical dotted lines indicate the true parameter values.

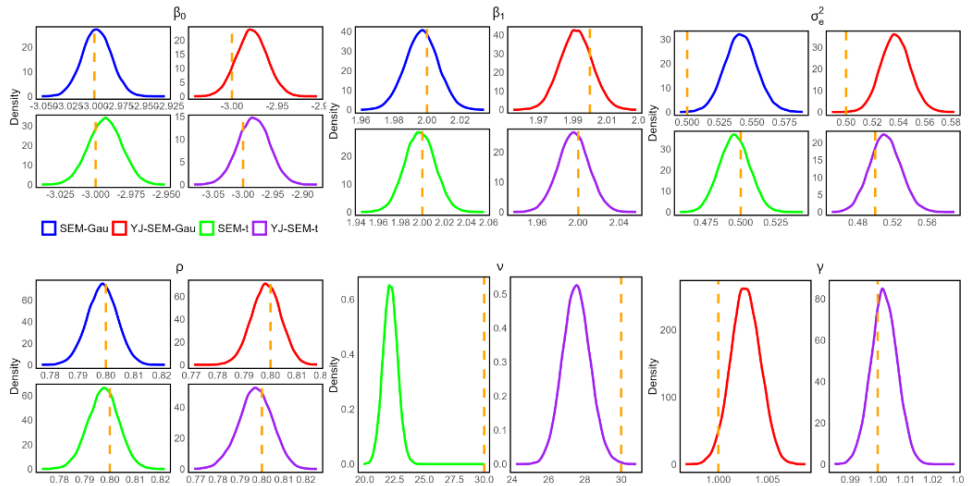


Figure S3: Posterior densities of some of the parameters for the SEM-Gau, YJ-SEM-Gau, SEM-t, and YJ-SEM-t models, fitted to the simulated dataset 2, using the VB method. The vertical dotted lines indicate the true parameter values.

### S7.2.2 Simulation study with missing data

This section presents further figures from Section 4.2 of the main paper.

Figures S4 and S5 compare the posterior densities of selected model parameters estimated using the proposed HVB method, applied to different SEMs with missing values, for simulated dataset 1 and simulated dataset 2, respectively.

As shown in Figure S4, the YJ-SEM-t model is able to recover the true parameter values more accurately than the other three models, as expected, since the simulated

dataset 1 was simulated using the YJ-SEM-t model. In contrast, as shown in Figure S5, all four models successfully recover the true values of the parameters.

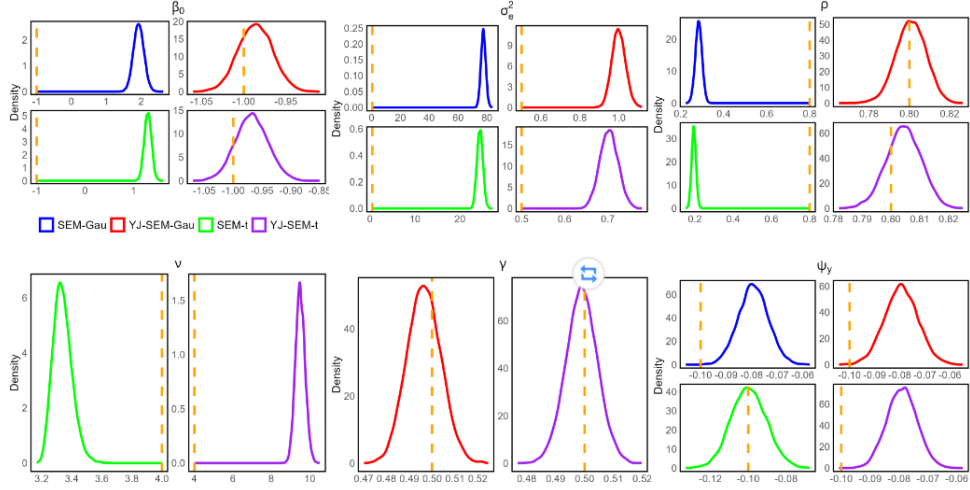


Figure S4: Posterior densities of some of the parameters for the SEM-Gau, YJ-SEM-Gau, SEM-t, and YJ-SEM-t models, fitted to the simulated dataset 1 with missing data, using the HVB method. The vertical dotted lines indicate the true parameter values.

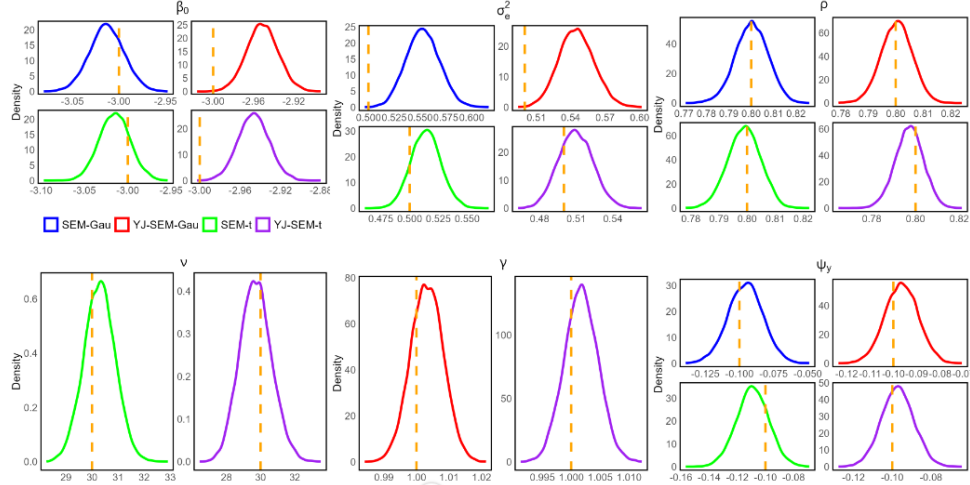


Figure S5: Posterior densities of some of the parameters for the SEM-Gau, YJ-SEM-Gau, SEM-t, and YJ-SEM-t models, fitted to the simulated dataset 2 with missing data, using the HVB method. The vertical dotted lines indicate the true parameter values.

The left panel of Figure S6 shows the kernel densities of the true missing values ( $\mathbf{y}_u$ ) and the kernel density of posterior means of the missing values at locations  $s_1, s_2, \dots, s_n$ , estimated from different SEMs for simulated dataset 2. All four models produce nearly identical densities of posterior means of missing values that closely match the density of the true missing values.

The right panel of Figure S6 presents the posterior density of the maximum missing value ( $\mathbf{y}_{u_{\max}}$ ) predicted by each SEM. The true value of  $\mathbf{y}_{u_{\max}}$  lies within the posterior distribution estimated by all models. These results are consistent with expectations, as all four models produce similar parameter estimates and DIC values (see Table 5).

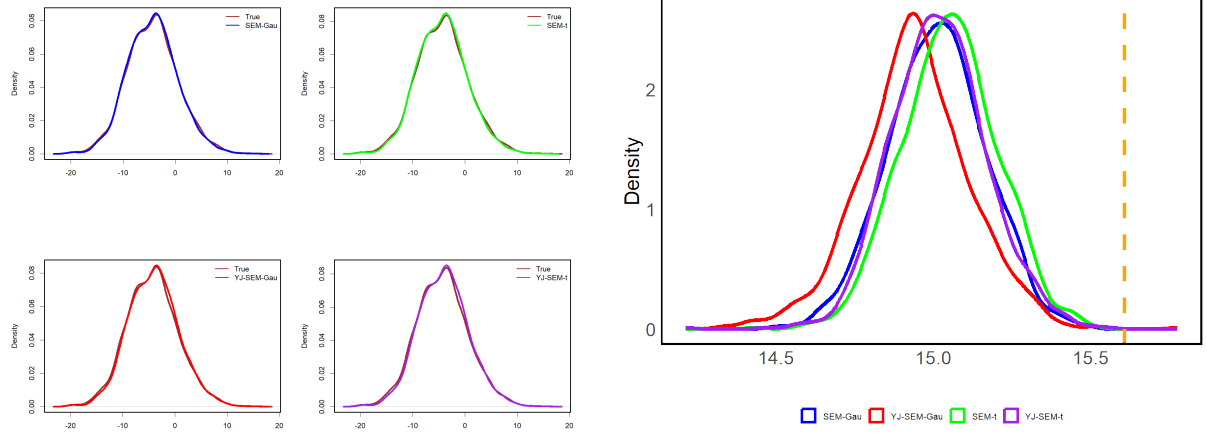


Figure S6: Left panel: The kernel densities of the true missing values ( $\mathbf{y}_u$ ) and the posterior means of the missing values ( $\mathbf{y}_u$ ) obtained using the HVB-AllB method for different SEMs for the simulated dataset 2 with missing values.

Right panel: The posterior density of the maximum missing value ( $\mathbf{y}_{u_{\max}}$ ) predicted by different SEMs for the simulated dataset 2 with missing values. The true value of the maximum missing value is indicated by the vertical line.

Figure S7 compares the posterior means and standard deviations of the missing values ( $y_{u_1}, \dots, y_{u_{n_u}}$ ) estimated by different SEMs for the simulated dataset 1 with missing values. The left panel compares the posterior means of the predicted missing values with their true values. The right panel compares the posterior standard deviations of the missing values estimated by the YJ-SEM-t model (x-axis) against those obtained from SEM-Gau, SEM-t, and YJ-SEM-Gau models (y-axis).

The posterior means of the missing values estimated by the YJ-SEM-Gau and YJ-SEM-t models are closer to the true missing values compared to those estimated by the SEM-Gau and SEM-t models. Additionally, the posterior standard deviations from the YJ-SEM-Gau and YJ-SEM-t models are nearly identical, whereas those from the SEM-Gau and SEM-t models deviate from the standard deviations obtained by the YJ-based models.

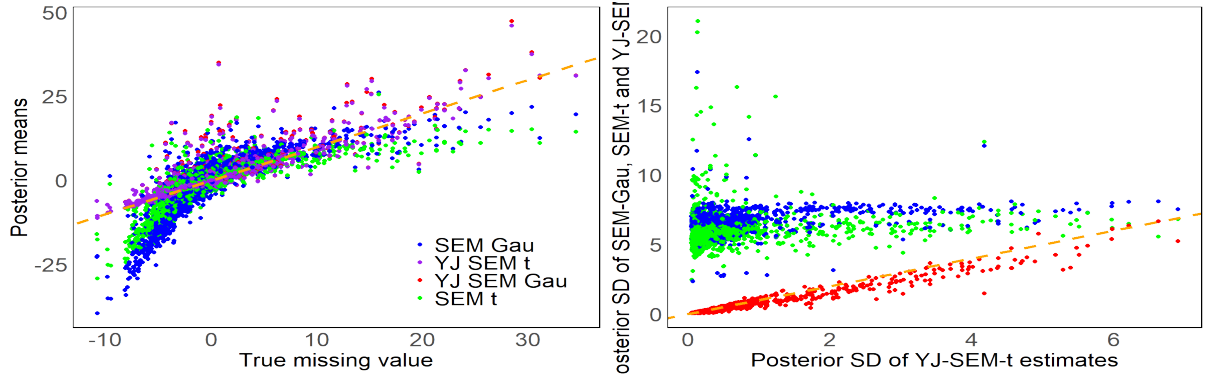


Figure S7: Comparison of posterior means and standard deviations of missing values for the simulated dataset 1: The left plot shows the comparison of the posterior means of predicted missing values from the SEM-Gau, SEM-t, YJ-SEM-Gau, and YJ-SEM-t with true missing values. The right plot compares the posterior standard deviations of the missing values from SEM-Gau, SEM-t, and YJ-SEM-Gau against those obtained from YJ-SEM-t.

Figure S8 compares the posterior means and standard deviations of the missing values  $(y_{u_1}, \dots, y_{u_{n_u}})$  estimated by different SEMs for the simulated dataset 2 with missing values. The left panel compares the posterior means of the predicted missing values with their true values. The right panel compares the posterior standard deviations of the missing values estimated by the YJ-SEM-t model (x-axis) against those obtained from SEM-Gau, SEM-t, and YJ-SEM-Gau models (y-axis).

The posterior means of the missing values estimated by all four models are close to the true values. Additionally, the posterior standard deviations from the SEM-Gau, SEM-t, and YJ-SEM-Gau models closely align with those from the YJ-SEM-t model, with YJ-SEM-Gau showing the closest match.

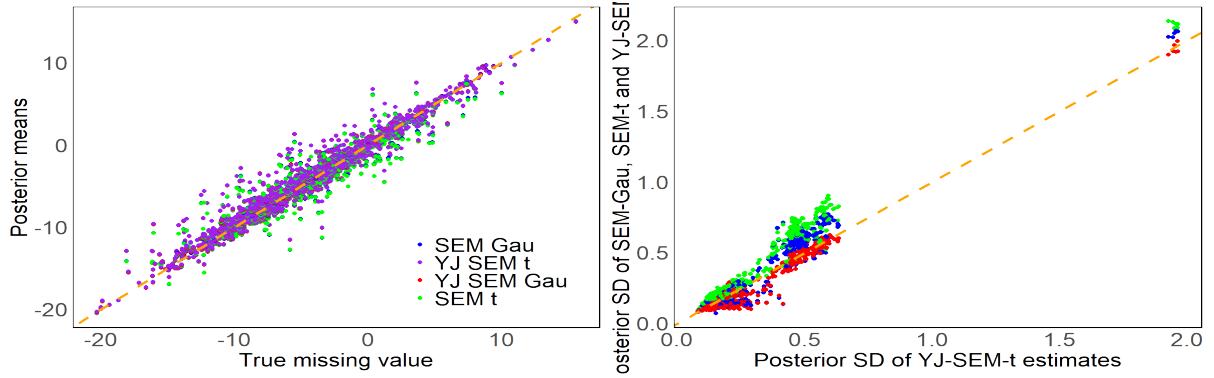


Figure S8: Comparison of posterior means and standard deviations of predicted missing values for the simulated dataset 2: The left plot shows the comparison of the posterior means of missing values from the SEM-Gau, SEM-t, YJ-SEM-Gau, and YJ-SEM-t with true missing values. The right plot compares the posterior standard deviations of the missing values from SEM-Gau, SEM-t, and YJ-SEM-Gau against those obtained from YJ-SEM-t.

## S8 Additional figures for real data application in Section 5

This section provides additional figures related to the real data application discussed in Section 5 of the main paper.

Figure S9 shows kernel density plots of house prices from the Lucas-1998-HP dataset. The left panel displays the distribution of house prices (in hundreds of thousands), while the right panel shows the distribution of their natural logarithms. For a detailed description of the Lucas-1998-HP dataset, see Section 5 of the main paper. As expected, house prices being strictly positive, exhibit right skewness, whereas their logarithms appear to be left-skewed.

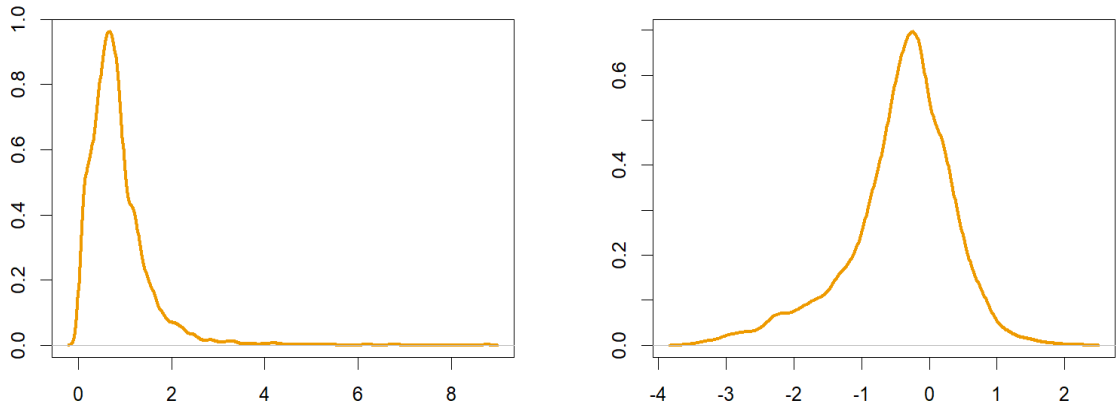


Figure S9: Kernel density plots of house prices from the Lucas-1998-HP data: The left panel displays the kernel density of house prices (in hundreds of thousands). The right panel shows the kernel density of the logarithm of house prices (in hundreds of thousands).

Figures S10 and S11 compare the posterior densities of selected model parameters, estimated using the proposed VB and HVB-AllB methods, across different SEMs (without and with missing values) applied to the Lucas-1998-HP dataset.

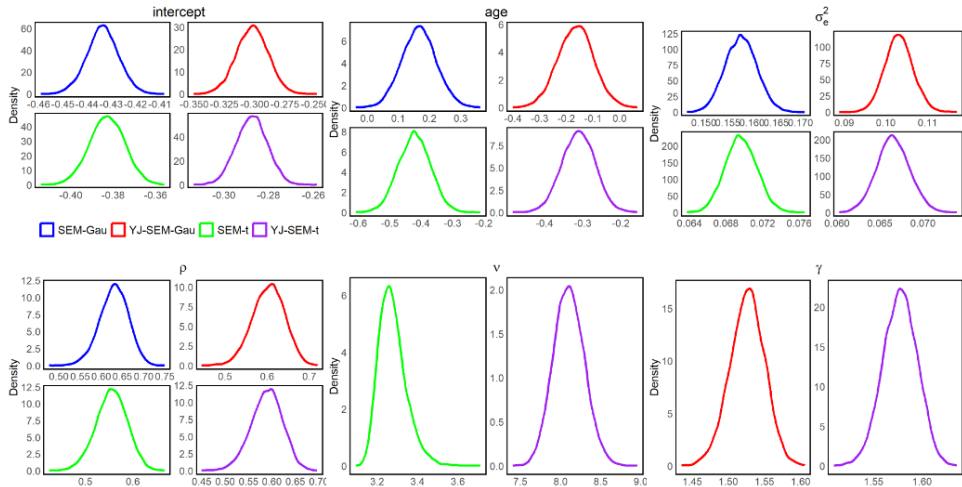


Figure S10: Posterior densities of some of the parameters of the SEM-Gau, YJ-SEM-Gau, SEM-t, and YJ-SEM-t models, fitted to the Lucas-1998-HP dataset without missing values, using the VB method.

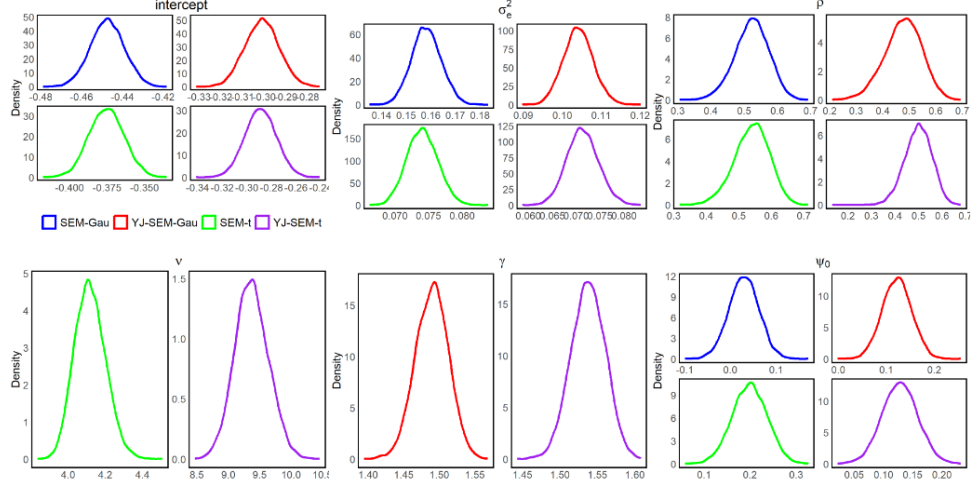


Figure S11: Posterior densities of some of the parameters of the SEM-Gau, YJ-SEM-Gau, SEM-t, and YJ-SEM-t models, fitted to the Lucas-1998-HP dataset with missing values, using the HVB-AllB method.

## S9 Convergence analysis

For the variational Bayes (VB) and hybrid VB (HVB) algorithms, convergence is assessed by examining the trajectories of the variational means of model parameters across iterations. For the Hamiltonian Monte Carlo (HMC) algorithm (Neal et al., 2011), convergence is evaluated by inspecting the trace plots of the posterior draws of model parameters.

Section S9.1 presents the convergence analysis plots for the simulation study described in Section 4 of the main paper. Similarly, Section S9.2 provides the convergence analysis plots for the real-data example discussed in Section 5 of the main paper.

### S9.1 Convergence analysis of simulation study

#### S9.1.1 Convergence analysis for Section 4.1

This section presents convergence plots from the simulation study designed to compare the performance of the VB approximation with the HMC algorithm, as described in Section 4.1 of the main paper. In this study, data are simulated from the YJ-SEM-Gau model, and the model is estimated using both VB and HMC methods.

Figure S12 presents trace plots of posterior samples obtained using the HMC algorithm for selected parameters of the YJ-SEM-Gau model with full data, after excluding burn-

in samples. Figure S13 displays the trajectories of the variational means for selected parameters across VB iterations. Both plots indicate that the algorithms have converged.

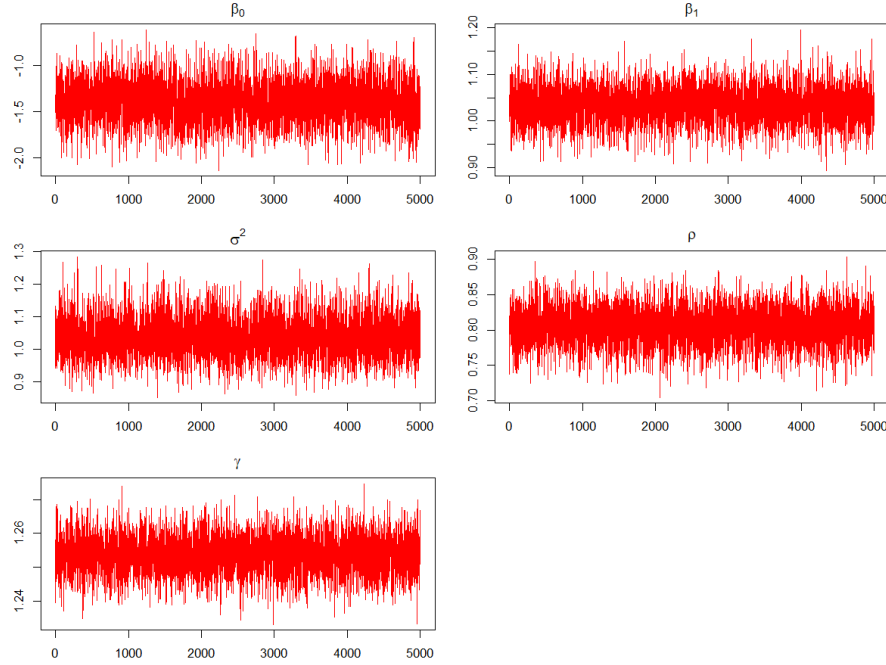


Figure S12: Trace plots of posterior samples obtained using HMC for selected parameters of the YJ-SEM-Gau model (without missing values), after excluding burn-in samples.

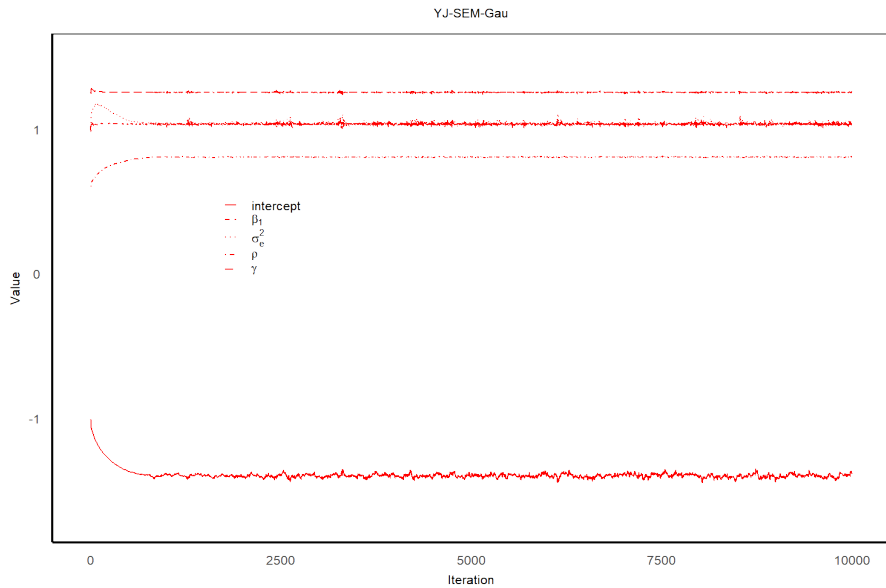


Figure S13: Trajectories of the variational means of selected parameters of the YJ-SEM-Gau model (without missing values) across VB iterations.

Next, missing values are introduced into the simulated dataset, and the YJ-SEM-Gau model is fitted using both the HVB-NoB and HMC algorithms.

Figure S14 presents trace plots of posterior samples obtained using the HMC algorithm for selected parameters of the YJ-SEM-Gau model with missing values, after excluding burn-in samples. Figure S15 displays the trajectories of the variational means for selected parameters across HVB-NoB iterations. Both plots indicate that the algorithms have converged.

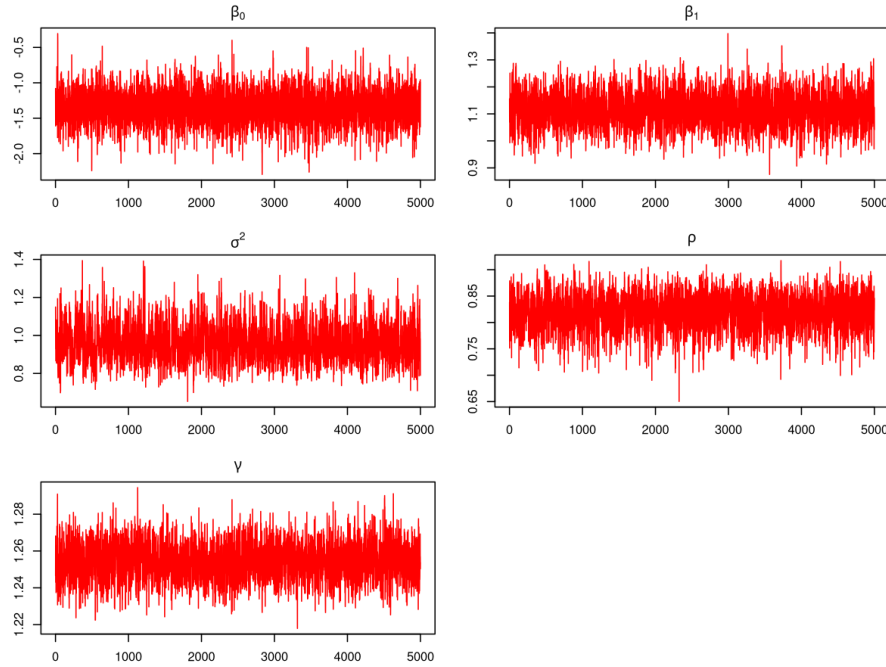


Figure S14: Trace plots of posterior samples obtained using HMC for selected parameters of the YJ-SEM-Gau model (with missing values), after excluding burn-in samples.

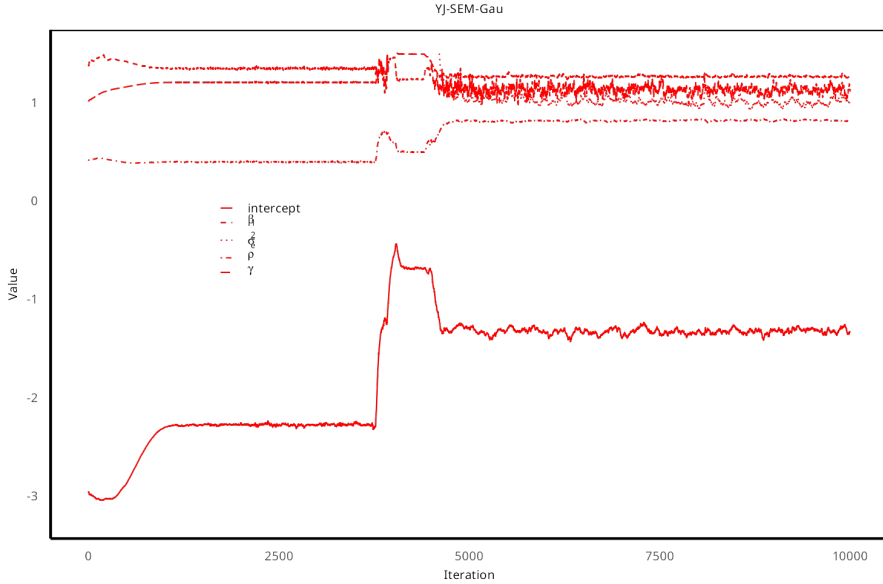


Figure S15: Trajectories of the variational means of selected parameters of the YJ-SEM-Gau model (with missing values) across HVB-NoB iterations.

### S9.1.2 Convergence analysis for Section 4.2

This section presents convergence plots from the simulation study conducted to evaluate the performance of the proposed SEMs, as described in Section 4.2 of the main paper.

Figure S16 shows trajectories of the variational means for selected model parameters of different SEMs fitted to the simulated dataset 1, without missing values. It can be observed that for each parameter in each model, the variational means converge by the end of the final iterations, indicating that the VB algorithms for all models have successfully converged.

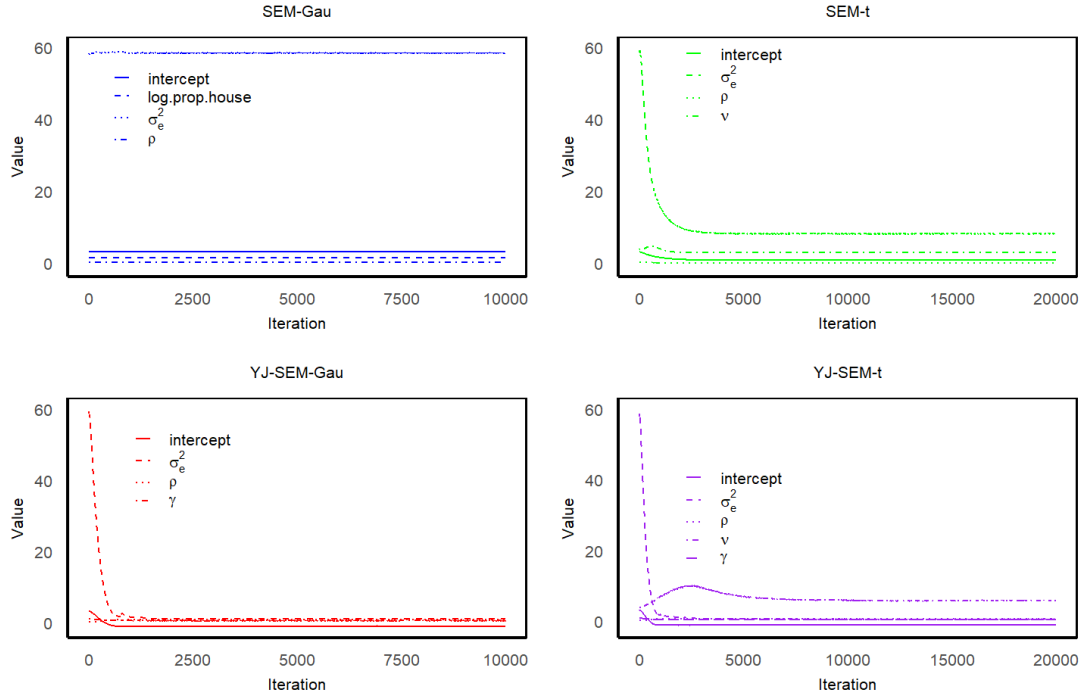


Figure S16: Trajectories of the variational means of selected parameters across VB iterations for different SEMs fitted on the simulated dataset 1.

Figure S17 shows trajectories of the variational means for selected model parameters of different SEMs fitted to the simulated dataset 2, without missing values. It can be observed that for each parameter in each model, the variational means converge by the end of the final iterations, indicating that the VB algorithms for all models have successfully converged.

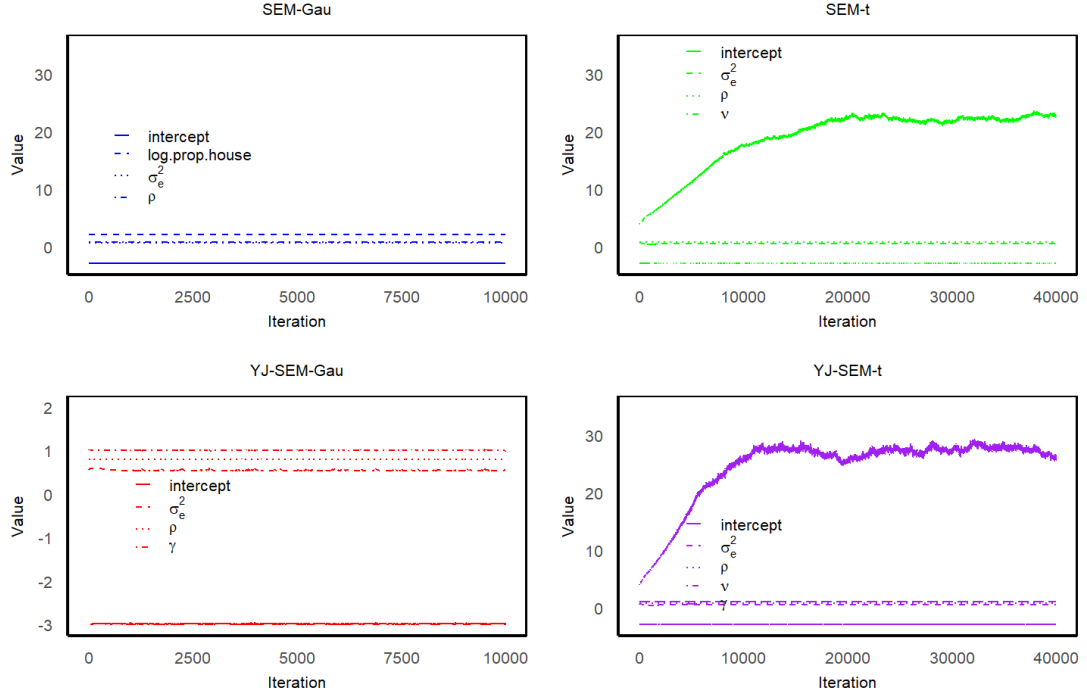


Figure S17: Trajectories of the variational means of selected parameters across VB iterations for different SEMs fitted on the simulated dataset 2.

Figure S18 shows trajectories of the variational means for selected model parameters of different SEMs fitted to the simulated dataset 1, with missing values. It can be observed that for each parameter in each model, the variational means converge by the end of the final iterations, indicating that the HVB-AllB algorithms for all models have successfully converged.

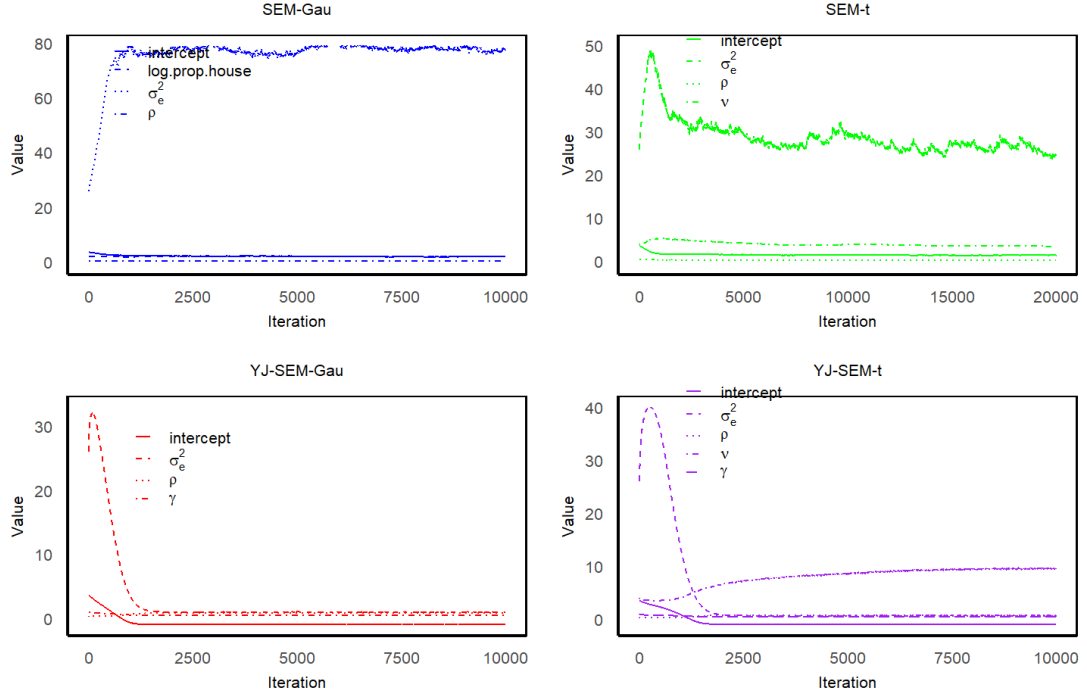


Figure S18: Trajectories of the variational means of selected parameters across HVB-AllB iterations for different SEMs fitted on the simulated dataset 1 with missing values.

Figure S19 shows trajectories of the variational means for selected model parameters of different SEMs fitted to the simulated dataset 2, with missing values. It can be observed that for each parameter in each model, the variational means converge by the end of the final iterations, indicating that the HVB-AllB algorithms for all models have successfully converged.

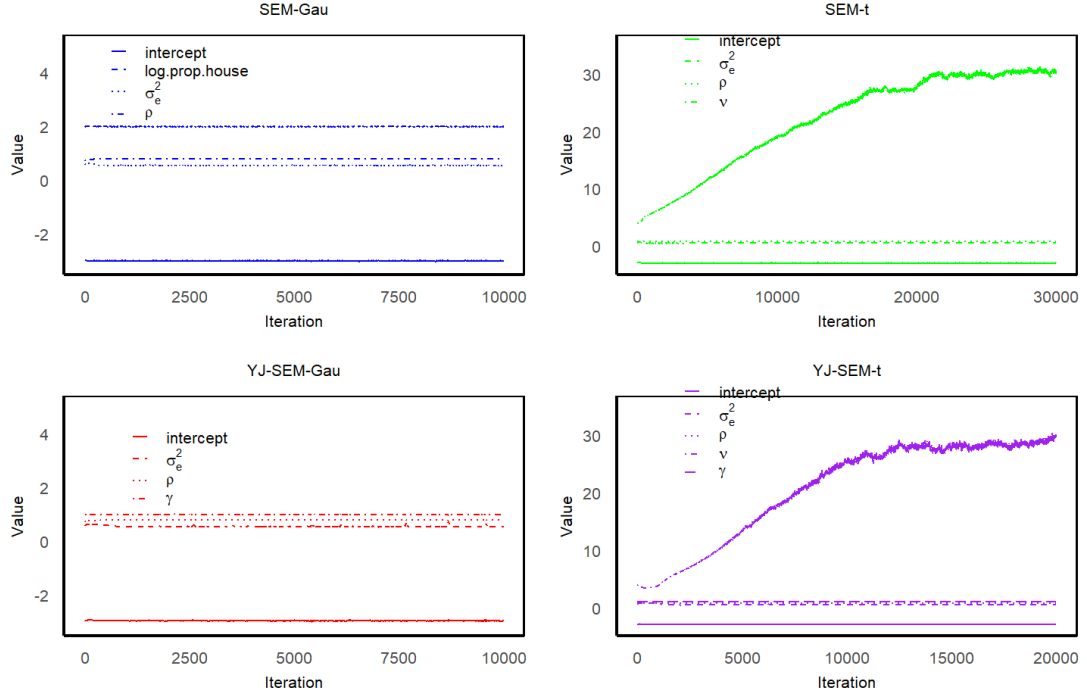


Figure S19: Trajectories of the variational means of selected parameters across HVB-AllB iterations for different SEMs fitted on the simulated dataset 2 with missing values.

## S9.2 Convergence analysis of real example

Figure S20 shows trajectories of the variational means for selected model parameters of different SEMs fitted to the Lucas-1998-HP dataset (full data). It can be observed that for each parameter in each model, the variational means converge by the end of the final iterations, indicating that the HVB-AllB algorithms for all models have successfully converged.

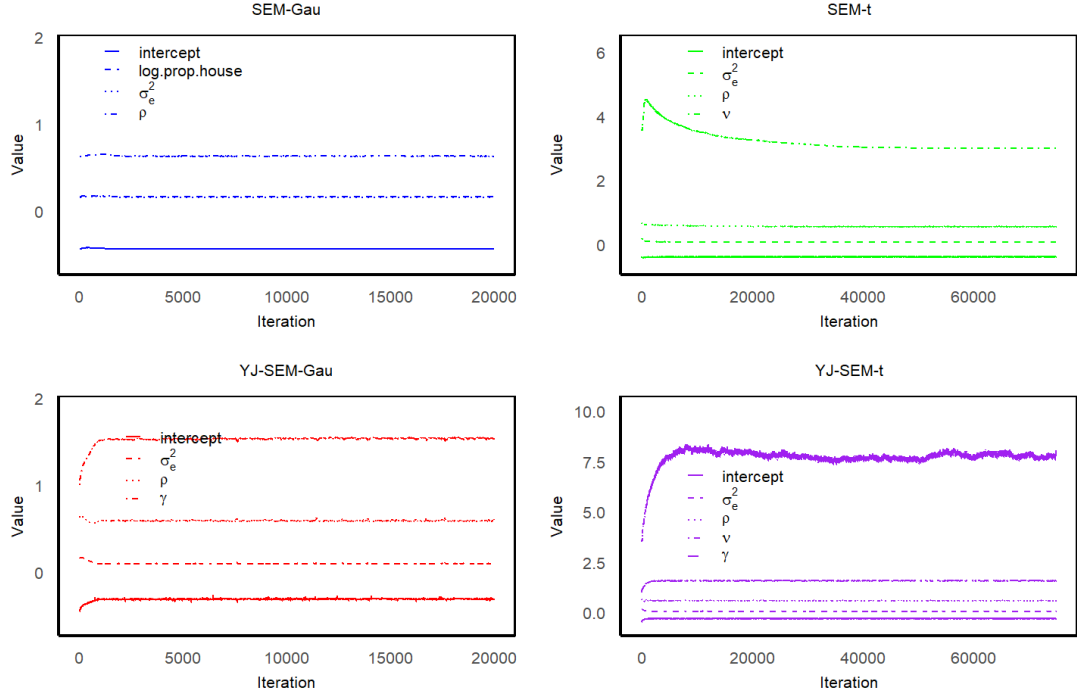


Figure S20: Trajectories of the variational means of selected parameters across HVB-AllB iterations for different SEMs fitted on the Lucas-1998-HP dataset without missing values.

Figure S21 shows trajectories of the variational means for selected model parameters of different SEMs fitted to the Lucas-1998-HP dataset, with missing values. It can be observed that for each parameter in each model, the variational means converge by the end of the final iterations, indicating that the VB algorithms for all models have successfully converged.

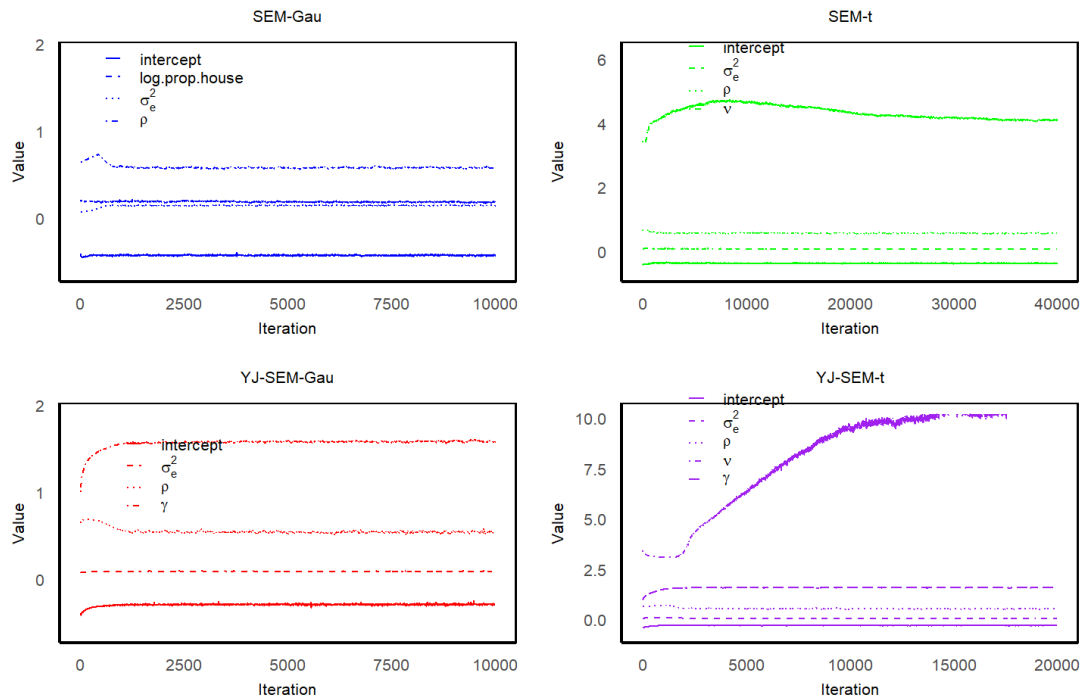


Figure S21: Trajectories of the variational means of selected parameters across HVB-AllB iterations for different SEMs fitted on the Lucas-1998-HP dataset with missing values.